NORTHWESTERN UNIVERSITY

Standardization of Automated Crack Monitoring Apparatus for Long-Term Commercial Applications

A Thesis

Submitted to the Graduate School In Partial Fulfillment of the Requirements

For the Degree

MASTER OF SCIENCE

Field of Civil Engineering

By

Markian B. Petrina

EVANSTON, IL

August 2004

Table of Contents

Table of Contents

Table of Contents

Acknowledgments

An advanced degree is always a challenging undertaking. It is even more so for someone who has been out of school for almost a decade, particularly if that individual decides to take an advanced degree in an area different than his undergraduate major. I found myself in this position, an Applied Mathematics major changing professions to Civil Engineering after a military career of over nine years. I could not have succeeded without the assistance of many people.

First of all, I thank my advisor, Professor Charles H. Dowding, who guided me through this interesting and educational thesis project. Long before that, Professor Dowding was my sponsor at Northwestern University when I was researching graduate schools. I am grateful to Professor Dowding for taking a genuine personal interest in me, helping me through the application process, and for the cordial rapport we maintained throughout my time at Northwestern.

Thanks also to Professor Richard J. Finno for his challenging and valuable instruction, and to Professor Raymond J. Krizek for his teaching, assistance, and sincere, helpful mentorship. I am also indebted to Professors Finno and Krizek for serving on my thesis examination committee. Finally, I am deeply grateful to Professor Edwin C. Rossow, for his help with structural engineering basics and classes, and his advice, both academic and professional; his contributions caused me to consider him an unofficial second advisor.

Returning to school from military service required the indulgence and assistance of my superiors. Major Lewis D. Carlisle, U.S. Air Force, Lieutenant Colonel Cynthia Lundell, U.S. Air Force, and Mrs. A. Cathy Deitering, all took the time and trouble to write

letters of recommendation. The generous policies of Mrs. Deitering, my branch chief, and her moral and administrative support at work, made my transition to civilian life smooth and uneventful.

My peers and collaborators had a great influence on this project, as well. I am indebted to the Infrastructure Technology Institute for funding my research and education, and to the ITI staff, in particular Daniel Marron, whose technical expertise made this project possible. I am also grateful to those of my peers and classmates who helped me with academics.

During most of my time in the graduate program, I had the distraction of a second house in Omaha, Nebraska. My attorney, Mr. James L. Stanton, provided wise counsel and assistance, and referred me to Mrs. Dianne Rogers, the upstanding and conscientious realtor to whom I am indebted for efficiently and smoothly selling my house.

Finally, my parents, Andrew and Irene Petrina, provided unstinting and generous support, both moral and material, from the time I decided to change careers through the end of graduate school. Their assistance, as well as the knowledge they would help me however they could, was a comfort to me during several difficult periods. I thank them for their generosity and encouragement, without which my return to graduate school would not have been nearly so successful.

Abstract

All structures have cosmetic cracks, which have no influence on structural integrity and usually remain unremarked until the structure's occupants sense ground vibrations. Such vibrations are often associated with engineering activity, but are rarely responsible for cracks. However, this is difficult to prove without scientific basis. Automated Crack Monitoring (ACM) provides this basis by measuring crack displacement with micro-measurement instruments and data logging systems. Previous work (Louis, 2000; Siebert, 2000; McKenna, 2002; Snider, 2003) has shown that temperature and humidity effects far exceed those of typical engineering-induced ground motion by as much as an order of magnitude.

Until recently, all ACM systems were considered research instruments. Though highly accurate, such apparatus was too unwieldy and expensive for widespread, commercially-viable installation. Simple, compact, and accurate ACM systems for commercial monitoring are necessary. Such apparatus would immensely benefit engineering reliant on ground vibration, by effectively demonstrating the relatively small contribution to wall crack opening and closing from engineering activity.

This thesis proposes methods to qualify commercial ACM systems under controlled laboratory and field conditions. An alpha-model commercial ACM apparatus, System X, was tested and evaluated with these methods to verify their validity. Rigorous testing is crucial to ensuring ACM equipment will perform adequately and provide unassailable information in real-world situations fraught with legal and financial consequences. The methods of this thesis are the first step in developing a reliable and defensible validation process.

List of Figures

List of Figures

List of Figures

Figures in Standalone Appendices

Appendix E. LVDT Mounting Procedures

List of Figures

Appendix F. Proposed ASTM Standard: "Qualification of Systems to Measure Micro-inch Crack Opening and Closing"

List of Tables

List of Equations

Equations in Standalone Appendix

Appendix F. Proposed ASTM Standard: "Qualification of Systems to Measure Micro-inch Crack Opening and Closing"

Chapter 1

Introduction

Automated Crack Monitoring (ACM) is an approach to measure micro-displacement of cracks autonomously with specialized sensors and data collection software and equipment. This thesis will describe laboratory qualification and field testing of ACM systems. Industries dependent on procedures that cause vibratory ground motion, such as quarrying and construction, can demonstrate the impact of these operations relative to naturally-occurring phenomena by installing ACM technology. At present, the only proven ACM equipment is research grade and is expensive, manpower-intensive, and uneconomical for commercial applications. As commercial systems become available, a standardized method to qualify them for field installation will be crucial.

In general, ACM measures the one-dimensional opening and closing of a crack, measured as relative motion between a target on one side of a crack and a displacement detector on the other side. A displacement sensor, such as a linear voltage displacement transducer (LVDT) or eddy-current gauge, is placed across a crack. A data logging computer records displacement measurements. Figure 1.1 shows the installation of an

LVDT, which consists of rod suspending a ferromagnetic core inside an electromagnetic LVDT coil; the rod is also attached to a bracket on the other side of the crack. An eddy-current sensor, unlike an LVDT, has no mechanical or moving parts. Though dissimilar in mechanical configuration, both rely on changes in an electromagnetic field to detect displacement. While operating principles differ, both sensors are viable alternatives to measure crack response.

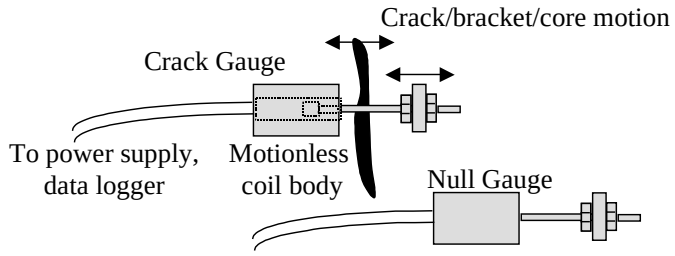

Figure 1. Sketch of an LVDT spanning a crack, with a null gauge nearby on an intact portion of the surface.

In an LVDT, the coil produces an electromagnetic field, which is converted to a voltage that becomes the output signal. The electromagnetic field, and its corresponding voltage output signal, both change when the ferromagnetic core moves linearly back and forth inside the coil. As the crack opens and closes one-dimensionally, the bracket-rod-core assembly moves with it, causing the core to move back and forth inside the coil. A data logger records voltages corresponding to core positions inside the coil. Voltage is converted to displacement units by a factor provided by the LVDT manufacturer. In the eddy-current gauge, a transmitter on one side of a crack illuminates the target on the opposite side of the crack with a constant electromagnetic field. Changes in relative positions of the transmitter and target modify the electromagnetic field; displacement measured by an output signal in volts, is a polynomial function of the field's changes.

This paper presents two qualification methods, one in the laboratory to determine suitability for deployment in the field, and one for testing performance in the field under

actual conditions. It is essential to understand ACM system performance and to qualify systems before they are installed in structures for which the ACM data has real-world legal implications. Rigorous, reliable, and credible methods that can be rationally applied and defended will ensure that ACM system performance is demonstrably adequate.

ACM definitions

There are three levels of monitoring that though similar are independent of each other. The first, Level I, records only long-term crack displacement history on the order of months, and is characterized by low sampling rates, e.g., one to several points per hour. Level II and Level III systems collect both high sample rate data (1000 points per second) during dynamic crack motion events, as well as low sample rate (Level I) data in the absence of seismic events. Simultaneous operation of Level I and Level II or III requires control software to detect vibration, trigger Level II or III data acquisition, and then return to Level I recording. Although Level II and III triggering methods differ, both require a seismic event to initiate collection via a complex combination of hardware and software. Level II and III qualification are not considered in this thesis.

Level I monitoring records the long-term environmentally-induced "opening and closing" crack displacement time history. Level I is sufficient for many applications where it is only necessary to show that dynamic events did not change the typical long-term crack response. Past work (Louis, 2000; Siebert, 2001; McKenna, 2002) has shown that the influence of environmental factors dominates crack displacement, and such movements exceed typical seismic displacement by up to an order of magnitude. Long-term response can be measured with one data point every hour. An optimum Level I data point is the average of a large number of points recorded over a short period to "average out"

electronic noise. Such filtering is not essential if daily crack movement is an order of magnitude larger than the noise.

Level I laboratory qualification requires a plate of homogeneous material with linear thermal expansion properties and a known coefficient of thermal expansion, α. The quantity α is defined as strain per degree of temperature and can be employed to predict the temperature-induced expansion-contraction that approximates one-dimensional crack motion. Level I monitoring memory requirements are relatively small (1-4 MB of data logger storage is generally adequate), and no trigger or additional programming is required as with Level II and III.

Level II monitoring records dynamic crack displacement at high sample rates (on the order of 1000 points per second) for a short period (3-5 seconds) during seismic events by triggering off ground motion. Level II is activated when a buried geophone detects ground particle velocity of a certain threshold; the industry standard for recording industrially-induced seismic events is 0.04 inches per second (ips). In addition to triggering, challenges include onboard computing capability and memory. The data logging computer must be capable of maintaining a buffer, temporarily terminating Level I data acquisition, initiating a high sample rate recording mode for several seconds, then returning to low sample rate recording.

Level III monitoring is similar to Level II except high sample rate data recording is triggered by the dynamic crack displacement itself without external geophone input. Level III requires significantly more computing power and memory than Level II, and is still under development. Complications include a “moving zero point” for the crack: over time, environmental factors expand and contract the crack, moving the “zero” point about

which the trigger is set. The baseline "zero" for a crack's relative displacement is its position at the moment before seismic effects begin to open and close the crack rapidly. The only difference between Levels II and III is the triggering method. Though it requires significantly more complex software and computing, Level III possesses the enormous advantage of requiring only a data logging computer and displacement sensors; no directly connected external geophones are necessary, and thus installation is simpler than for a Level II system. However, it will still be necessary to record the ground motion for compliance and regulatory purposes.

Chapter 2

Laboratory Qualification: Theoretical Background

Physical Parameters

Before ACM sensors can be deployed to the field, they must be shown to work properly in laboratory conditions. Several tests determined the consistency of sensor performance: sampling, linearity, noise, and resolution as described in Chapters 3, 4, 5, and 6 respectively; Appendices A and C treat linearity and resolution, respectively, in greater detail. This chapter focuses on background calculations that determine parameters for equipment and experimental setup.

The first stage of system qualification is to determine linearity of the system. System X, the ACM system under evaluation, has LVDTs and a data logger; its linearity was assessed on both aluminum and plastic. Since ACM systems are deployed for months or even years, they must be reliably linear, i.e., not deviate from their centerline, under numerous environmental changes over that time.

An aluminum plate (α = 13.1 μin/in/°F) was the initial standardization surface (Siebert, 2000). Although suitable for high-resolution research systems, its thermal

expansion behavior may be too small for detection by commercial systems designed to balance capability and affordability in measuring theoretically large crack responses. Furthermore, α of aluminum, though high for a metal, is low compared to α of a wall crack, requiring a different material for more faithful representation of a wall's thermal behavior. For these two reasons, Ultra-High Molecular Weight Polyethylene (UHMW-P), also known as "poor man's Teflon®" (α = 110 μin/in/°F) was also employed for thermal expansion testing. An incidental benefit is the modest cost savings; a 12"x 12"x ¾" plate of Aluminum ($150 in 2003) costs roughly five times as much as an 18"x 24"x ¾" plate of UHMW-P ($35 in 2003).

Data Collection Calculations

ACM also requires a thorough understanding of system technical limitations, particularly measurement range and resolution. Sensor range is easily obtained from a manufacturer and is usually included in technical literature packaged with a sensor; LVDT measurement ranges vary; those investigated herein have ranges of 0.1 inches, two orders of magnitude larger than necessary for ACM. However, the sensor's suitability must still be verified.

The equation to calculate expansion and contraction of a test material with linear thermal expansion properties is

$$\delta_{tot} = \alpha * L * \Delta T \qquad \text{(Equation 2.1)}$$

where δ_{tot} is total displacement, α is the coefficient of thermal expansion (units: [micro-length]/[length]/[degree Temperature]), L is width of gap, i.e., the spacing between the detector and target (units: [length]), T is temperature of the test material (units: [degrees]), and ΔT is temperature change over the course of an experiment = $T_{max} - T_{min}$.

Expansion and contraction changes L at most on the order of 10^{-3} inches over an entire test on the large-thermal-displacement plastic described later; thus, L, which is usually in the neighborhood of 0.5 to 0.75 inches, is assumed to remain constant. Temperature varies cyclically, and predicting ΔT in the test environment requires knowledge of current temperature cycles and trends. This equation is employed to calculate the theoretical displacement a sensor is expected to measure over the experiment's temperature range. During the laboratory qualification of the ACM systems described, the expansion measurements were conducted in a garage with no heating or cooling control.

Subsequent displacement calculations build on Equation 2.1 to determine voltage range "gates." A constant should be added so all data is collected even during unexpected, extreme temperature swings inducing large movements. For example, $0.2^* \delta_{tot}$ yields the quantity $\delta_{collection} = \delta_{tot} + 0.2^*\delta_{tot} = 1.2^*\delta_{tot}$. If Equation 2.1 yields a predicted displacement of $\delta_{tot} = 250$ μin, then the range adjustment is $0.2^*250 = 50$ μin, and $\delta_{collection} = 300$ μin.

A sensor system whose data collection range can be adjusted should be set to collect $\delta_{collection}$ on either side of the starting voltage. For a sensor with a collection range of ±10 Volts (V), the sensor's starting position should be adjusted as close as reasonably possible to 0 V on the data logger; for a sensor with a range of 0-5 V, the starting point should be around 2.5 V.

A slightly different approach is necessary to set voltage ranges for sensors with nonlinear output. The eddy current sensors have a nonlinear conversion from voltage to displacement in the form of a fifth-order polynomial. The voltage from which the displacement range is the same on either side does not necessarily coincide with the voltage from which voltage range is the same on either side.

This is not a concern with an LVDT whose Scale Factor will be in units of Volts/[length], which can be inverted as it is simply a conversion factor equal to unity. Applying the scale factor, the equation to derive voltage "gates" is

$$V_{gate} = \pm\delta_{collection} * \text{Scale Factor} \qquad \text{(Equation 2.2)}$$

and for the example, assuming a scale factor = 200 V/in and a voltage range of ±300μin, V_{gate} = ±300μin * 200 V/in = ±300x10^{-6} in * 200V/in = ±0.06 V. If sensor voltage range is exceeded, that sensor is incompatible and a sensor with a larger range must be substituted.

Data analysis depends on system and test-specific resolution. System resolution is the number of incremental "steps" into which the data logger's Analog-to-Digital (A-D) converter can divide the data. It is necessary to know the processing power of the data logger, defined as "bits" (such as an 8-bit or 12-bit processor). The number of steps is defined as two to the power of the processor bits, or $2^{\text{processor bits}}$. Thus, a 12 bit processor has 2^{12} = 4096 steps.

Resolution for the voltage collection "gates" selected in Equation 2.2 is the smallest voltage increment a system can detect, defined as $\delta_{min,\ measured}$ where

$$\delta_{min,\ measured} = \frac{V_{gate(\max)} - V_{gate(\min)}}{2^{processor\ bits}} * \text{Scale Factor} \qquad \text{(Equation 2.3)}$$

Thus, for a 12-bit processor set to collect a range of ±0.06 V, and a sensor with scale factor 200 V/in, the smallest increment the sensor can record is

$$\delta_{min,\ measured} = \frac{0.06\,V - (-0.06V)}{2^{12}} * \frac{1\,in}{200\,V} = \frac{0.12\,in}{4096 * 200} = 1.4\text{x}10^{-7}\text{in} = 0.1\mu\text{in}.$$

For large volumes of raw data collected pointwise without averaging, it is possible to see repetition of certain decimal portions of the collected values in any small range of values.

If predicted displacement is estimated as 250 μin, and data resolution is 0.1μin/point, then there will be roughly 250/0.1 = 2500 measurement steps, or increments, in the 250 μin range. For gradually-changing data like that collected in ACM, in the absence of large temperature changes and corresponding displacement "jumps," a graph consisting only of raw points may appear virtually continuous with such high resolution.

In the linearity test, sensors are attached to a plate of known α, and a data logger records sensor displacements and plate temperature. Data are plotted on a hysteretic curve of measured displacement versus calculated displacement, the latter a function of temperature and α.; linear regression methods then determine the best-fit line and standard deviation from that line for each sensor's data for each test. Chapter 4 and Appendix A discuss this data analysis in detail.

The y-axis of this plot is displacement detected by the sensor. In previous trials, the x-axis was reported as temperature (Louis, 2000; Siebert, 2000), which gives no information about expected displacement as a function of α and L. New methods appearing herein plot calculated displacement δ, where

$$\delta = \alpha * L * T \qquad \text{(Equation 2.4)}$$

on the x-axis, where δ is reported in the same units as sensor displacement, generally microinches (μin) or micrometers (μm). The quantity δ is a slightly modified version of Equation 2.1; each temperature data point corresponds to a sensor displacement data point taken at the same time. Once again, L is taken to be constant. Each measured displacement point should have a corresponding plate temperature, T.

All values of δ are relative to one another. If the same constant is added to or subtracted from each point δ, the range of δ values can be shifted as necessary for plotting.

As described previously, the minimum δ value in a data set was usually subtracted from every δ value in that set, ensuring that the plot of measured displacement versus δ remains in the first quadrant (+x, +y).

Calculations for the α-predicted theoretical line are also based on Equation 2.1. On a plot of measured displacement versus calculated displacement, the endpoints of the α-predicted line are the origin, (0,0) and (δ_{tot},δ_{tot}) as determined by Equation 2.1; this line's slope is always unity. By contrast, on plots of measured displacement versus temperature, the slope varies as a function of L. An ideal system's data points would follow the α-predicted line exactly; however, real-world systems have a certain amount of data scatter, and sensor details such as length of the LVDT rod may control small displacement system sensitivity.

Sometimes it is necessary to change the line's position in relation to the hysteretic data. To shift the line up and down, add a constant value to both endpoints' y-axis values; right or left by adding a constant to the x-axis values.

Chapter 3

Laboratory Qualification: Equipment and Sampling

Experimental setup

Level I experimental setup varied little from that shown in Figure 3.1 for both aluminum and UHMW-P. These plate hysteresis qualification methods were those

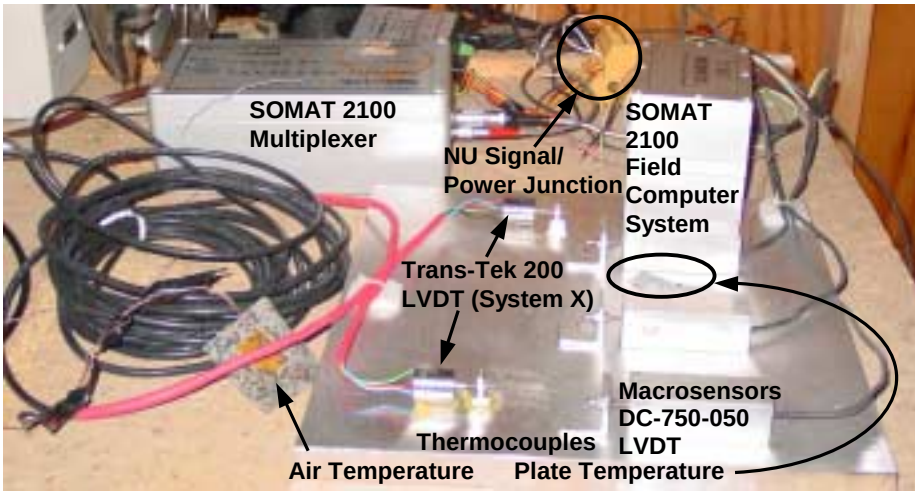

Figure 3.1 Representative plate-testing setup: Macrosensors 750-050 LVDTs for NU system, Trans-Tek 200 LVDTs for System X mounted on aluminum.

developed by Louis (2000). Aluminum plate testing incorporated a SOMAT 2100 Field Computer System data logger, while UHMW-P testing incorporated the more advanced,

higher-capacity SOMAT eDAQ. The following describes technical details for plate qualification tests.

Northwestern University (NU) Baseline Systems

The SOMAT 2100 records six significant figures and has a 12-bit Analog-to-Digital (A-D) converter. Plate temperature is measured with a thermocouple whose signal is converted to logger format in a 2100-compatible SOMAT Multiplexer. The 2100 can store up to 4MB of data, including the set-up program which is roughly 5-10KB for ACM processes. Typical data files are 1.5-2MB in the proprietary SOMAT format. The compact 2100 system's onboard processing capability is limited. Data download is via serial cable to a laptop PC, and a typical data file transfer takes roughly 15 to 20 minutes. Communications for programming the logger from the PC were similarly slow. LVDT signals are fed into the 2100 input channels via a signal junction bridge, the odd-shaped piece in the background of Figure 3.1.

The UHMW-P plastic plate tests incorporated the SOMAT eDAQ, which collects 20 channels of data to six significant figures and has a 16-bit A-D converter. The thermal expansion of UHMW-P is almost an order of magnitude higher than that of aluminum; however, the eDAQ's higher A-D definition allows a resolution of 0.1 μin, roughly equal to that of the 2100, albeit for a greatly increased displacement range. An onboard processor is capable of averaging and similar computing operations. A 512MB PC-MCIA card provided additional memory and would have allowed more memory-intensive collection options, though none were utilized at the plate test stage. The thermoucouple is linked through the Super MCJ Thermocouple-to-Analog connector acting as multiplexer for the eDAQ. The non-SOMAT thermocouple adaptor data is less stable than that of the

2100, leading to fluctuations which had to be reconciled via time-based rolling averages. An Ethernet port allows fast, stable communication between PC and data logger.

SOMAT proprietary software was employed to program the data loggers and to download and perform analysis of the data. Setting up and downloading the 2100 was accomplished with SOMAT TCS (version 2.0.1); the corresponding eDAQ software was SOMAT TCE-eDAQ (version 3.7.2). SOMAT has since issued new versions of both packages. Data export to text files for further processing with Excel and MATLAB was accomplished via SOMAT WinEase, now superseded by SOMAT Infield.

In both stages, a Macrosensors DC-750-050 "infinite resolution" LVDT was the baseline sensor. "Infinite resolution" measurements are theoretically limited only by data logger A-D resolution. The LVDTs receive power from a regulated power supply and send signals to the logger via a junction bridge. Aluminum plate NU sensors were light-to-medium duty indoor-only LVDTs with power/signal leads hard-wired into the back of the coil, similar to those mounted at the Franklin, WI field test site (Louis, 2000). The UHMW-P testing substituted outdoor for indoor versions of the same sensor; these LVDTs have a military-specification ("mil spec") waterproof connector on the back, which also allows their power/signal leads to be disconnected without removing the sensor from its test surface.

Both systems were programmed to collect a "burst" of points at 1000 Hz for 0.1 seconds, yielding 100 points (101 points on the eDAQ, whose software allows only an odd-number of data points for bursts) every five minutes. Each 100-point burst was averaged to eliminate system noise, as explained in Chapter 4. Temperature data were collected as individual points. The 100-point bursts were averaged onboard the eDAQ,

although 2100 data was averaged on a separate computer. The SOMAT systems, particularly the eDAQ, could have accommodated more programming options; the methods described were chosen to balance a reasonable number of data points per hour with minimizing electronic noise.

Laboratory qualification: System X

System X was an alpha-generation, commercial, off-the-shelf system being evaluated, and consisted of a proprietary data logger, signal-power junction box, and Trans-Tek 200 "Infinite Resolution" LVDTs. Whereas the NU SOMAT systems were unwieldy, complex, and flexible, System X was compact, simple, and single-task dedicated. LVDT signals traveled to the data logger via the junction box; most settings, including data logger collection range and sampling frequency, were factory pre-set for both components, and inaccessible to end-users. The system was capable of recording to four significant figures; however, to maximize flexibility, collection range was set such that the 12-bit A-D converter resolution was only about 0.035 mils (≈1μm). Users select System X output units of mills or μm; for all collection runs described herein, System X output was in mills, and subsequently converted to μin and μm. To maximize data integrity, end-users have no access to raw data.

Provisions for a geophone were not used. Downloads were to a laptop PC via serial cable in a manner similar to the SOMAT 2100, with a similar download rate. Although System X could be programmed on a PC program via serial connection, it was easier to enter commands directly through the data logger's simple, easy-to-understand keypad and display. The manufacturer of System X provided proprietary software for data download and analysis.

System X samples data continuously at 1000 Hz and records the peak voltage signal for a user-selected time period. Though the sampling frequency cannot be changed, the end-user selects one of 13 data recording periods varying from one second to one hour. The manufacturer-recommended recording rate is one point per minute, which optimizes data density and system data storage. Qualification testing was conducted with sampling rates of one to six points per minute (ppm), with little apparent difference in data quality on aluminum, and moderate improvement in curve smoothness with more ppm for UHMW-P.

Data acquisition: technique and commentary

When collecting points at periods of once every few minutes or longer, it is best to average each individual point to remove the influences of electronic noise and anomalous spikes. A collection rate of 1000 Hz and a period of 0.1 to 1.0 seconds ensure a sufficient number of points for a averaging. A balance must be established between number of points and length of collection; an excessively-long period may begin to include actual displacements. One second is sufficiently short that any displacement will be too small for measurement; thus, all valid points will be in a similar range, and yield the sensor's instantaneous displacement after averaging out the quasi-sine-wave, produced by the power supply, distorting them. For such collection, 1000 Hz for one second yields 1000 points for averaging, which may overwhelm some systems' computing or memory capacity, in which case 1000 Hz for 0.1 seconds yielding 100 points has proven adequate.

A far less desirable option which does not average out anomalies is recording the instantaneous value of the sensor at the collection time. Such collection will capture points completely at random. Based on the data collected for this thesis, this method appears

unlikely to collect a series of spurious values. If the recording period for a single point, e.g., once per minute or once per five minutes, remains constant. This method may be viable for electronically "quiet" systems with limited memory.

A highly inadvisable technique is to record the largest-magnitude value for a given period. As previously mentioned, electronic anomalies are likely to appear as large deviations from a series of values consistent with each other. Recording the maximum value for a given time period virtually guarantees the anomalous points defining the collection period. Such spurious data may adversely affect both raw and averaged data, the latter if the anomalous point's magnitude is large enough to skew averaged data considerably.

Mathematical averaging computations often produce points with finer resolution than theoretically possible for the system. This means averaged data points have values that fall between resolution "steps." ACM Level I monitors smooth, gradual changes in displacement as a function of time. Large random displacements from the norm are not typical, as with seismic response that is recorded by completely different Level II and III data collection processes. Therefore, data points whose values fall between the quantum values defined by A-D "steps" are theoretically possible. This is acceptable, if the averaged points produce a curve that follows a pattern consistent with shape and magnitude of a similar plot of raw points. Where large, abrupt deviations are the norm, such as monitoring intermittent impacts, averaging is not advisable, as it eliminates important information.

Chapter 4

Laboratory Qualification: Hysteresis and Linearity

Data Processing

Once collected, the data must be analyzed properly. System X could be set to record numerous data points per minute, as it was several times during plate testing. Figure 4.1 demonstrates the recommended technique for averaging such data with multiple points per minute.

When the logger collects more than one point per minute, it is necessary to choose a "baseline" point around which the others will be averaged, in Figure 4.1 the final point of a given minute. For a one-hour rolling average (as in the laboratory qualification process), the average of the following is taken: 1) the baseline value; 2) the values of all preceding points from the same minute; 3) the points from the preceding 30 minutes (or all preceding points if less than 30 minutes of data is available); 4) the points from the subsequent 30 minutes (or all subsequent points for less than 30 minutes of data). System X had different collection methods, and so a sorting routine selected a point for every fifth minute to correspond to the NU data's point collected every five minutes. The 24-hour rolling average takes the one, one-hour rolling average point for every hour and averages it with

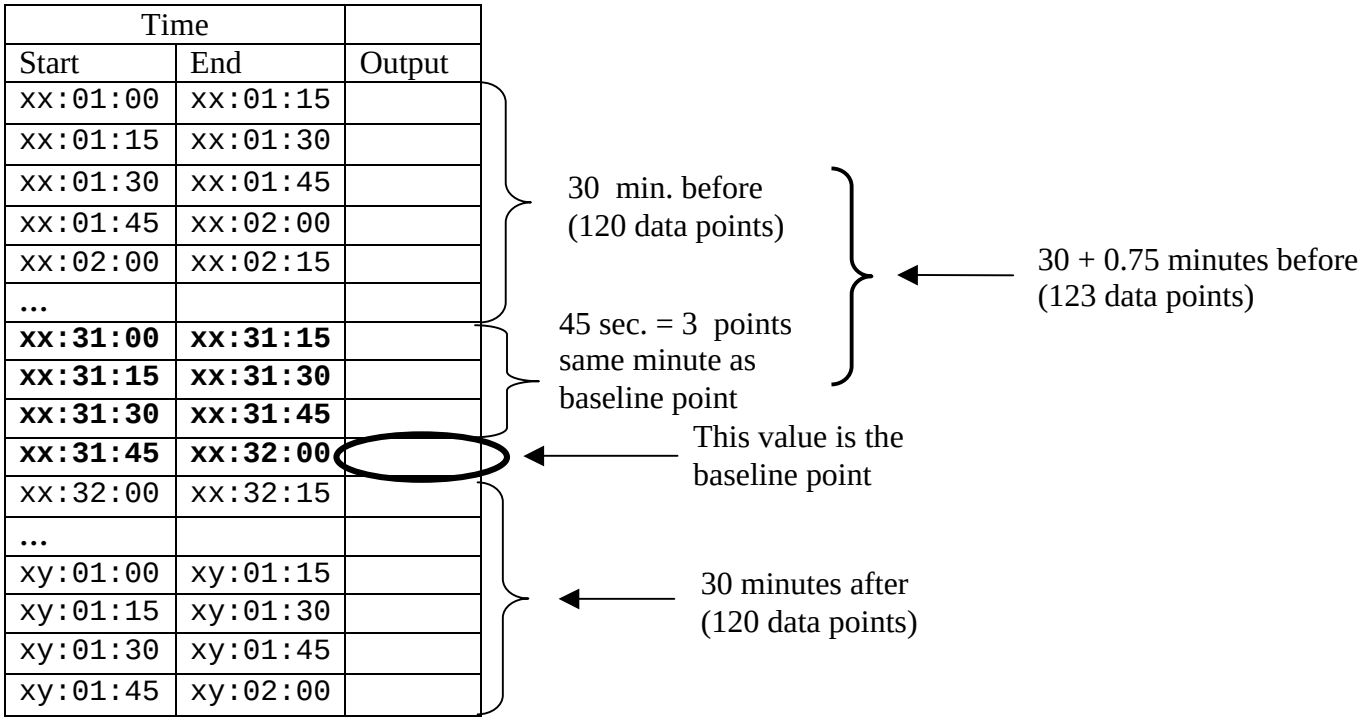

Figure 4.1. Rolling time data averaging scheme, where there is more than one point in a given time period.

the 12 hours preceding and following. Spreadsheets are not recommended for such averaging and sorting, as spreadsheet files become large and unwieldy for such operations.

Figure 4.2 demonstrates data processing and presentation to be applied to hysteretic and time history plotting; both processing and presentation are possible in either a computer program or a spreadsheet. Figure 4.2 shows the application of Equation 4.1 to adjust data so that all points appear Quadrant I of a plot and Equation 4.2, which adjusts plotted data for the first displacement point to be equal to zero. Please see Appendix D, "Data Processing," for more details on averaging and data handling.

Plate test hysteresis/linearity

The hysteretic behavior of NU systems and System X was compared to the α -predicted hysteresis, the gray broken line that always has a slope of 1, in Figure 4.3. Measured displacement points are not absolute; it is necessary only to maintain the same differential between all values relative to each other. In this way, plots may be shifted by adding or subtracting a constant. To keep all values of measured displacement positive, as for all hysteretic plots herein including Figure 4.3, the minimum measured displacement value is subtracted from all points. In addition, either raw data or α-predicted line data is shifted for the intersection of these two sets of data to be centered. For time histories, the first measured displacement value is subtracted from all data points in the set.

Figure 4.3a summarizes NU system data for a representative aluminum trial, with a tight hysteretic loop and the sensor detecting more displacement in this range than predicted by a function of α. Data deviation from centerline is minimal. Figure 4.3b represents a System X sensor on aluminum; plot jaggedness results from system noise and low resolution. Such data sets prompted a change to UHMW-P plastic, a test surface with

	A	B	C	D
1	Time	MS2	MS2 zero	MS2 pos
2	hrs	μin	35.3	-60.0
3	0.00	35.3	0.0	95.3
4	0.08	35.1	-0.2	95.1
5	0.17	34.9	-0.5	94.9
	A'	**B'**	**C'**	**D'**
1	Time	MS2	MS2 zero	MS2 pos
2	hrs	μin	=B3	=MIN(B4:B1546)
3	0	35.3237	=B3-MS2.0.822	=B3+60
4	=B4+5/60	35.0791	=B4-MS2.0.822	=B4+60
5	=B5+5/60	34.8517	=B5-MS2.0.822	=B5+60

Figure 4.2. Spreadsheet showing calculations. Columns A-D show actual data; Columns A'-D' show the calculations in the corresponding cells A-D. B is averaged displacement data.
Equation 4.1. For Time History with x axis, Column A; y axis, column C, such that y-axis starting point equal to zero, Equation 4.1 repeats through Column C, illustrated in Column C'; here, MS2.0.822 is the variable name defining the quantity in Cell B2/B'2. Explanation of variable: MS2 means Macrosensors LVDT collected by SOMAT data channel 2; 0 means shift all values such that the first value is zero; 822 is data start date.
Equation 4.2 is seen in column D'. It places all data in Quadrant I (+x, +y) of an x-y plot: cell D2 finds the minimum of all values in column B = -60μin, which is subtracted from all column B values to shift all column D values ≥ 0.

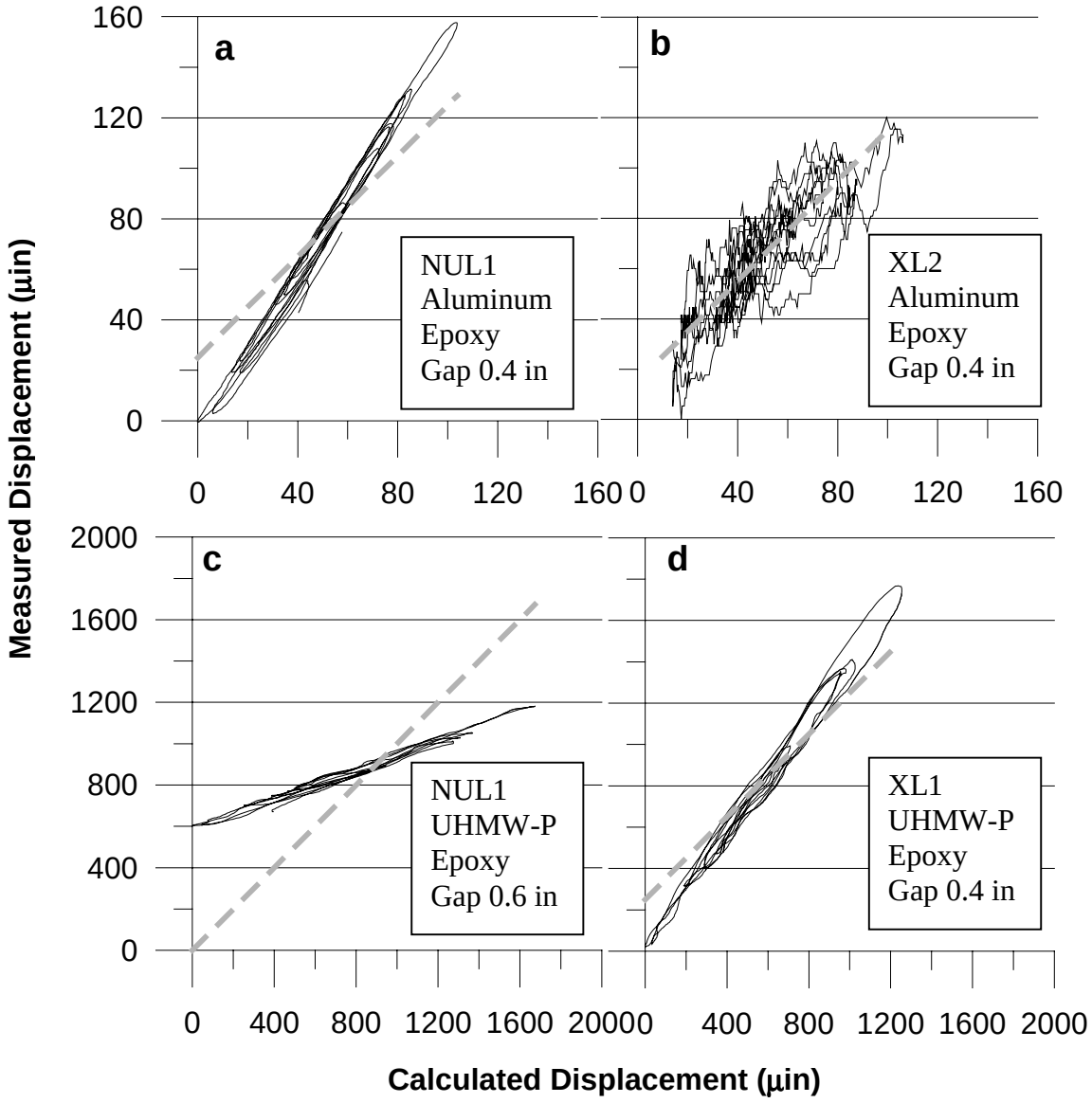

Figure 4.3. Sensor hysteresis on two different materials; dashed line is predicted response as a function of α.
a-b. Aluminum plate trials; a. NU LVDT connected to SOMAT data channel 1 (NUL1) , b. System X LVDT connected to System X data channel 2 (XL2);
c-d. UHMW Polyethylene plate; c. NUL1, d. XL1. The System X plot becomes significantly smoother for larger displacements.

larger thermal displacement, which more closely approximates actual crack movement.

With the increased thermal expansion of the UHMW-P plastic surface, System X linearity and data clarity increased significantly. Figure 4.3c depicts less displacement than predicted for the NU system, although the data are again highly linear with low hysteresis. Figure 4.2d depicts System X displacement, which exceeds calculated displacement. The jaggedness is largely eliminated as larger displacements include far more 35μin A-D increments than did the aluminum test, thus providing a larger number of data points. This is demonstrates adequate System X linearity for ACM, since thermal expansion characteristics of cracks (Snider, 2003) are more like those of UHMW-P than aluminum.

The data's deviation from the α-predicted line in Figure 4.3 is of minor significance; linearity is more important. Figure 4.4 summarizes "goodness of fit," which defines the degree of linearity, which is itself defined by a data set's linear regression best-fit line. A linear regression standard deviation from the best-fit line for each data set divided by the that data set's corresponding $\delta_{net,\ measured} = \delta_{max,\ measured} - \delta_{min,\ measured}$, yields dimensionless variance. The magnitude of variance is inversely proportional to linearity.

Only the NU system was analyzed for the aluminum trials because on aluminum, System X resolution was too low for meaningful variance analysis. During the first three aluminum trials in Figure 4.3, both NU sensors were attached to the aluminum plate by applying epoxy to the entire underside surface in contact with the plate. During the third trial data input channels were flipped, i.e., the NUL1 (NU LVDT connected to 2100 collection channel 1) was switched to channel 2 and vice versa.

For the last two aluminum trials, both sensors were removed and carefully re-attached. NUL1 was reattached to the plate with just a ½ inch strip of epoxy near the front

of the sensor housing; NUL2 was attached as before, ensuring the entire bottom surface was thoroughly coated with a thin layer of epoxy. NUL1 and 2 were re-connected to channels 1 and 2 respectively, though this change seemed to make little difference. Epoxy hardening often requires several days, possibly accounting for the there was a relatively large change in NUL1 variance between the aluminum trial beginning on Day 25, the day the sensors were newly attached, and Day 33. However, NUL2 remained in the same consistent pattern as before for these two trials.

Figure 4.4 shows a variance of only four to ten percent for both sensors in all configurations, indicating linear behavior. Such changes as flipping the inputs for Trial 3, or changing the attachment technique did not perceptibly affect performance. These small variances for extremely-small magnitude displacements measured with an electro-mechanical system, attest to a high-quality collection system.

For the plastic sheet trials, variance for both the NU eDAQ system and System X were even smaller, particularly for the NU system as shown in the last three data sets of Figure 4.4. Variance remained virtually constant at one percent for NUL1 and five percent for NUL2 among the three trials, once again demonstrating consistency and strong linearity. System X performance was less consistent, though XL1 (System X LVDT number 1) and XL2 each deviated among their respective trials by less than two percent. During these trials, the only variation was flipping XL1 and XL2 inputs between Trials 7 and 8.

The results reported in Figure 4.4 validate LVDT stability for ACM even under conditions which changed by as much as 15°C (30°F), which far exceeds the likely temperature range inside a home, the likeliest structure to have instrumentation installed.

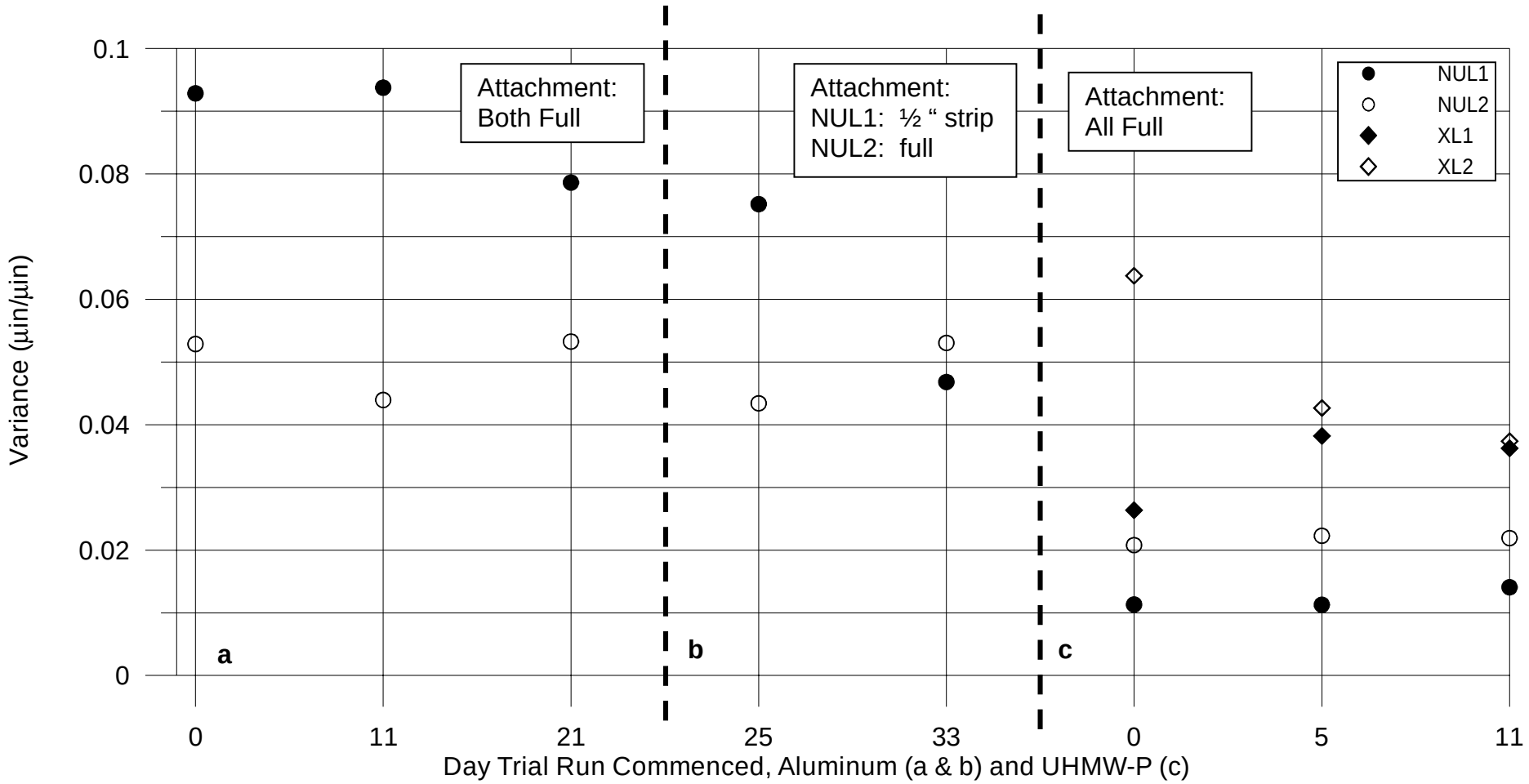

Figure 4.4. Variance from "best fit" line, the quotient of standard deviation and total displacement, for linearity-hysteresis tests similar to those of Figure 4.3. a. Aluminum, NUL1 and NUL2 both fully-attached; b. Aluminum, NUL1 attached with only a ½ inch strip near the front of the sensor housing, NUL2 fully attached; c. Ultra high molecular weight polyethylene, all sensors fully attached.

Chapter 5

Laboratory Qualification: Noise Analysis

Significance of noise

When measuring displacements of small magnitude such as in ACM, system resolution and electronic noise become critical factors. High system resolution alone does not ensure adequate data collection. A "noisy" system can easily defeat even the finest-resolution equipment. Micro-measurements described herein derive displacement from voltage signal changes on the order of 10^{-3} V and smaller, which correspond to micro-displacements detected by displacement sensors. Voltage changes are converted to engineering units via manufacturer-supplied conversion factors as explained previously.

Successful data collection depends heavily on "clean" electrical signals; electronic noise is a voltage signal not corresponding to input from a sensor and is usually a voltage value outside the reasonable range of data surrounding it. Even more insidious is the noise signal similar to the signals surrounding it, a credible anomalous point. The large deviations, voltage "spikes," are unpredictable, large-amplitude deviations from the normal

signal, and are interpreted during data analysis as displacement, which introduces error into measurements. There are two types of noise: systematic and random.

Systemic Noise

Systemic noise is regular, usually sinusoidal, and usually corresponds to the power supply's frequency. Examples of systemic noise for the Kaman eddy-current gauge and Macrosensors LVDT at a field installation appear in Figure 5.1. Random noise is easily distinguished as a regular pattern resembling a sine wave. Such interference can be eliminated from Level I monitoring data by averaging a series of points, the reason for the "burst" collection-averaging technique for NU data. The NU field data in Figure 5.1, however, is from Level II recording, which consists of simple point collection and cannot be averaged. Such noise can on the order of 5-10 μin for the eddy-current sensor and 40 μin for the LVDT, though the plate test LVDTs were significantly quieter.

Random Noise

Random noise consists of irregular, unpredictable signals, which can be anything from random electron activity to poor internal electrical connections within the system itself to outside electromagnetic signals. Table 5.1 and Figure 5.2 illustrate some examples of random noise. Note the different scales of Figures 5.2a and 5.2b. If noise is a large proportion of the total signal, it will obscure valid data by establishing a range of uncertainty around the valid data.

However, noise spikes that deviate noticeably but affect neither the overall coherent pattern of raw data points nor the final averaged line, are of minor consequence. Figure 5.3 shows System X data from a plastic plate test during a period with several obvious, but inconsequential, noise points. The plot is from the same data as Figure 6.1 appearing later

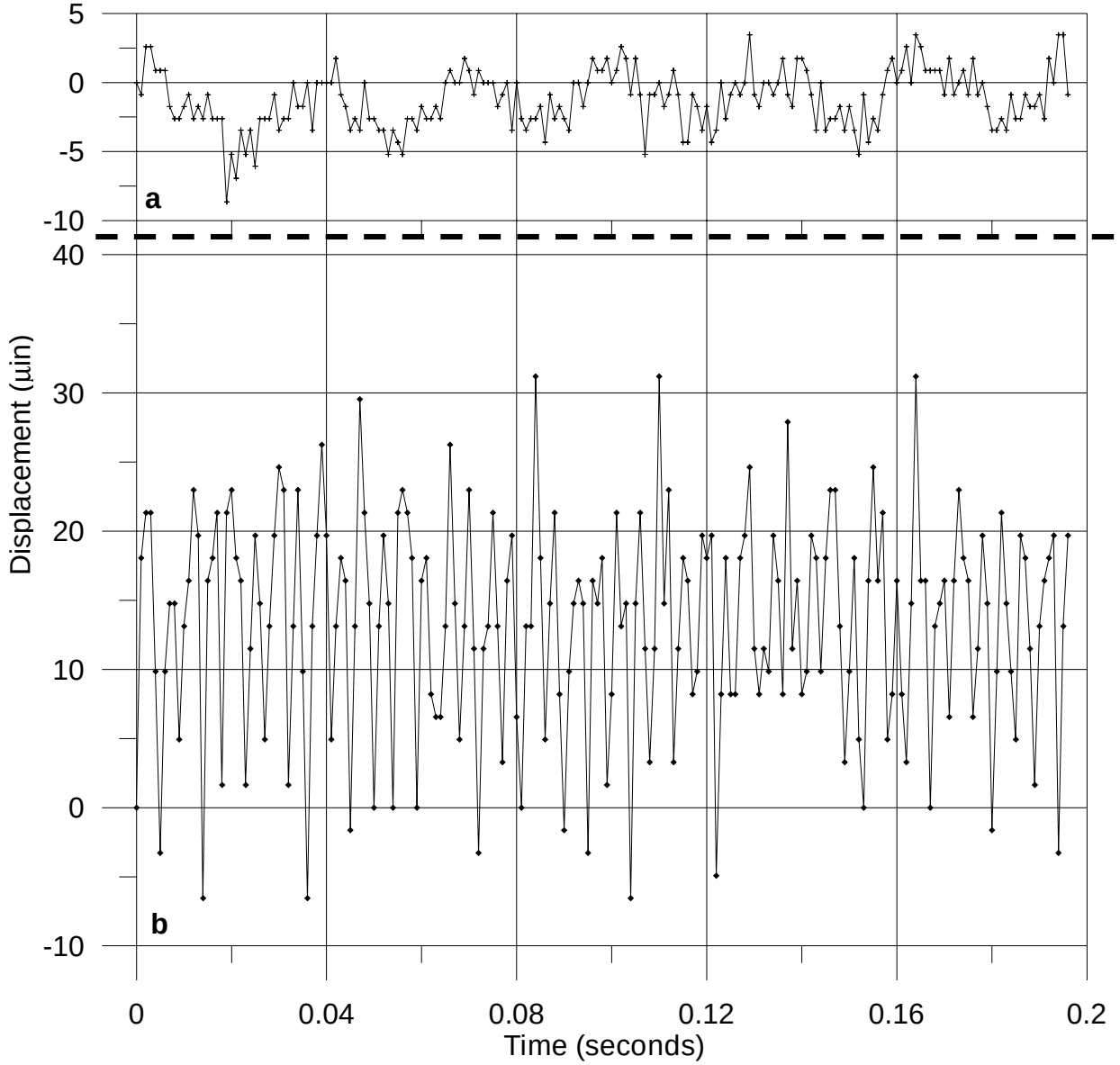

Figure 5.1. Systemic noise plot, first 0.2 seconds of 3 second data set of raw data points collected at 1000 Hz for seismic event. Some slight undulation of the overall pattern indicates early-arriving seismic displacements. Noise appears as large-amplitude undulations resembling sine waves, readily apparent in both plots. a. NU Eddy-current crack gauge; b. NU crack LVDT.

Time	System X Null mills	System X Crack mills
6:17:00	14.45	13.15
7:17:00	14.45	13.22
8:17:00	14.42	13.37
9:17:00	15.83	13.91
10:17:00	14.42	13.51
11:17:00	16.40	22.29
12:17:00	14.63	13.12
13:17:00	14.45	13.12
14:17:00	14.45	13.12
15:17:00	14.45	13.19
16:17:00	14.42	13.22
17:17:00	14.45	13.33
18:17:00	19.37	13.22
19:17:00	14.56	13.15
20:17:00	14.53	13.12
21:17:00	15.03	13.66
22:17:00	14.49	13.15

Table 5.1. System X data excerpt, 31 March 04; highlighted cells show exceptionally noisy data for both channels. Normally, the Null channel had far more anomalous points. The largest jump, in the Crack column between 11:17:00 and 12:17:00, is 9170 μin (233 μm).

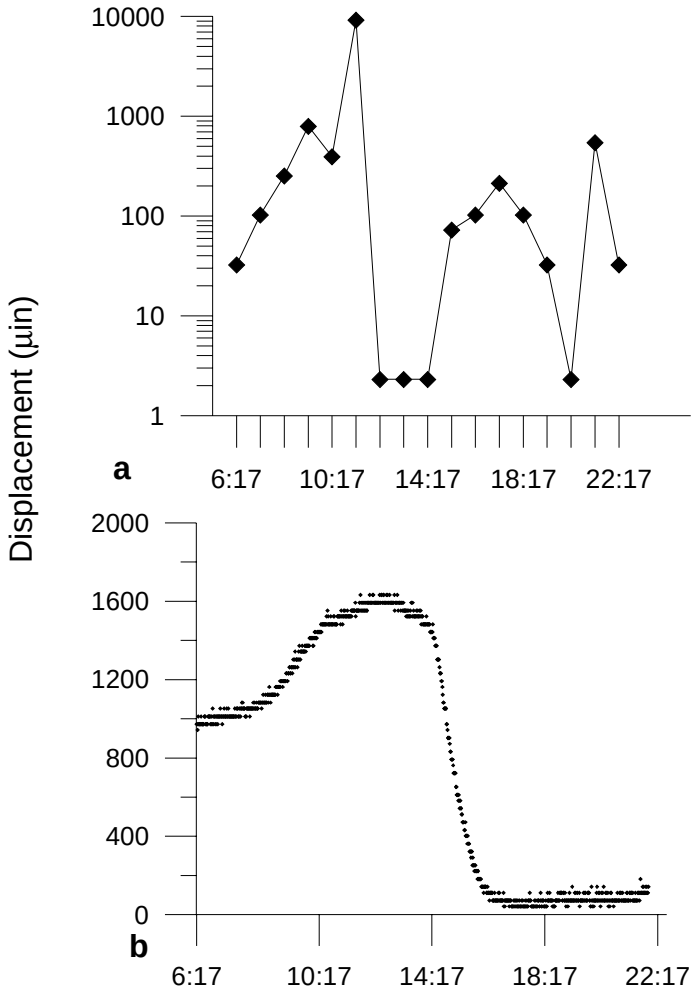

Figure 5.2. Collection method comparison; note different scales of plots. a. One point per hour, XLC data from Table B1. All points converted to μin and shifted to be greater than zero for plotting on logarithmic scales. b. Raw data for a similar 16-hour period, collection at manufacturer-recommended 1 ppm.

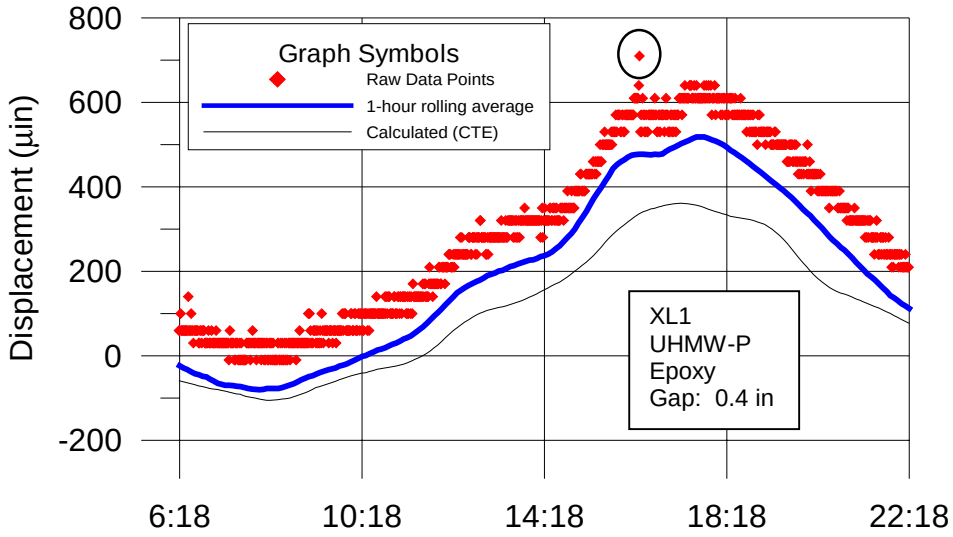

Figure 5.3. Time history for System X plastic plate test. The noise spike (circled) is one of several (see Figure 6.1d), but does not obscure the overall pattern of the raw points. The average follows the raw point pattern (which is offset upward for visibility) almost exactly. Noise appears to have little, if any, influence.

in this paper, and the time of day (starting 06:17, ending 22:17) corresponds to Figures 5.2a-b.

Some experimentation with the data logging system is necessary to determine its ambient noise level. For a mass-produced, financially-feasible commercial ACM system, noise may be unavoidable but can be minimized with careful internal architecture and construction. An adequate "quiet" system will have noise on the order of several microinches or less, most of which should be the unavoidable sinusoidal power supply signal, which does not disappear even when alternating current is converted to the direct current required by most such systems.

Figure 5.4 illustrates the best method to resolve power supply noise by averaging bursts of data, which are large numbers of points recorded at high frequency in a short time. As described previously, NU systems collected 1000 Hz bursts for 0.1 second, yielding 100 points; averaging largely canceled out sinusoidal interference and

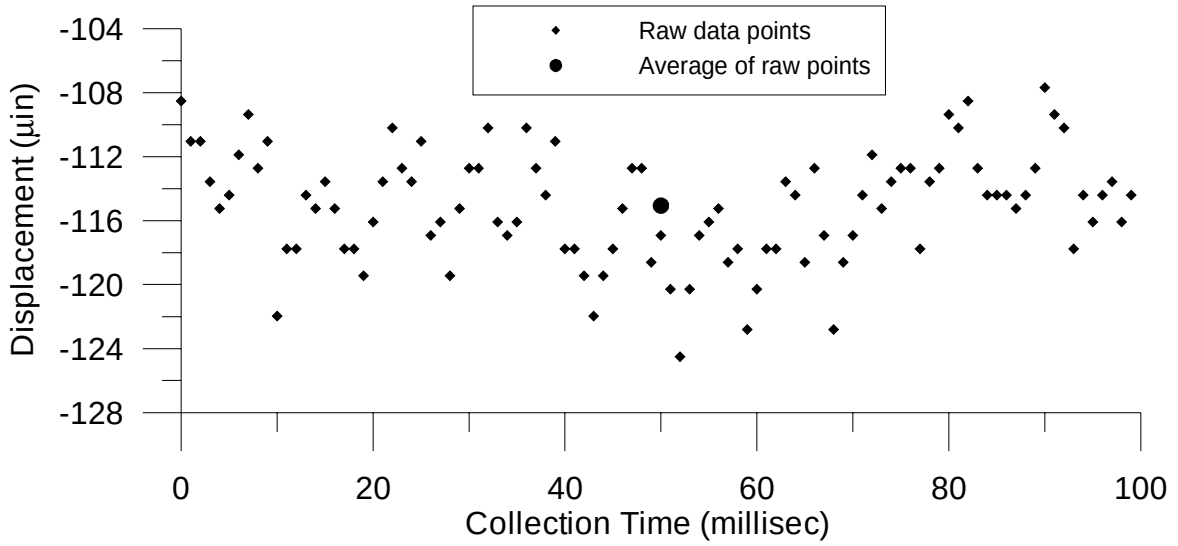

Figure 5.4. 100-point raw data burst in a 0.1 second time interval. The dot in the center represents the average of the 100 points. Note sinusoidal pattern of systemic noise even during this brief period.

significantly mitigated spikes. Collecting single points for a given time period risks allowing a spike to define the data for that collection period.

The System X data logger does not presently collect bursts, and its performance illustrates several shortcomings of single-point collection. Since System X records the largest-magnitude voltage signal for a given time period, spikes inevitably enter the data set; the probability of an anomalous point is directly proportional to the length of collection interval.

Spikes are unavoidable for the "maximum signal per period" collection method; however, shorter collection intervals mitigate the inevitable spikes by introducing a larger number of points around it. If a noise spike corresponding to 500 µin is the highest-magnitude signal in a 60-minute period, for a collection interval of: 1) one point per minute, it will be one of 60 points in an hour, with 59 other points to average it away; 2) one point per hour, the spike becomes the data point for that hour, thus compromising and invalidating an entire hour of data.

Chapter 6

Laboratory Qualification: Data System Resolution

Significance

Resolution corresponds closely to noise; noise spikes in a lower-resolution system are often larger since probability dictates that the A-D converter will round the signal up to the next A-D step at least half the time. Higher resolution systems also provide data sets in which even small anomalies are detectable. High resolution is therefore doubly important for high-quality data.

Resolution and small movements

Adequate resolution is important for credible data, as is illustrated in Figure 6.1. In each of these four plots, the thin line represents CTE-predicted displacement, each diamond-shaped point represents a point of raw data (in the case of the NU systems, the average of a 100-point burst), and the thick line represents the one-hour rolling average (the average of each data point with data points a half-hour before and after). Each line is adjusted such that displacement = 0 at time = 0, as explained in Chapter 4. The NU systems' resolutions of less than 1 μin result in virtually continuous plots of individual

points, as step size is less than 1% of total displacement, seen in Figures 6.1a and 6.1c, whereas the 35 μin resolution of System X makes the steps easily visible in Figures 6.1b and 6.1d.

Aluminum expansion and contraction is not large even during summer days with large temperature swings; Figure 6.1 data was taken in a garage with no climate control, 6.1a-b 12-14 August 2003, 6.1c-d 3-5 September 2003. For aluminum (α = 13.1μin/in/°F) with a 0.5 inch (1.3 cm) gap, total displacement is on the order of 70μin (1.75 μm) as in Figure 6.1a; Figure 6.1b calculated displacement is three times as large because the gap is 1.5 in (3.8cm), a function of a relatively long factory-stock LVDT rod for System X. Figure 6.1a,with resolution exceeding 1 μin, has roughly 100 points for the displacement range; and as a result, the averaged data is smooth and even. However, in figure 6.1b, System X with its 35 μin resolution has only four discrete steps in a total range three times as large, yielding uninformative averaged data resembling a spiky horizontal line, at best tenuously related to α-predicted displacement. Large noise spikes appear at times 0, 34, and 46-47 hours, well outside the range of the other points. A low-resolution system does not perform well when expansion and contraction is small. The absence of large-magnitude anomalous points in Figure 6.1a reinforces the importance of averaging each individual data point as previously described.

Resolution and movements comparable to structural wall cracks

Cracks in residential structures move far more per degree of temperature change than does aluminum, meaning that aluminum is not an appropriate material to qualify the type of ACM system being considered. Therefore, ultra-high molecular weight

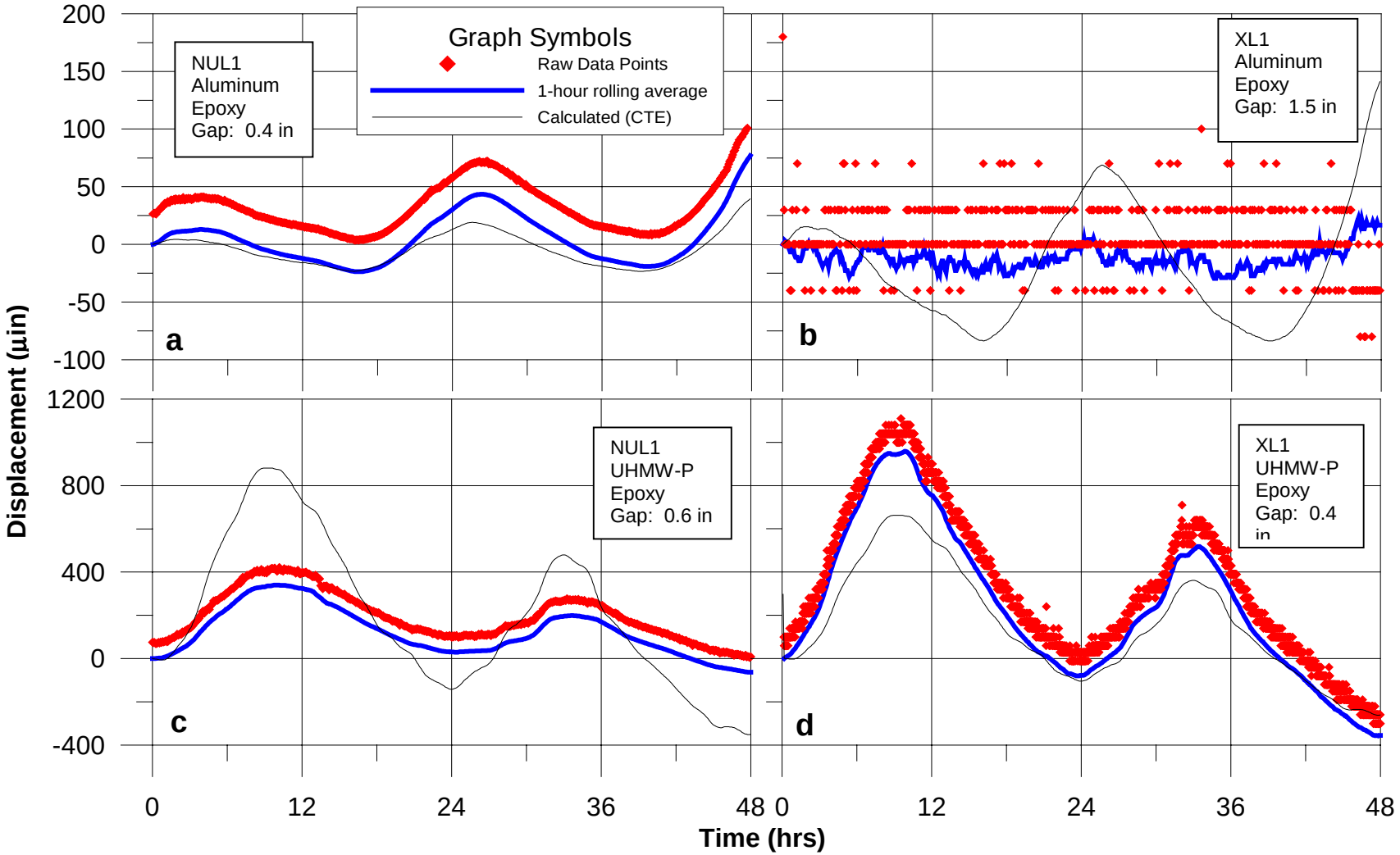

Figure 6.1. Time histories for plate tests. All point plots and averaged plotted offset for visibility. On aluminum: a. NUL1 showing fine-resolution point plot nearly equivalent to averaged plot; b. XL1 showing low-resolution points and averaged line plot only vaguely resembling theoretical plot. On UHMW Polyethylene: c. NUL1 showing fine-resolution point plot nearly equivalent to averaged plot; d. XL1with same resolution as in b, points now form a recognizable pattern; same magnitude anomalies now a far smaller percentage overall.

polyethylene, a plastic whose temperature-expansion properties are more similar to those of structural cracks, was chosen; its α of 110 μin/in/°F is eight times that of aluminum. The results are illustrated in Figures 6.1c and 6.1d. Here the α-predicted movement is far larger for both; that in Figure 6c is slightly larger than that of Figure 6d because of a larger the gap, 0.55 as opposed to 0.4 inches. The α-predicted line is not as smooth as in Figure 6.1a-b because the temperature data was less consistent; the modification to adapt a non-SoMat multiplexer to function with the SoMat eDAQ was not entirely successful.

Performance characteristics such as resolution and sensitivity are similar for both the two different NU systems and System X on both aluminum and plastic; however, expansion and contraction is far greater on the plastic. The small anomaly at hour 13 in Figure 6.1c is the only disruption in the point-wise plot, which otherwise appears continuous and linear itself; the one-hour rolling average is similarly smooth. Figure 6.1d shows how large displacements mitigate low resolution. Although the individual points are still clearly visible and form discrete levels every 35 μin, these collections of points now have a distinguishable shape overall. Systemic noise spikes, whose magnitude remains constant, are now much smaller in relation to total displacement. The averaged line is smooth and provides data whose shape corresponds closely to that predicted by α.

Overall, NU system response is larger than that calculated by α on the small-displacement aluminum, while response is smaller on the significantly more expansive plastic sheet. The opposite is true for System X. Sensor system response appears to vary with displacement regime, indicating that a sensor system should be qualified on material with thermal expansion properties similar to those of the surface to be monitored in the field.

This relative sensitivity is of no consequence for either system, since crack movement always occurs at the crack, and the attachment effects are measured by the null gauge. A null gauge would measure the wall material α and attachment sensitivity of the LVDT or other displacement detection device, and the gauge across the crack would measure the crack and wall response. The difference between crack and null gauge measurements is the crack response. Noise is only a significant factor when crack displacement is small, a situation which rarely occurs.

Chapter 7

Laboratory Qualification: Sensors

Physical arrangement of sensors

Among the most important ACM factors is sensor configuration, including attachment to the surface, mechanical design, and operational configuration. Configuration effects are shown in Figures 7.1 and 7.2.

Adhesive effects

LVDT attachment with deformable adhesive possessing a high α value results in significant nonlinearity, as seen in Figure 7.1. The top line of the plot shows hysteresis of XL1 attached to the plate with ordinary "hot glue," showing two distinct periods of instability. The hot glue replaced the standard adhesive, 90-second epoxy, which is both stable and quick-setting. The hysteretic plot near the x-axis represents XL2 attached to the test plate with epoxy. The difference in both gross displacement and stability is significant.

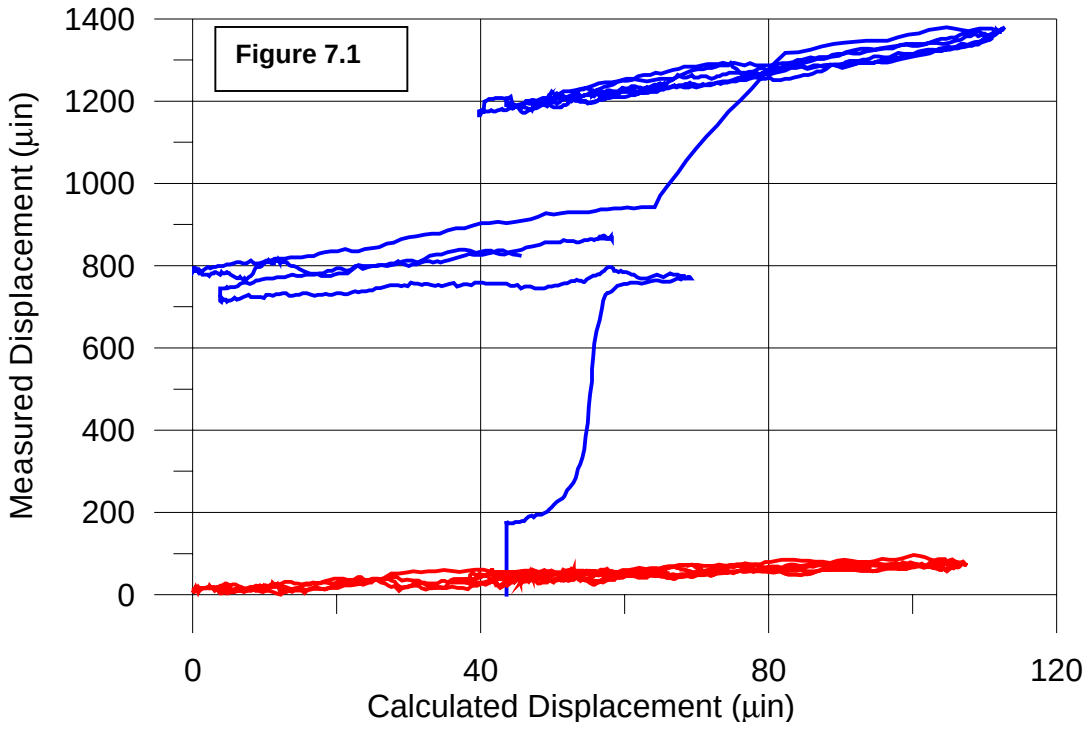

Figure 7.1. Hysteresis with excessive-α adhesive ("hot glue") (upper line) with hysteresis of simultaneously-run second sensor attached with low-CTE epoxy for comparison (lower line). The epoxy was the standard adhesive for LVDTs.

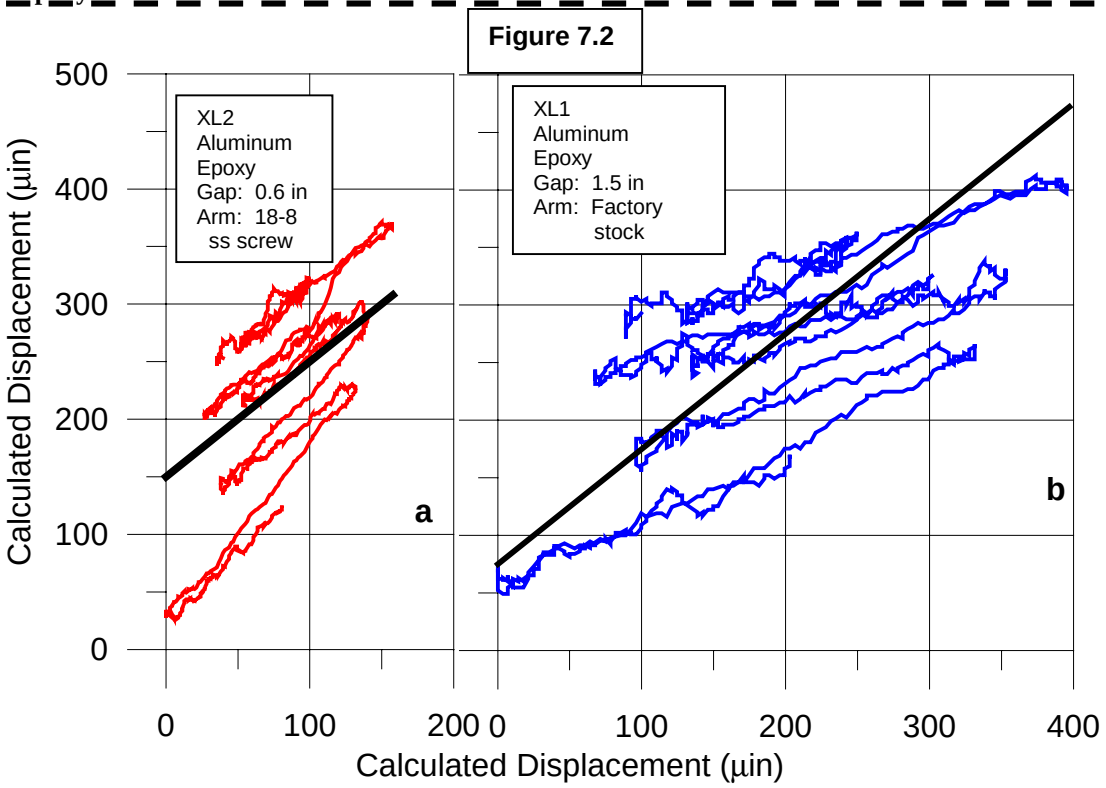

Figure 7.2. Nonlinearity from magnetism: a. 18-8 stainless steel screw as LVDT rod causing magnetic disturbances; b. Factory-stock nonmagnetic 312 stainless steel rod, affected by nearby magnetism.

Magnetic effects

Magnetism adversely affects an LVDT, which is dependent on an electromagnetic field for measurements, as illustrated in figure 7.2a and 7.2b, which show data "wandering" from the centerline, too inconsistent for ACM. The core-supporting rods standard with Trans-Tek LVDTs required gaps on the order of 1.5 inches, which seemed to affect response adversely, likely due to thermal effects on the metal rod. With great difficulty, one such rod was threaded almost its entire length, enabling the bracket to be placed closer to the coil, creating a smaller gap (see Figure 7.3), and system response improved.

The NU systems' Macrosensors LVDTs come with cores that must be attached to nonmagnetic(18-8) stainless steel screws; threaded from top to bottom, screws provide flexibility with setting gap width. Accordingly, single cores were obtained from Trans-Tek, but tiny 1-72 threads limited the availability of apparently suitable screw material to 16-6 stainless steel, which is classified essentially non-magnetic, but apparently contains enough magnetic material to disrupt the Trans-Tek LVDTs. Only one sensor was had a screw rod, but both sensors' data was affected; Figure 6b was similar for both sensors. During the screw-rod trial, sensor attachment and data collection techniques were no different than at any other time. Therefore, it is reasonable to conclude that magnetism in the screw must be responsible for the nonlinearity.

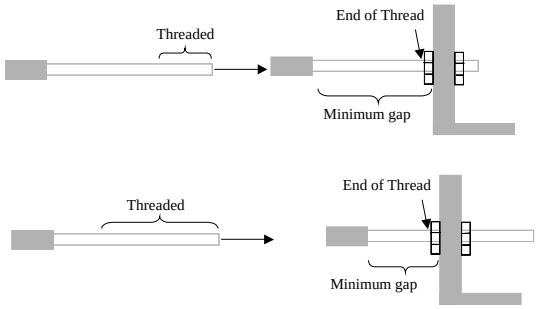

Figure 7.3. Decreasing gap by increasing rod's threaded length; LVDTs perform better with smaller gaps.

Chapter 8

Field Qualification: Background

As a result of the UHMW-P trials, it was concluded that System X with a short-rod LVDT would perform adequately on a wall crack, whose α would be similar to the UHMW-P, and System X was installed alongside existing NU sensors in an occupied residence. NU has had sensors at this site from 2000 onward (Siebert, 2000; McKenna, 2002); this house is several hundred feet from a quarry where quarrying blasting causes measurable ground motion and structural vibration. The System X ACM installation was to verify past results and validate the commercial system under consideration.

System X and the NU LVDT were compared to the Kaman sensor to evaluate their performance. System X was installed on a ceiling crack already instrumented by two NU sensors, a Macrosensors HSD-750-050 LVDT and a Kaman eddy-current gauge, shown in Figure 8.1 The NU eddy current (Kaman) sensor was chosen as the baseline for crack motion because of its minimal vulnerability to thermally-induced metallic expansion and measurement without attachment across the crack.

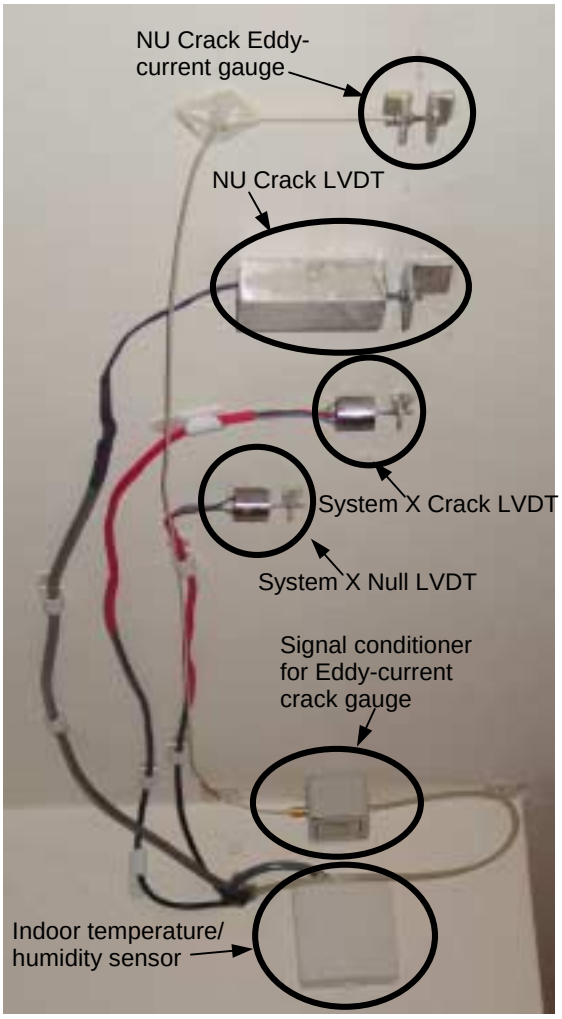

Figure 8.1. Sensors on ceiling crack at field test site, house near quarry, Franklin WI.

NU systems are connected both to ground motion detection (seismograph) and crack sensors. A geophone in the yard of the house detects three channels of ground particle velocity (lateral, transverse, and vertical); a microphone detects air blast intensity. Ground motion above 0.04 inches per second (ips), the blasting industry standard detection threshold, triggers a three-second, 1000 Hz Level II recording mode for all crack and null sensors. This combined Level I / II monitoring requires complex wiring illustrated in Figure 8.2

It was decided to test only the Level I capabilities of System X since Level I environmentally-induced displacement is the predominant crack displacement phenomenon. System X Level II capabilities will be tested in the future, and possibly Level III when that technology matures sufficiently; at present, however, no one, not even NU, has a system capable of Level III monitoring.

During the initial stages of its deployment, System X was checked frequently and its data downloaded often to ensure proper operation. When System X proved reliable for recording long-term data given sufficient memory, maintenance and downloads became

less frequent. Confidence in the system grew to the point that it was often allowed to run to the limits of its memory capacity.

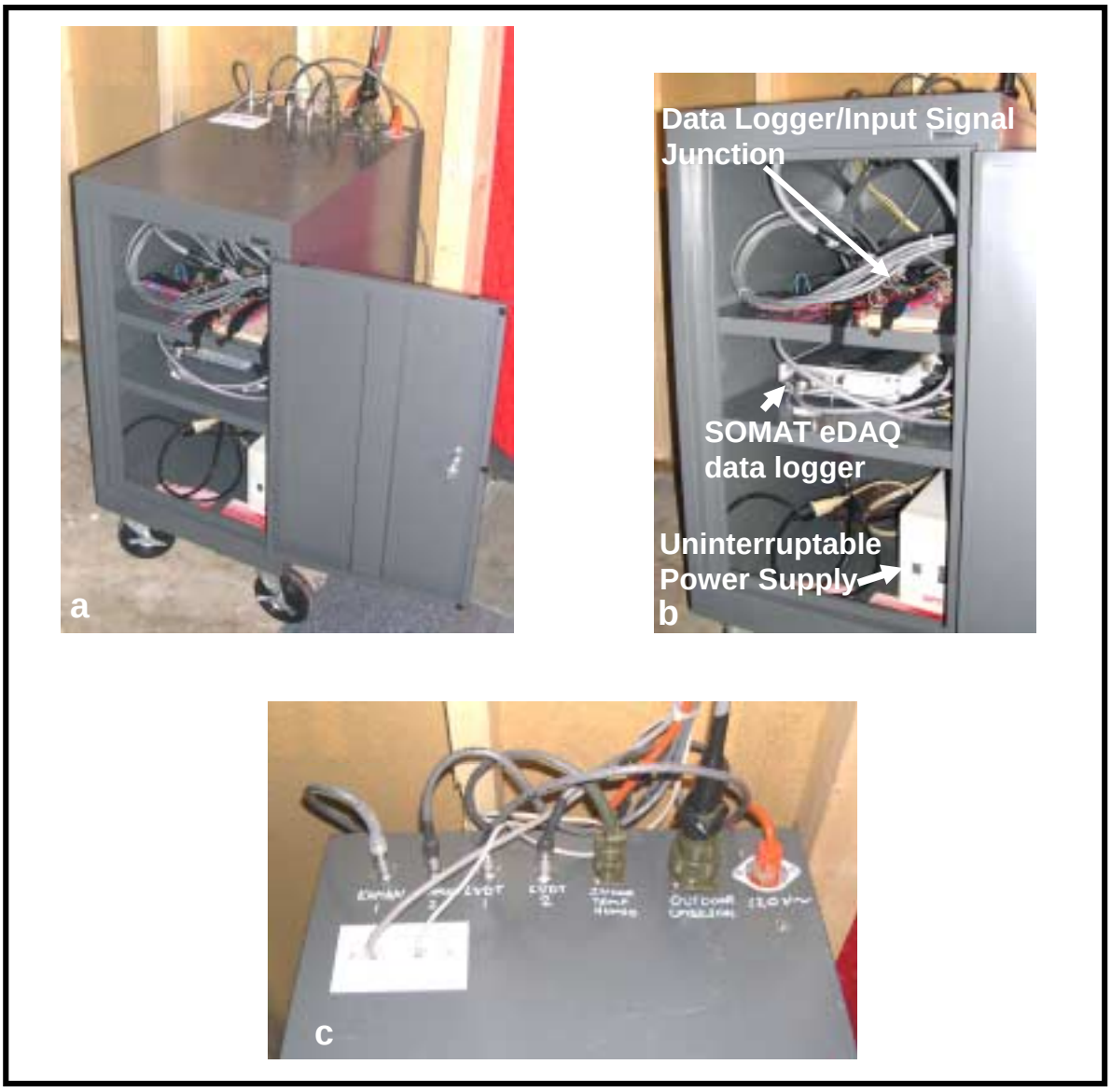

Figure 8.2. NU data logger system installation, Franklin WI. a. Cabinet in basement showing interior and input/output wires; b. detail of interior, showing closeup of logger/input signal junction, data logger, and uninterruptible power supply battery; c. detail of cabinet top, showing communication wiring links into cabinet.

Chapter 9

Field Qualification: Data and Results

Environmental effects on ACM installations

Qualifying a new ACM system in the field requires accurate environmental data and already-qualified sensors for comparison. Environmental factors and system performance are summarized for a six-week period from 18 March to 27 April 2004 in Figure 9.1; the gray lines in represent hourly plots of one-hour rolling averages; the black lines, hourly plots of 24-hour rolling averages. The one-hour average depicts often large daily variations in temperature and humidity, while the 24-hour average removes the jaggedness of hourly fluctuations, producing a longer-term representation of weather trends or fronts.

Indoor humidity and temperature patterns are similar to their outdoor counterparts, but significantly smaller in magnitude as shown in Figures 9.1a-d. The temperature plots are more similar to each other than those for humidity. Even an enclosed, insulated structure will experience similar temperature change *patterns*, which can be transmitted relatively easily even through well-insulated walls; magnitude is the only significant

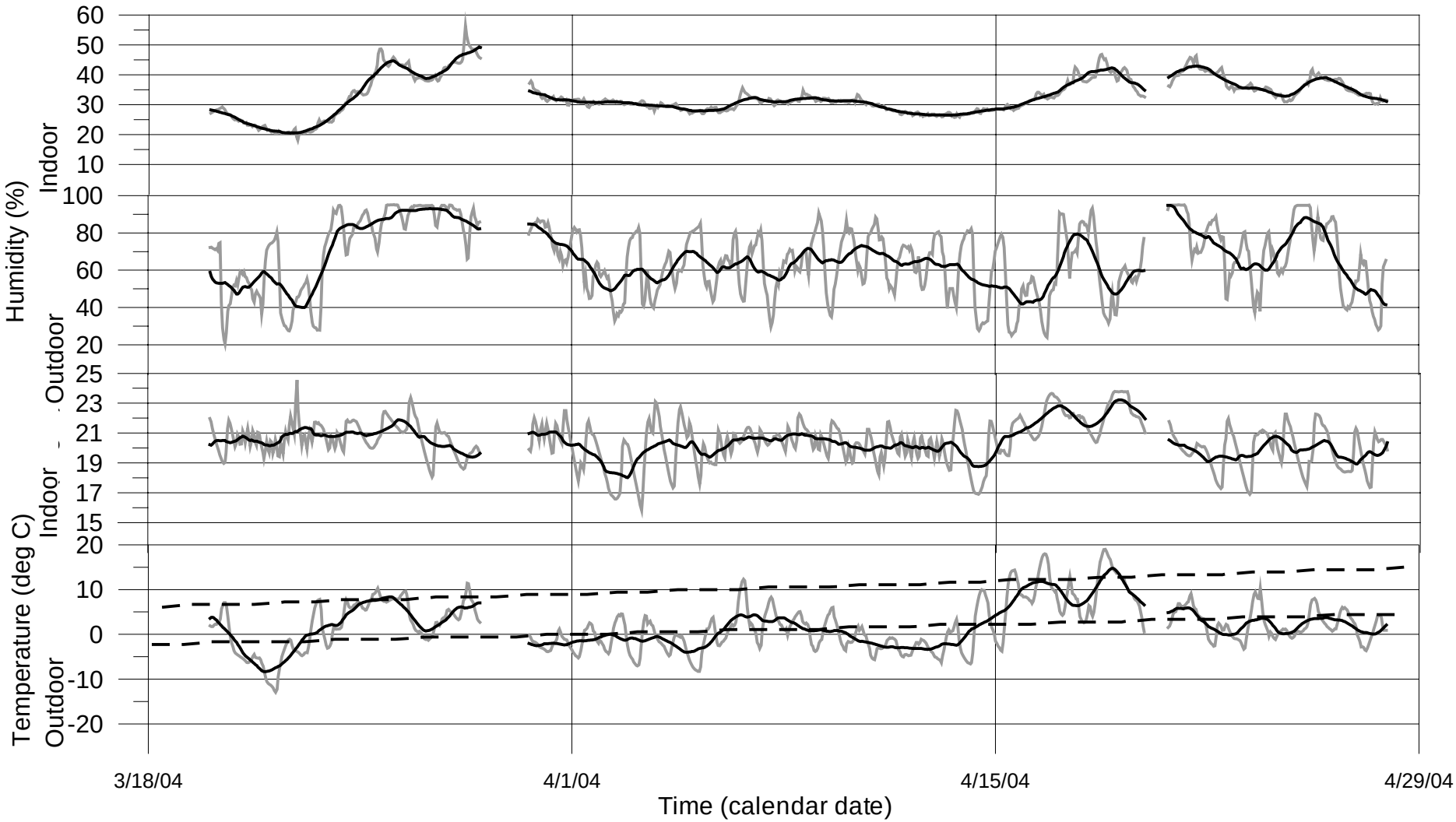

Figure 9.1. Environmental data for six-week period at Franklin, WI test site. Gray jagged lines: one-hour rolling average; black lines: 24-hour rolling average. This period was considered because crack displacement began to track with temperature during this time. a. Indoor humidity; b. Outdoor humidity; c. Indoor temperature; d. Outdoor temperature; dashed lines represent National Weather Service average daily highs and lows.

difference, e.g., 14 – 21 Apr, outdoor temperature change, 18°C, indoor temperature change, 4°C. However, a structure contains relatively static, isolated air volume which will not undergo the same moisture fluctuations as outdoors, since structures are shielded from factors affecting atmospheric water content, e.g., wind, rain fronts, direct sunlight, etc.

Since ACM systems must be able to measure changes in displacement under varying environmental conditions without being affected themselves, it is appropriate to compare their performance at a time when these factors are likely to dominate collection. Starting during the six-week period in Spring 2004 shown in Figure 9.1, the motion of the crack began corresponding closely to temperature patterns. As windows and doors were opened in milder weather, the influence of artificial environmental modifiers (furnace, humidifier, etc.) waned, leading to more synchronization of the crack with atmospheric influences.

The NU eddy current baseline system and System X closely follow temperature changes as seen in Figures 9.2a-c, with both sensors' spikes and valleys similar to those of temperature. Figure 9.2c also demonstrates that System X, though not as responsive in magnitude of measurement as the NU eddy current system, follows a nearly-identical displacement pattern. The magnitude of System X peaks and valleys were smaller than those of the NU Kaman, and the actual shapes were flatter and less well-defined in the hourly averaged readings. This discrepancy between the NU Kaman and System X was somewhat mitigated by the 24-hour rolling average, which by its nature flattens peaks and valleys to show frontal environmental effects. This correspondence validates System X for Level I crack monitoring.

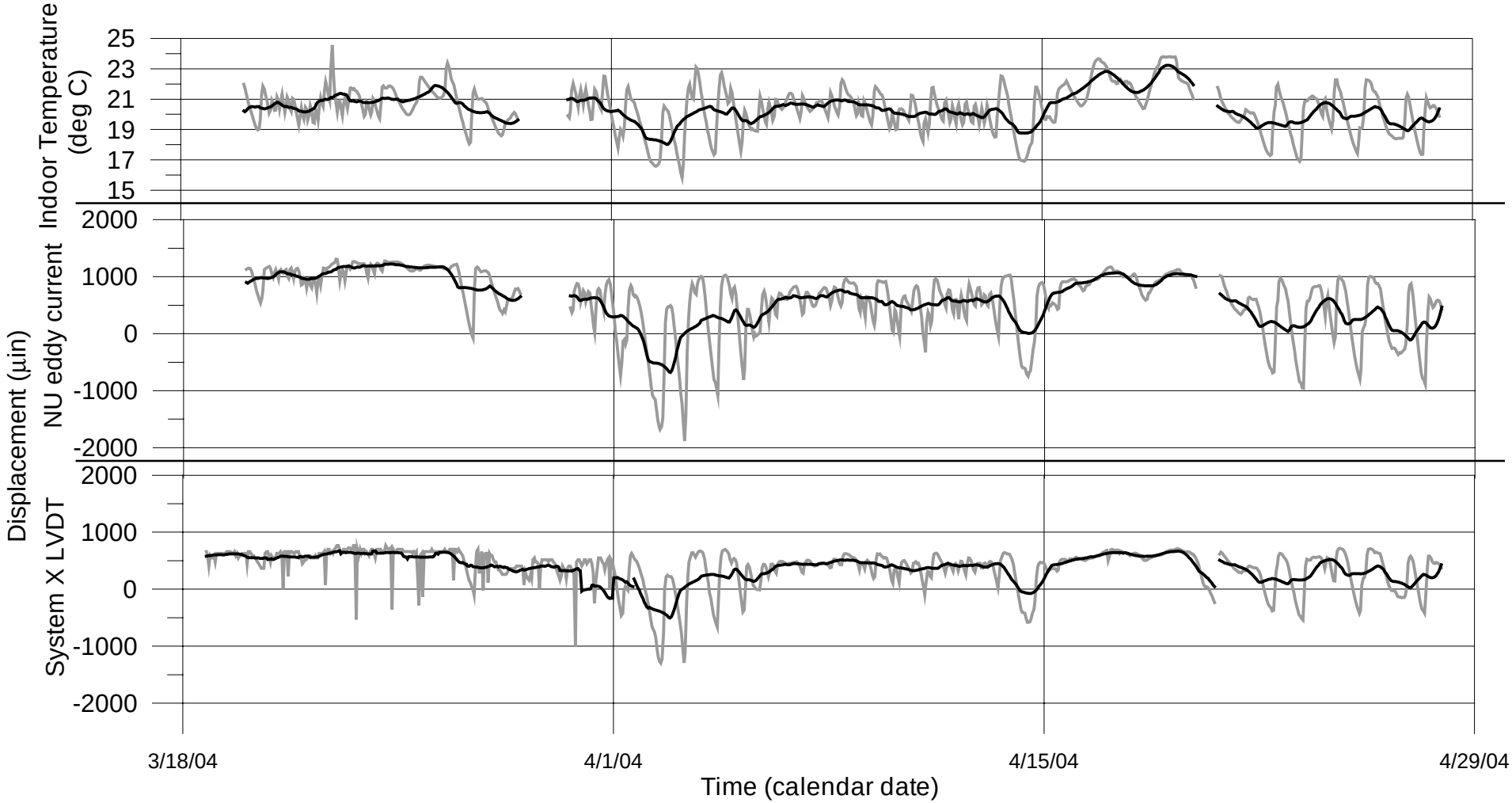

Figure 9.2. a. Temperature time histories (gray jagged: 1 hour rolling average; black: 24-hour rolling average) compared to displacement time histories for b. NU eddy current crack gauge and c. System X LVDT crack gauge. During this period, the both ACM systems follow indoor temperature trends closely. The 18 March –1 April 24-hour average temperature is almost flat, while the hourly trend varies. The crack sensors' 24-hour average matches the temperature 24-hour average more closely than the hourly, demonstrating that crack movement is more trend-like than instantaneous.

Validation of measurements

The crack, not the ceiling material itself, is the dominant factor in these displacements, as shown in Figure 9.3, comparing the System X null gauge with the System X crack gauge. Although occasional spikes indicate the System X null gauge channel is subject to electronic noise, the displacements of the intact portion of the ceiling are a fraction of the displacements of the crack. This verifies that the sensor is measuring the displacement of the crack, not the displacement of the wall material.

The null gauge channel appeared more sensitive than the crack gauge, which led to more frequent spurious null gauge signals, however, the crack gauge also occasionally had noise issues, though not as extreme or as frequent. Even so, the displacements over time, even in the course of a single day, combined with the effects of averaging, essentially overwhelm such noise data and make it irrelevant. Though there may be a certain amount of data roughness locally, when taken over the entire time period and compared to the other sensors, it is not possible to discern any significant difference.

Large changes in weather have been shown to influence wall cracks greatly; a comparison of large humidity changes (20-30%) in a house in an arid area were shown to change crack displacement by several thousand μin (Snider, 2003). This is another indication that noise intrusion even in a moderately noisy system will have little long-term effect; noise will remain constant and surround the data in a small envelope, whose effect will be further reduced by 24-hour averages. Therefore, when overall displacements are large, even moderate noise does not detract from the ACM system's ability to detect data as it should.

Consistent fidelity to a baseline known "true" displacement pattern, not necessarily identical magnitude, is the hallmark of an adequate data system. A consistent-value percentage deviation can become a multiplier to define "true" movement. Such a multiplier could be derived during extended trials in a controlled environment with large, but gradual, changes for an LVDT-based system. For long-term Level I measurement, instantaneous displacement measurement is not critical as long as the large-magnitude movements are accurately recorded within a reasonable time. As figure 9.2 shows, System X and NU displacements patterns are virtually indistinguishable; though one may lag the other due to clock time issues, in the end System X does measure what it should.

Field test analysis

While it has been shown above that the sensitivity of System X is sufficient for measuring typical structural crack expansion, it remains to investigate the adequacy of System X for measuring dynamic response. At the same site, maximum crack response for the ceiling crack was 202 μin for a 0.09 ips vertical ground motion and 114 dB air blast (McKenna, 2002). The typical ceiling crack displacement was 90 to 130 μin for vertical ground motion from 0.03 to 0.12 ips (McKenna, 2002); these displacements are three to four times greater than the 35μin resolution of System X. Thus, it appears that System X resolution is sufficient to record dynamic response. System X capability to measure both long-term and dynamic response with the same system is called dual mode; however, the system did not operate in this mode during this evaluation period.

The best baseline system would likely consist of a purely electro-magnetic sensor not dependent on relative motions of metal parts or cross-crack attachment. The Kaman eddy-current gauge is such a sensor, mini-radar which measures displacement by detecting

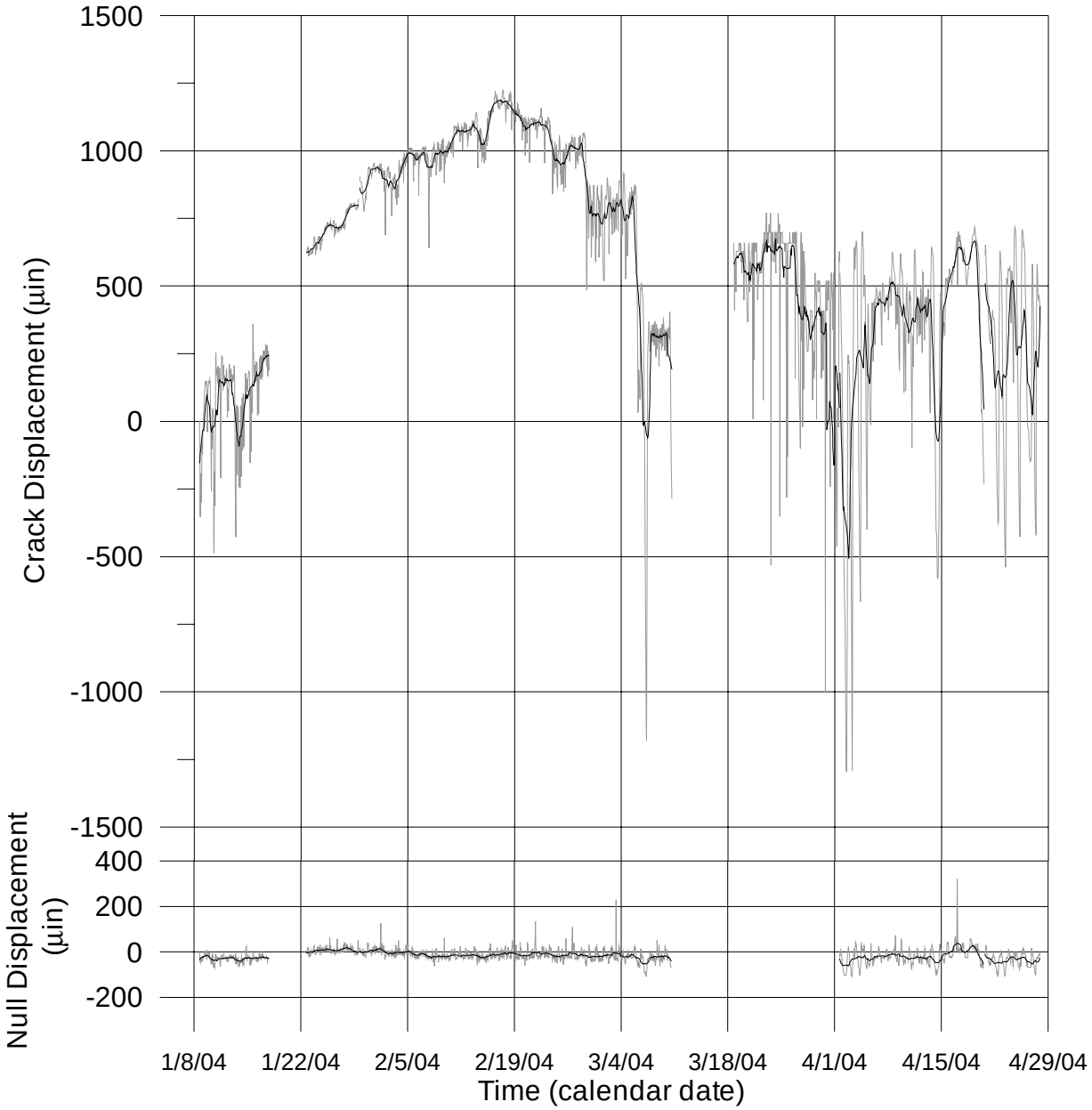

Figure 9.3. Comparison of System X Crack and Null gauges over the entire duration of the trial. During the winter months, the crack displacement did not correspond to any particular environmental factor. When the house was less insulated from outdoor weather patterns, the time history of 18 March 2004 and onward follow temperature closely. Although the null gauge also begins to follow temperature on the uncracked ceiling starting 18 March, it still contributes very little. The period from 18 March – 1 April are not plotted in this section due to data anomalies; see Appendix B, "Field Testing," for details.

changes in a quasi-constant electromagnetic field between source/detector and target. Such systems are relatively insensitive to environmental factors likely to be encountered at an ACM installation. They have no moving parts and therefore are not subject to metal-mass inertia errors, and their measurements are not dependent on mechanical apparatus many times larger than the actual displacement.

A system whose deviation relative to a baseline system is essentially constant as System X is, as shown in Figure 9.1, can be can be deemed reliable. Although System X does not record as much displacement as the NU baseline system Figure 9.1 demonstrates that System X deviation from the baseline eddy-current sensor is consistent.

Comparison of the three sensors' responses to crack expansion in Figure 9.1 shows that both System X and NUL have the same sensitivity and the displacement measured by each is some 75% of the eddy-current gauge measurement. Crack behavior is nonlinear because of the inhomogeneous, nonlinear nature of sheetrock and wood. Thus, field testing is a useful extension of laboratory plate testing; for further explanations and details, please see Appendix B, "Field Testing."

It is important to validate these differences are minor compared to the small (10%) ratio of the blast-induced dynamic crack response to long-term response. The somewhat-surprising reversal of performance, where System X was more responsive on plastic and less responsive in the field than NU Systems, indicates the importance of field testing. Benign, controlled laboratory testing is no substitute for actual field testing, but is a crucial step in qualifying sensors for field testing. It is the final step, field testing under actual conditions that determines system suitability for actual ACM.

Chapter 10

Conclusions and Recommendations.

Scope

Development of laboratory and field qualification procedures for Automated Crack Monitoring (ACM) system performance has been described for Level I monitoring, which entails measurement of long-term crack response where data are acquired at one to several points per hour. The developed procedures were followed in evaluating Northwestern University systems as well as an alpha-generation commercial product, System X.

Similarly, the necessity for further qualifying the systems for Level II and Level III monitoring, which measure crack response to seismic events, was recognized. Both Level II and Level III involve recording one to ten seconds of high sample rate crack displacement data (1000 points per second), and differ only in triggering method. Level II, a mature technology, triggers recording from an external geophone that detects ground motion, while Level III, still being developed, triggers collection from dynamic crack displacement itself. Ultimately, it will be necessary to develop Level II and Level III qualification techniques in future work.

As a result of applying Level I procedures, the following conclusions and recommendations were made. They are grouped into the following categories: system characteristics, sensor specifics, data collection and processing, laboratory testing, field testing, and an overall assessment.

System characteristics

High-resolution, electronically stable systems are critical for valid ACM data collection. Individual components must all be suitable and sufficiently capable. To investigate a full system thoroughly, every part of the system (data logger, sensors, electronic junctions, software if possible) should be evaluated separately, as the error may lie in more than one component.

Although noise is unavoidable, it should be minimized. System resolution should exceed the noise level to minimize uncertainty around the data. The smallest noise level consistently achievable is on the order of 10 μin or slightly less. Given the larger movements of cracks, such a low level of noise is not necessary; systems with as much as 70μin of intermittent, peak-to-peak noise have been found adequate.

The highest possible system resolution is important to provide data as accurate as possible and to minimize noise magnification due to analog-to-digital (A-D) conversion rounding. However, for the large, long-term displacements encountered in ACM, resolution with step sizes as large as one-seventh of the total displacement is adequate. This appears to be the practical limit for typical ACM displacements; the actual limit for step sizes as a fraction of overall displacement is a matter for further investigation.

Sensor specifics

Both eddy-current and linear voltage differential transducer (LVDT) sensors are acceptable for ACM measurements. The eddy-current gauge is more desirable as a baseline sensor since it has no mechanical attachment across the crack and is not susceptible to as much metallic expansion and contraction as an LVDT. However, an LVDT with strong linearity as determined by hysteretic testing is also acceptable.

The attachment method is important because an adhesive with excessive coefficient of thermal expansion (α) or creep will result in nonlinearity and unusable data. A strong, quick-setting epoxy with low coefficient of thermal expansion has been found to perform acceptably for long-term ACM monitoring after a settling and hardening period of several days.

Magnetism is another potential source of nonlinearity. When customizing sensor components to make them more suitable for ACM, it must be ensured that the new components do not cause magnetic interference. This concern requires at least one test under laboratory conditions with all other factors held constant.

Data collection and processing

Data collection and processing play a significant role in reducing systemic noise. Three different collection methods were investigated. The most desirable method involved averaging a large number of points from short bursts at high sampling rates. This approach eliminates unavoidable sinusoidal systemic noise and greatly mitigates isolated large-magnitude spikes, or other anomalous false data points.

Recording single points at small, regular time intervals minimizes the possibility of collecting random noise spikes. With such a collection method, anomalous noise will be

collected rarely and randomly, and will then be averaged with a large number of non-noise data points. However, this method is not recommended because of the large amount of system memory required.

The least desirable method is recording single peak values obtained at high sampling rates for a given collection interval, especially over long collection intervals. With this technique, the likelihood of noise defining the response increases in proportion to the length of the collection interval. Peak value collection virtually guarantees the presence of numerous large spikes in the data. To mitigate such anomalous points, it is necessary to collect over more numerous short intervals and average the collected points. However, increasing the number of points increases the amount of system memory required, as described above.

Laboratory testing

A material that responds linearly to thermal change is necessary to test displacement systems under controlled conditions. Sensors are affixed to this material, their displacement is recorded, and the calculated and measured responses are compared. The thermally induced expansion between sensor and target should be on the same order as that expected for cracks. Materials with a small coefficient of thermal expansion, α, such as aluminum, are not capable of sufficient thermal displacement to evaluate commercial systems, given typical sensor-target gaps, and may unfairly disqualify such systems. Materials with large α, such as ultra-high molecular weight polyethylene, are recommended. The magnitude of α for a material is a matter of engineering judgment and a function of the system's purpose: informational, scientific, legal, etc.

Laboratory testing is necessary to evaluate linearity, resolution, and noise of a system. Thermally-induced natural expansion is measured and hysteretic variation about the least-squares, best fit response line is determined. These responses recorded by a system under evaluation should be compared to those of the baseline system. A system should be sufficiently linear and its averaged data should be sufficiently sensitive to track calculated response. Linearity is sufficient when the variation about the best-fit line of the hysteresis plot is small compared to the crack response.

It is crucial to test a system consistently, with as little setup variation as possible between trials. Anomalies can be more easily identified and evaluated, particularly those affecting sensor performance, if only one factor is changed during evaluation test runs.

Field testing

Field testing is essential to system qualification because it subjects ACM monitoring equipment to actual conditions not reproducible in the laboratory. Systems that have not passed linearity assessments in the laboratory should not be deployed to the field. Untested modifications should not be installed in the field, particularly in "for the record" installations with legal or professional consequences. Field installations should consist of a sensor placed across a crack and a "null" sensor attached to the same, but intact, material.

Once deployed, ACM system output must be monitored carefully at the beginning to ensure proper recording. Anomalous data should be carefully examined; if the fault lies with the system, it should be thoroughly re-evaluated in laboratory tests with necessary modifications. When proven reliable under field conditions, the ACM system and its data may be left unattended for longer periods. At this stage, the rate of data collection

becomes an economic decision for a monitoring firm, involving economic trade-offs for personnel deployment and data analysis.

Commercial components have proven adequate for micro-displacement crack measurement for Level I monitoring, and as demonstrated by the NU system, Level II monitoring is possible. Level III monitoring remains under development.

Assessment

Applying the conditions and techniques discussed previously, the alpha model of System X was found to be adequate for long-term, Level I ACM data collection. This result demonstrates that resolution does not have to be particularly fine, although it must be sufficient for raw data to track the actual crack displacement without mathematical manipulation. Level II qualification was not investigated.

References

Dowding, C.H. (1996). *Construction Vibrations*, Prentice Hall, Upper Saddle River, NJ.

Haldar, A. and Sankaran, M. (2000). *Probability, Reliability, and Statistical Methods in Engineering Design*, John Wiley & Sons, Inc., New York, NY.

Louis, M. (2000). *Autonomous Crack Comparometer Phase II*, M.S. Thesis, Department of Civil and Environmental Engineering, Northwestern University, Evanston, IL.

McKenna, L.M. (2002). *Comparison of Measured Crack Response in Diverse Structures to Dynamic Events and Weather Phenomena*, M.S. Thesis, Department of Civil and Environmental Engineering, Northwestern University, Evanston, IL.

Siebert, D.R. (2000) *Autonomous Crack Comparometer*, M.S. Thesis, Department of Civil and Environmental Engineering, Northwestern University, Evanston, IL.

Snider, M.L. (2002). *Measurement and Analysis of Weather and Geodynamic Excitation-Induced Crack Displacements from Blasting in Connecticut and Construction Equipment in Las Vegas*, M.S. Thesis, Department of Civil and Environmental Engineering, Northwestern University, Evanston, IL.

SoMat Ease version 3.0 (1999). SoMat Corporation, Champaign, IL.

SoMat TCE eDAQ, version 3.7.2 (2002). SoMat Corporation, Champaign, IL.

SoMat TCS for Windows, version 2.0.1(1999). SoMat Corporation, Campaign, IL.

Appendix A

Hysteretic Testing for Laboratory Qualification

Introduction

Before an automated crack monitoring (ACM) system can be deployed to a field test site, it must be characterized properly, to ensure that: 1) it is linear under various environmental conditions it is likely to encounter; 2) it is consistent in its data collection; and 3) it can be relied upon to function properly. Tests described below were conducted on aluminum and plastic plates with known linear thermal expansion characteristics to qualify a sensor system to measure the expansion and contraction of cracks in actual structures. These "laboratory" tests, with the number of variables limited as much as possible, were conducted in a residential garage without climate control, a far more severe test than in the average house where temperatures typically stay within a small range. In all, there were eight trials. Each was plotted two ways. First, as a time history compared to temperature time history to ensure the sensor system consistently followed the same pattern as temperature. Second, as a hysteretic plot of measured displacement versus calculated displacement predicted by the coefficient of thermal expansion. A best-fit linear

regression line was fitted to this hysteretic data and became the focus of several data analysis procedures. Northwestern University (NU) systems with known, reliable performance were a baseline against which System X, the first commercial, off-the shelf ACM system, was compared.

Qualification surface material

The first tests were conducted on aluminum, whose coefficient of thermal expansion (α) is 13.1 μin/in/°F. This α induces small displacement compared to a crack on a wall or ceiling. Typical gaps between target bracket and displacement detector during these trials were 0.4 to 1.5 inches, with a maximum temperature differentials of 24°F. Thus, maximum calculated displacement from equation 2.1 was 500 μin for a 1.5 inch gap, though a more usual value was roughly 100μin for the standard gap sizes of 0.4 to 0.5 inches. Such half-inch gaps experienced expansions of less than 10μin per degree Fahrenheit of temperature change, typically over a period of fifteen minutes or more. System X recorded displacements at intervals of 1-minute or less; the NU SOMAT system recorded at 5-minute intervals. Thus, displacements between measurements would have been sufficiently small to require extremely sensitive apparatus to detect it.

The small displacements led to the conclusion that aluminum, with its unrealistically small α compared to an actual wall, was inadequate to test System X. Ultra-High Molecular Weight Polyethelene (UHMW-P), with α = 110 μin/in/°F which corresponds more closely to those of a wall or ceiling, replaces aluminum as the test surface material. Gaps ranged from 0.4 to 0.6 inches, with similar maximum temperature differences as aluminum; however, under conditions similar to those of the aluminum tests, expansion for half-inch gaps was calculated between 1250 and 1850 μin, a significant

increase that more closely matches the wall crack expansions, requires far lower resolution, and allows a much higher tolerance for system electronic noise. The more sensitive SOMAT eDAQ replaced the 2100, which proved beneficial: the eDAQ's 16-bit processor yielded slightly better resolution than the 2100's 12-bit processor (0.07 μin vs 0.1 μin) on a testing material with α an order of magnitude larger. An incidental benefit was the modest savinSystem X between a 12"x 12"x ¾" plate of aluminum ($150 in 2003) and a 18"x 24"x ¾" plate of UHMW-P ($35 in 2003).

There were several disadvantages to UHMW-P, also called "poor man's Teflon®" because of its high thermal expansion and its Teflon-like slickness. The bond between epoxy attaching sensors to the plate and the plate itself was much weaker because of the slippery nature of the plate. Large thermally-induced movements also appeared to weaken the bond through mechanical fatigue, and when the weather turned cooler, the epoxy-plate bond became brittle enough to require extremely careful handling. The bonds of the 90-second quick-setting epoxy, did not weaken with the metal of the LVDT bodies or with the aluminum plate under cooler conditions, leading to the conclusion that an epoxy-plastic bond is not as strong.

Linearity determination

Linearity was determined by plotting a hysteresis curve, measured displacement versus calculated displacement, for each data set, then determining a variance from the best fit line. Measured displacement, $\delta_{measured}$, plotted on the y-axis was the output from an ACM micro-measurement system. Calculated displacement was derived from equation 2.4 ($\delta_{calculated} = \alpha*L*T$) and plotted on the x-axis, where α and gap width, L, are constant and temperature, T, has a distinct value for each data point corresponding to a measured

displacement value. The $\delta_{calculated}$ and $\delta_{measured}$ values are shifted by taking the minimum value for each set of data, then subtracting that value or smaller from every point in each data set respectively; in this way, all data points are ≥ 0 and the hysteretic curve plots in Quadrant I (+x, +y). The slope of the theoretically-predicted line is unity.

Two NU and one System X data logging systeNU collected experimental data; Figure A1 shows a representative setup with the SOMAT 2100 Field Computer System and its associated equipment, and the LVDTs for System X which is being qualified. Appendix E shows summaries of system and sensor performance. See also Chapter 3 for detailed descriptions of the systeNU and sensors whose data is described below.

Testing conditions

The sensors were mounted on the test plates in a garage without environmental controls during summer, 2003; Table A1 (found at the end of this Appendix) summarizes relevant setup factors and temperature. The maximum temperature changes for a test run varied from 13°F to 24°F for the aluminum plate, deployed from June to July 2003, and 20 to 27°F for the UHMW-P plate deployed from late August through early September 2003.

Both NU SoMat systems have been thoroughly characterized and deemed suitable for such collection in past work (most recently McKenna, 2002; Snyder, 2003); the collection of System X data was the primary purpose for these tests. The collection period for System X varied from one to four points per minute (ppm); the manufacturer recommends 1 ppm collection to optimizes data density with available memory. Earlier tests showed that collecting one point per five minutes with produced erratic, often incomprehensible, data as noise and large data steps from the lower resolution tended to predominate. System X capacity is 20 data files of 1440 points each, corresponding to one

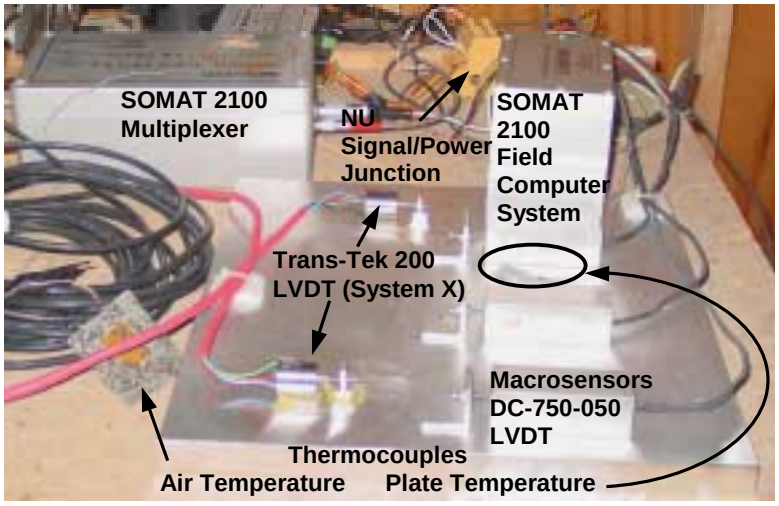

Figure A1a. Representative plate-testing setup: Macrosensors DC-750-050 LVDTs for NU system, Trans-Tek 200 LVDTs for System X mounted on aluminum plate.

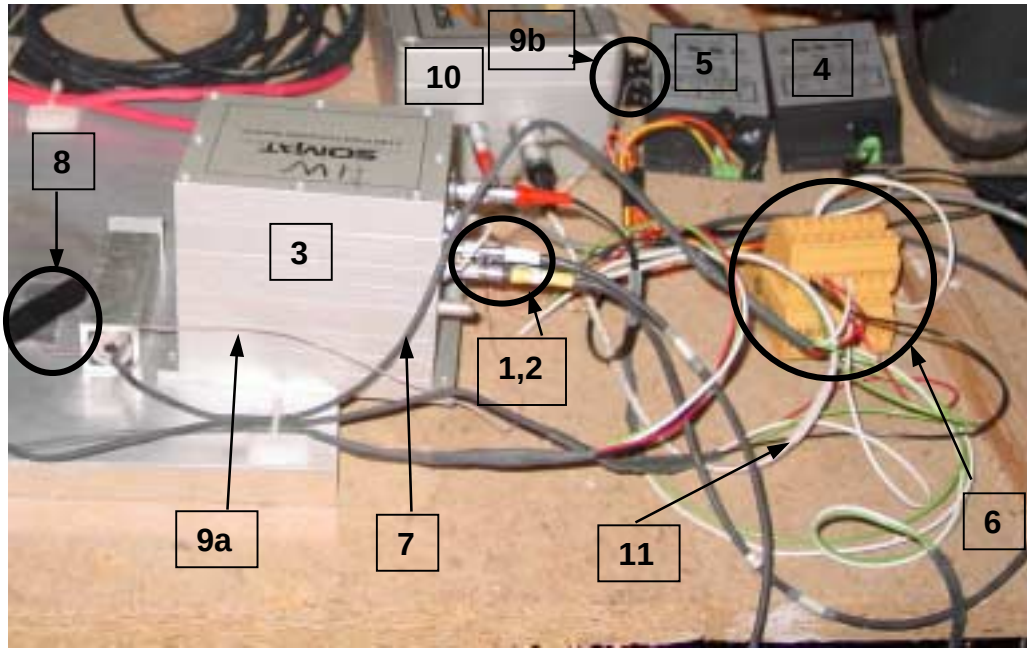

Figure A1b. Plate test set-up equiment close up. (1) and (2) are data channel inputs to the SoMat 2100 data logger (3) powered by an AC-to-DC converter regulated power supply (4). The LVDT power source (5) transforms 120 V AC electricity to DC and provides three inputs, ±15V and ground, to the signal/power junction (6). LVDT wire bundle enclosed in electrical shrink-tubing (7) transmits DC power from (5) and LVDT output signals via (6)to (1 or 2). The taped-down sensor (8) is the thermocouple, which measures aluminum plate temperature, and transmits data via wire (9a) and two-prong connector (9b) to the multiplexer (10), which converts data to 2100 format and sends it via cable (11) to the data logger (3).

file per 24-hour period for one ppm collection or 24 minutes per record for the maximum 1 point per second collection rate.

Trial runs varied from four to ten days. The difficulty with ACM testing is that the process cannot be speeded up, particularly under natural conditions. Conceivably, the process could be accelerated somewhat inside a regulated temperature cell capable of inducing temperatures from 10 to 25 °C; however, even this would require gradual changes to simulated natural daily temperature fluctuations, because large, abrupt changes are uncommon in nature.

Gap size plays a significant role in the performance of the system when the LVDT's metal connecting rod is subject to its own α-induced thermal displacement. Table A1 also shows that on several occasions, the best-fit slope of long-rod setups deviated significantly more from 1.0 than a short-rod setup, whose gap size is closer to field deployment gap sizes. It was concluded that longer rods were less responsive than shorter rods. Table 3 shows that during UHMW-P tests, when both XL1 and XL2 had short rods, the slope of each sensor's hysteretic plot was much more consistent and closer to 1.0

Results

Figure A2 shows hysteresis plots representing data for both System X sensors; Figures A2a-b and A2c-d represent the same two data sets, respectively, with different x-axes. System X LVDT 1 (XL1) has a 1.5 inch gap length as a function of the Trans-Tek manufacturer's standard stock rod; the XL2 gap is smaller, with a more standard ACMgap length.

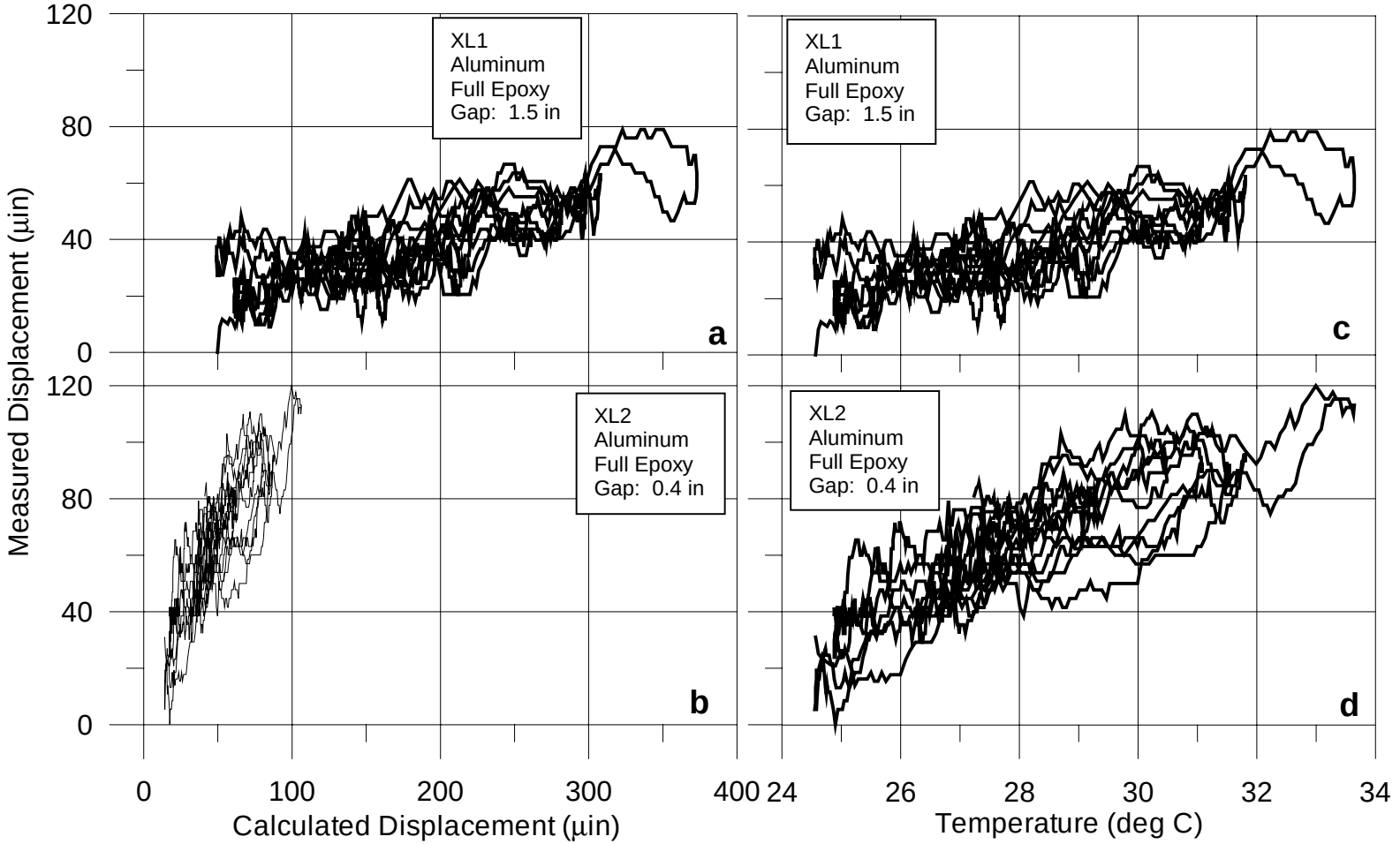

Figure A2. Comparison of hysteresis both System X sensors on aluminum, same trial, plotted with different x-axes. Despite one-hour rolling average of data, small System X A-D steps on a small-displacement material result in data Jaggedness. a-b. X-axis as calculated displacement =α*L*T; the gap size, L, defines the appearance the plot; a. XL1 has a gap—and therefore calculated displacement—four times that XL2 in b. c-d. X-axis as temperature; plots appear almost the same, despite the large difference in gap size. Far more information is available with calculated displacement as the x-axis.

Calculated displacement, $\delta_{calculated} = \alpha*L*T$ from Equation 2.4, is the predicted response as a function of gap size; Figure A2a-b clearly shows the influence of L. A rough predicted response and can easily be determined by subtracting x_{max}-x_{min}; for XL1,this value is 325 μin, for XL2, 70 μin. The x-axis values will always be accurate because they are a function of temperature; predicted response for The XL1 gap is four times larger than that of XL2 gap, in proportion to the respective gap sizes rounded to 1.5 and 0.4 inches, respectively. The actual response of XL1 (Measured Displacement) is far smaller than predicted, whereas the response of XL2 is somewhat larger than predicted, indicating that either the XL1 and XL2 sensors or data logger channels are, respectively, less and more responsive than predicted. The Measured Displacement vs Calculated Displacement plot displays a great deal of information not available when the x-axis is simply temperature.

In previous work (Siebert, 2000), hysteresis was always plotted with temperature on the x-axis, showing the relationship between temperature and hysteretic behavior as in Figures A2c-d, which plot the same data with a different x-axis as in Figure A2a-b. Similar sensors with the same data logger yield plots almost identical regardless of gap size. Unlike when the x-axis is Calculated Displacement, it is impossible to determine gap effects and sensor response, with an x-axis of Temperature.

The decreased responsiveness of the longer rod could be a function of the metal in the arm, the sensor itself, the data channel electronics, or a combination of the three. As previously discussed, it was the under-response of long LVDT rods that led to the conclusion that shorter arNU perform better. As a result, shorter rods were custom-ordered from Trans-Tek, as we were unable to fabricate such rods at NU.

Figure A3 shows representative plots of NU Macrosensors LVDTs on aluminum. The smoothness and consistency of NU data is the result of linear sensors, small A-D steps on the order of 0.1μin, and a one-hour rolling average of data. The "clean" appearance of data in Figure A3, in contrast with the jaggedness of System X data in Figure 2, is a function of A-D step size, and illustrates the crucial importance of 1) high data resolution as a function of A-D conversion; 2) the importance of matching A-D resolution with material. As previously discussed, aluminum was not suitable because its small displacements do not accurately simulate a wall or ceiling.

The importance of A-D compatibility with material is further illustrated in the contrast between Figures A4a and A4b. Figure A4a, a System X hysteresis plot for aluminum, is jagged and uneven despite data averaging because of the small number of A-D steps in $\delta_{calculated}$. The data from UHMW-P plastic in Figure A4b, however, is markedly smoother, because the material, with $\delta_{calculated}$ containing over 50 A-D steps, is compatible resolution in addition to having high α which better simulates structural crack behavior.

As has been mentioned, ACM data can be dependent on the differences between channels of the same ACM system, as illustrated in Figure A5 for System X. Reversing inputs on produces noticeable changes in the appearance of data. Figure A5a displays time history data for back-to-back trials, where the input channels were swapped on halfway through the test, i.e., XL1 input swapped from channel 1 to 2 and XL2 from channel 2 to 1. During the first test, XL1 appears more responsive than XL2, but XL1 responsiveness decreases when plugged into channel 2. Note the data jump at hour 148 in Figure A4b, and though the collection frequency changes between the data sets (2 ppm for the first half

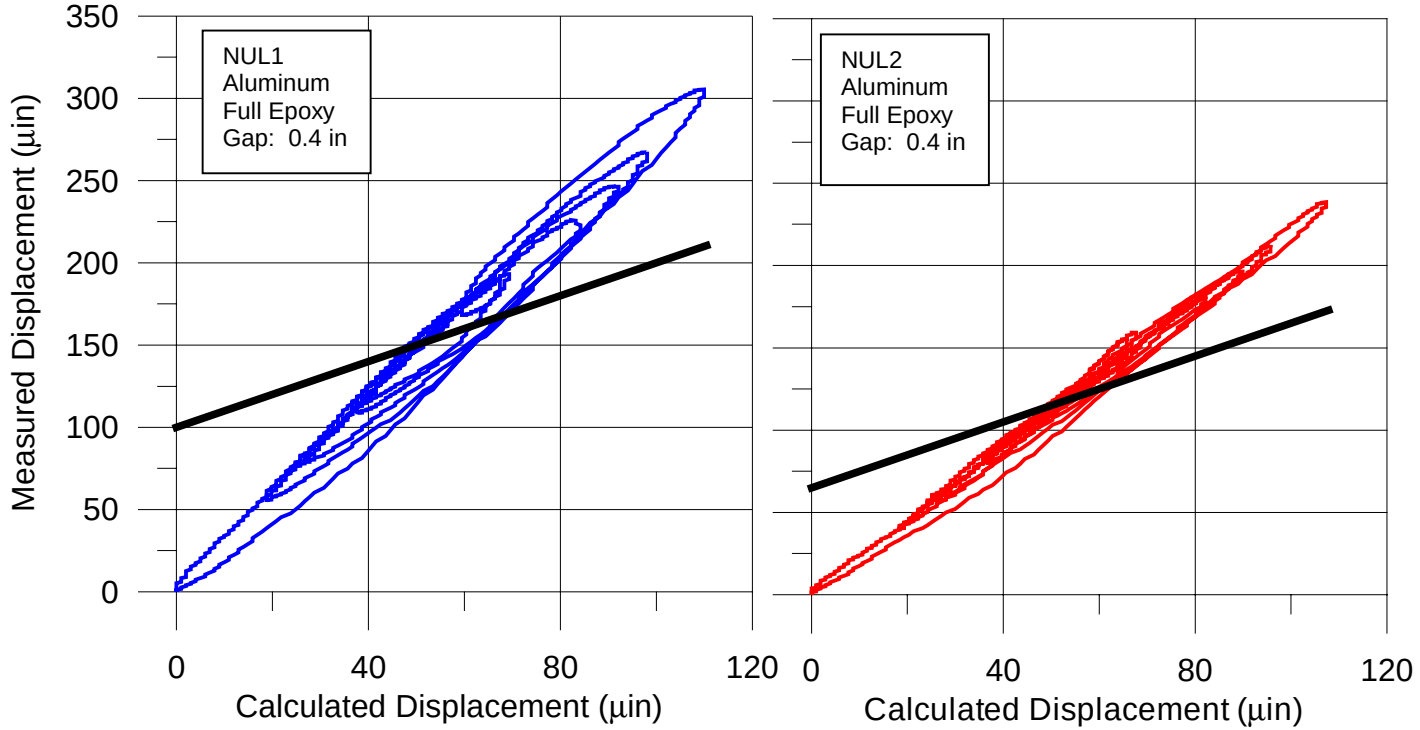

Figure A3. Hysteresis for NU Macrosensors LVDTs on aluminum. Small A-D step size and one-hour rolling average results in smooth, "clean" looking data. The loop tightness is a function of the sensor, and indicates linearity, which is discussed both in Chapter 6 and later in this Appendix. The heavy dark line in both plots represents α-predicted theoretical displacement.

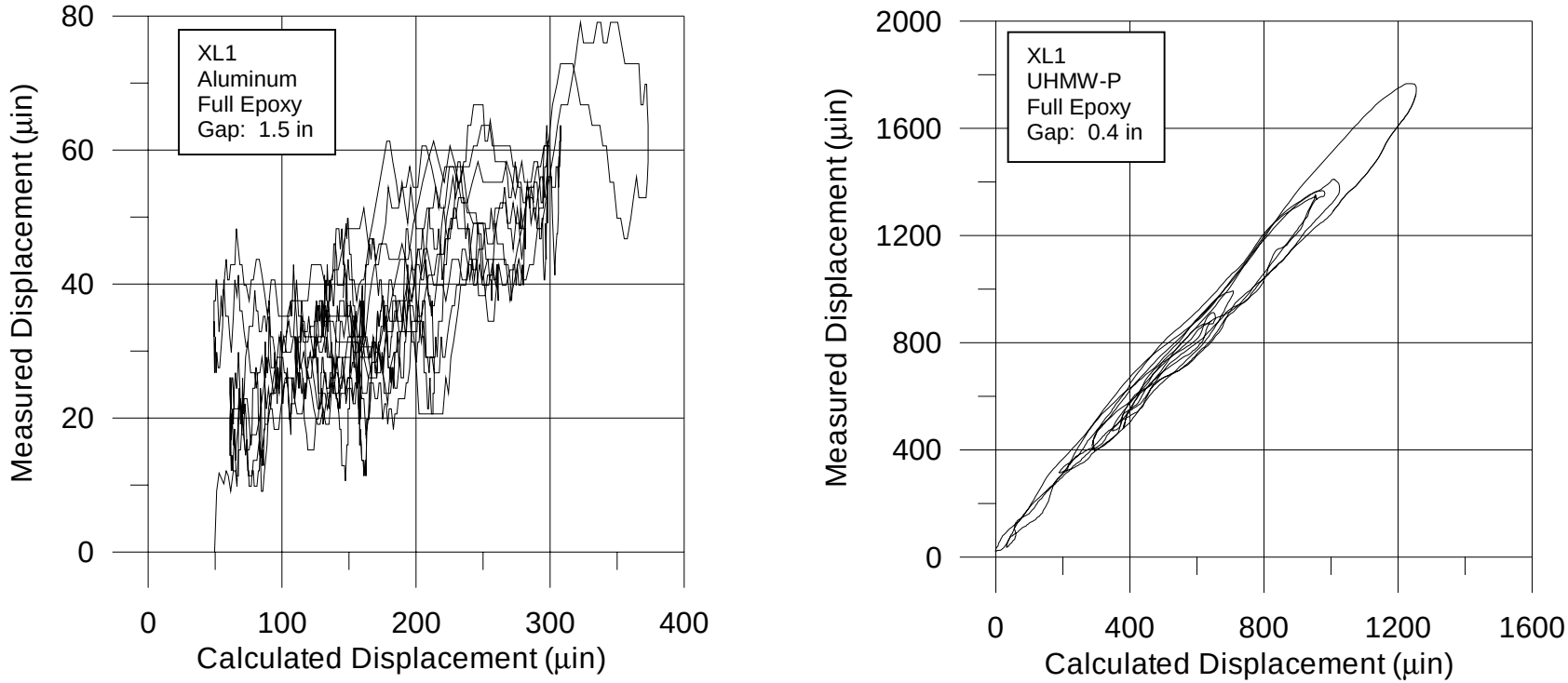

Figure A4. Note different scales. Correlation between data collection system A-D resolution and test surface displacement. This figure illustrates the importance of testing ACM systeNU on surfaces that accurately represent field conditions. a. System X sensor on aluminum, whose extremely small displacements do not accurately simulate structural cracks to be measured in the field; b. System X sensor UHMW-P plastic sheet, whose displacements per degree of temperature are significantly higher than those of aluminum and realistically simulate structural crack displacement.

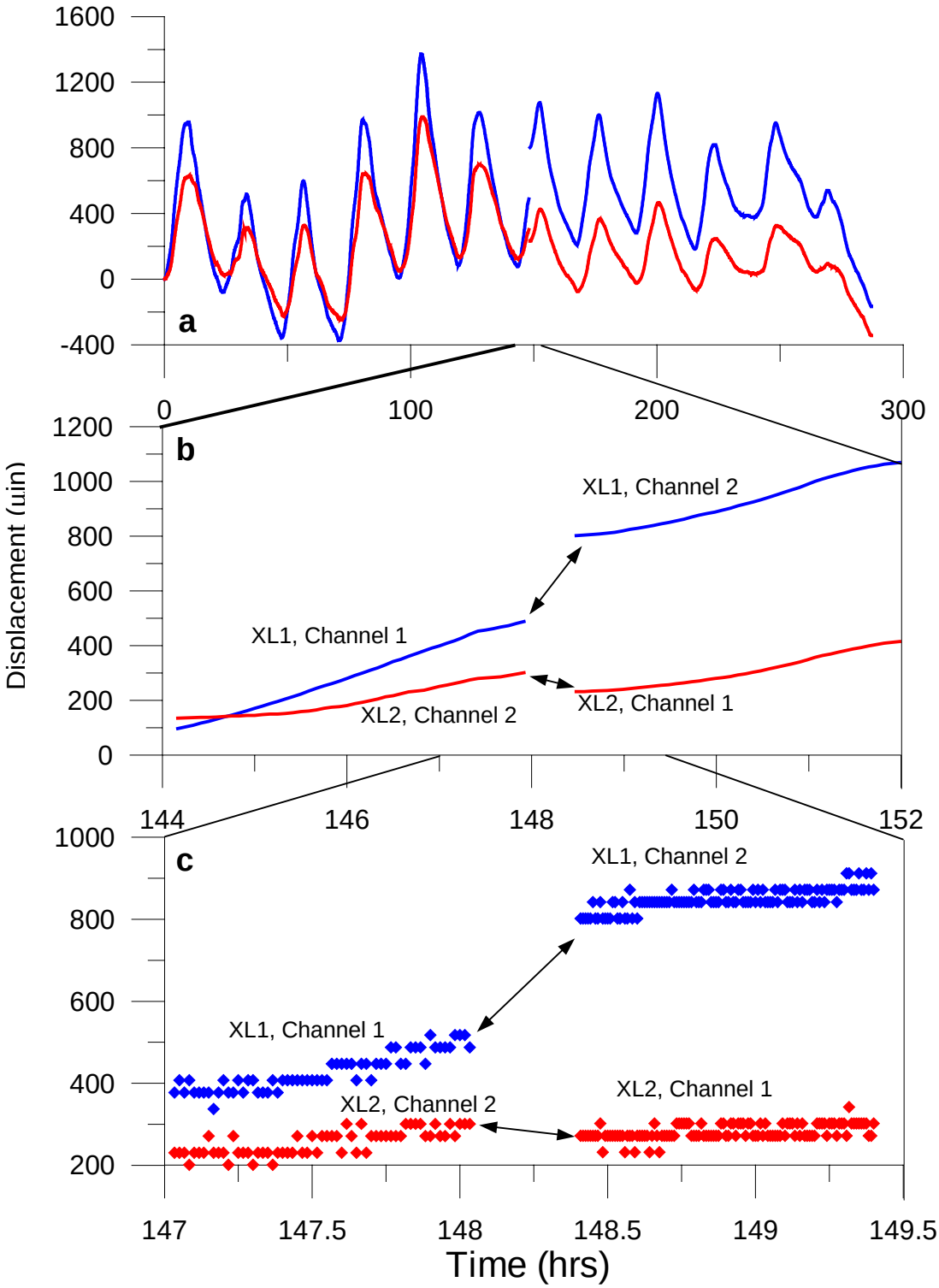

Figure A5. Time history for two consecutive tests run on UHMW-P plastic plate, showing visible changes in collection with data channel swap, XL1 from System X data channel 1 to 2 and XL2 from channel 2 to 1. a. Time history for entire two-test period with jumps when channels are swapped. b. Closeup of jumps after sensor-input channel swap. c. Further closeup of jumps, showing points, demonstrating that data collection remained consistent; it was the channel change that caused disturbance. (Note: before the swap, data is collected at 1 ppm, afterward at 2 ppm, accounting for increased density of points from hour 148.5 onward.)

of the test, 2 ppm for the second half) no appreciable effect on the collection data. When linked to channel 2, XL2 is less responsive, while response increases noticeably at hour 148 when XL2 is re-routed to channel 1. Other experimental results bear out this anomaly; channels 1 and 2 perform significantly differently in the field (see Chapter 9 and Field Test Appendix describing System X performance 18 March to 1 April 2004); channel 1, the nominal null sensor input, experiences more electronic noise which may indicate higher sensitivity to electrical signals than channel 2.

However, although there is a jump and the data plot does get offset significantly, this change in channel does not affect the quality of the data, seen in Figure A6 for Trials in A6c. There is virtually no change in variance, the quotient of deviation from data set's best fit line and $\delta_{measured}$ between the last two trials, when the channel swap occurred. Variance is inversely proportional to linearity: the lower the variance, the less deviation from the best-fit line, and therefore the higher the linearity.

Although there were detectable changes in the actual data plots, the system remains linear. Similarly, Figure A6a also shows linearity as changing little when a similar sensor-channel swap is done between NUL1 and 2 and channels 1 and 2 between the second and third trials. In fact, there is some change in variance, although the plots of the data appear relatively unchanged. In the trials of Figure A6a, regardless of input channel, NUL2 always had a tighter hysteretic loop than NUL1; Figure 3 plots data from the first trial in A6a, which is representative of all results in Figure A6a.

Similarly, there is little linearity change in Trials 4-5, when the sensor adhesive for attachment to the aluminum plate was changed. As discussed in Chapter 4, the adhesive configuration made little difference to linearity.

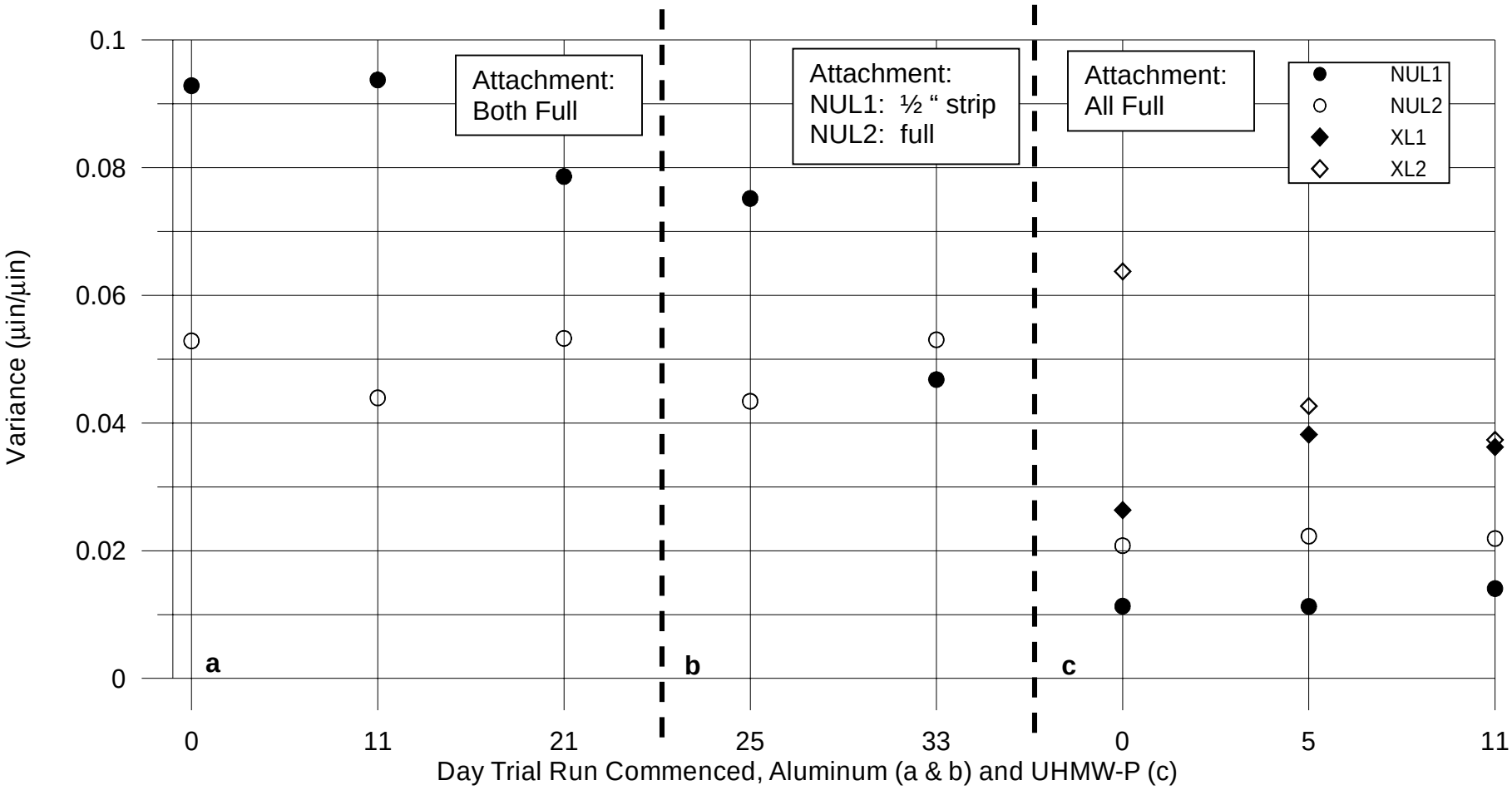

Figure A6. Variance from "best fit" line, the quotient of standard deviation and total displacement, $\delta_{measured\approx}$, for linearity-hysteresis tests. a. Aluminum, NUL1 and NUL2 both fully-attached; b. Aluminum, NUL1 attached with only a ½ inch strip near the front of the sensor housing, NUL2 fully attached; c. Ultra high molecular weight polyethylene, all sensors fully attached.

One significant difference is the appearance of the hysteretic loops shown in Figure A7, for data displayed in Figure A6b. Figure A6a is representative of the appearance of NUL1 during both trials. NUL1 is attached per usual procedure: the LVDT itself is contained in a square aluminum tube to make attachment easier. The entire surface of the tube in contact with the plate was carefully coated with epoxy. In contrast was attached to the aluminum plate by only a half-inch strip at the very front of the LVDT assembly. Figure A7b-c shows two distinct sets of loops for the two trials of NUL2. Interestingly, despite this small discontinuity, Figure A6b shows that the linearity of NUL2 is still quite good, in one case better than that of NUL1 which does not have any discontinuities. This is likely because despite presence of a discontinuity resulting in two distinct hysteretic loops for the NUL2 plots, both loops are noticeably tighter than the single loop of NUL1which has no discontinuity or offset.

A reliable, stable logging computer ideally exercises little, if any, influence on the data, regardless of input channel, and variations if present are small. Consistency is crucial, not necessarily adherence to the α-predicted line, since all measurements are relative, not absolute. Indeed, changing conditions render it virtually impossible to find an "absolute" zero displacement—which could be derived from any one of a number of historical minimum temperature points.

Although ideally there should be no variation between signal channels, the presence of such variation does not necessarily disqualify a system. If sensitivity or internal processing is the issue a simple modification should resolve it. However, if it is an intractable design flaw, if the performance of each such system produced is consistent, it should be acceptable provided the end-user is aware of the variation and the manufacturer

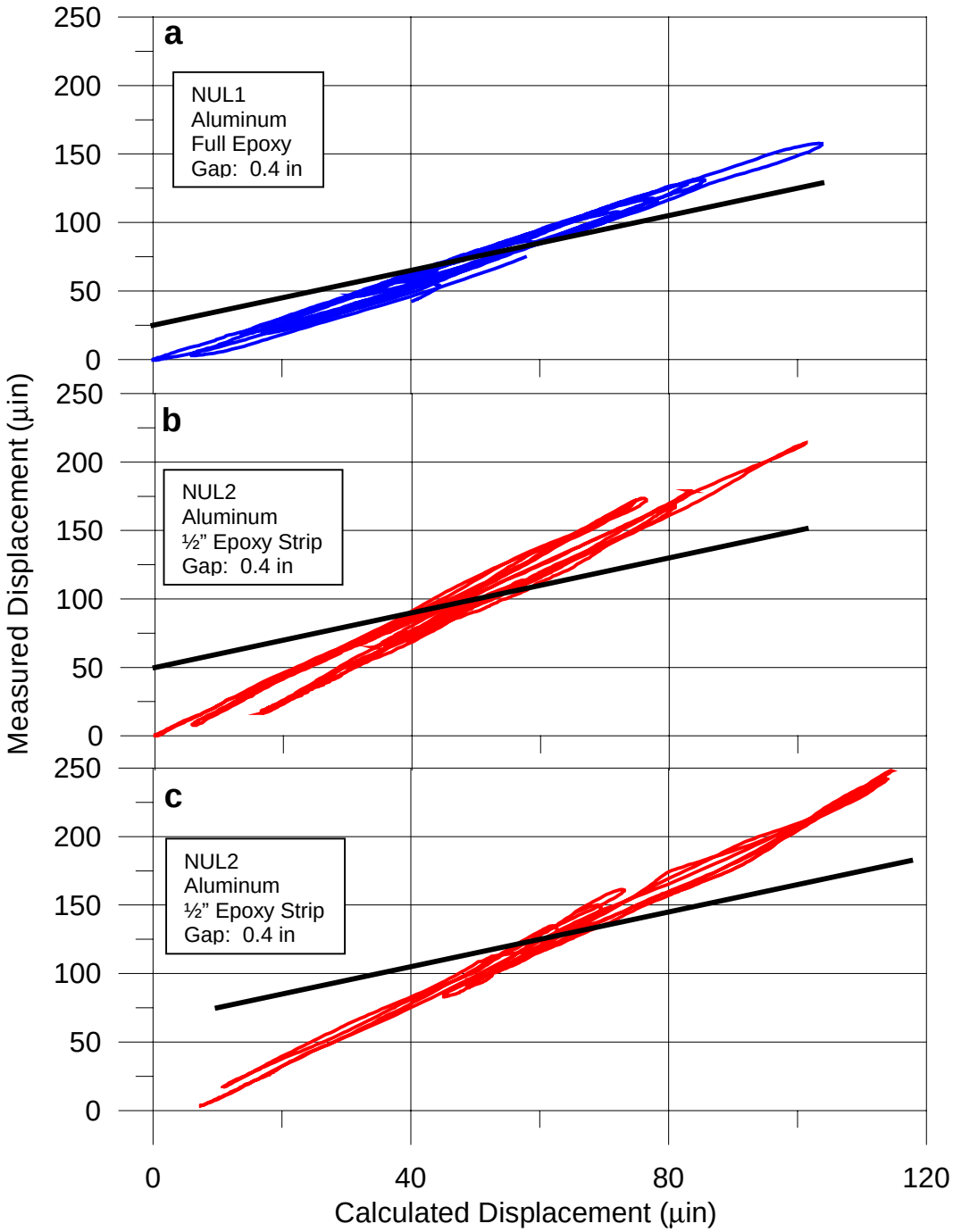

Figure A7. Comparison of attachment method. a. hysteretic behavior with epoxy applied to the entire coil-plate interface; b and c, only a ½" strip of epoxy at coil-plate interface. Discontinuities in both cause two distinct hysteretic loops, tighter in both b and c than in a.

provides clear, detailed methods to resolve the issue, though this such a "workaround" is not recommended due to the potential for error by the end-user and subsequent false data carrying the threat of legal liability.

As discussed in Chapter 7, however, adhesives with excessive α can completely invalidate ACM data due to thermal instability, as shown in Figure A8. Figure A8a compares behavior of XL1, attached to the aluminum plate with ordinary "hot glue," and XL2, attached to the plate with the epoxy normally used. Figure A8b shows that despite the significant difference in performance between the hot-glued XL1 and XL2, XL2 behavior is consistent with other System X trials on aluminum (see Figure A2). In contrast, XL1 is the large plot on the top with numerous "levels," showing radical nonlinearity in the form of a loose, wandering hysteretic loop at the bottom level, which itself falls between two ranges of great instability. By comparison, Figure A8b shows that XL2 is not significantly tighter or more linear than normal, serving to increase the emphasis between the hot-glued sensor behavior and the tightly-linear appearance of XL2 near the x-axis of Figure A8a.

A high-α adhesive like hot glue, sufficient for many macro-applications, falls far short of adequate for micro-measurement for several reasons, as can be determined from Figure A9. Figure A9a shows the time history of temperature during this test, and Figure A8b shows how XL2 follows the same displacement pattern, indicating acceptable behavior, though the resolution is far from ideal. Figure A9c, however emphasizes the resolution problem with two stages of instability. The first is the initial radical nonlinearity, depicted by the almost-vertical displacement line, in a small temperature

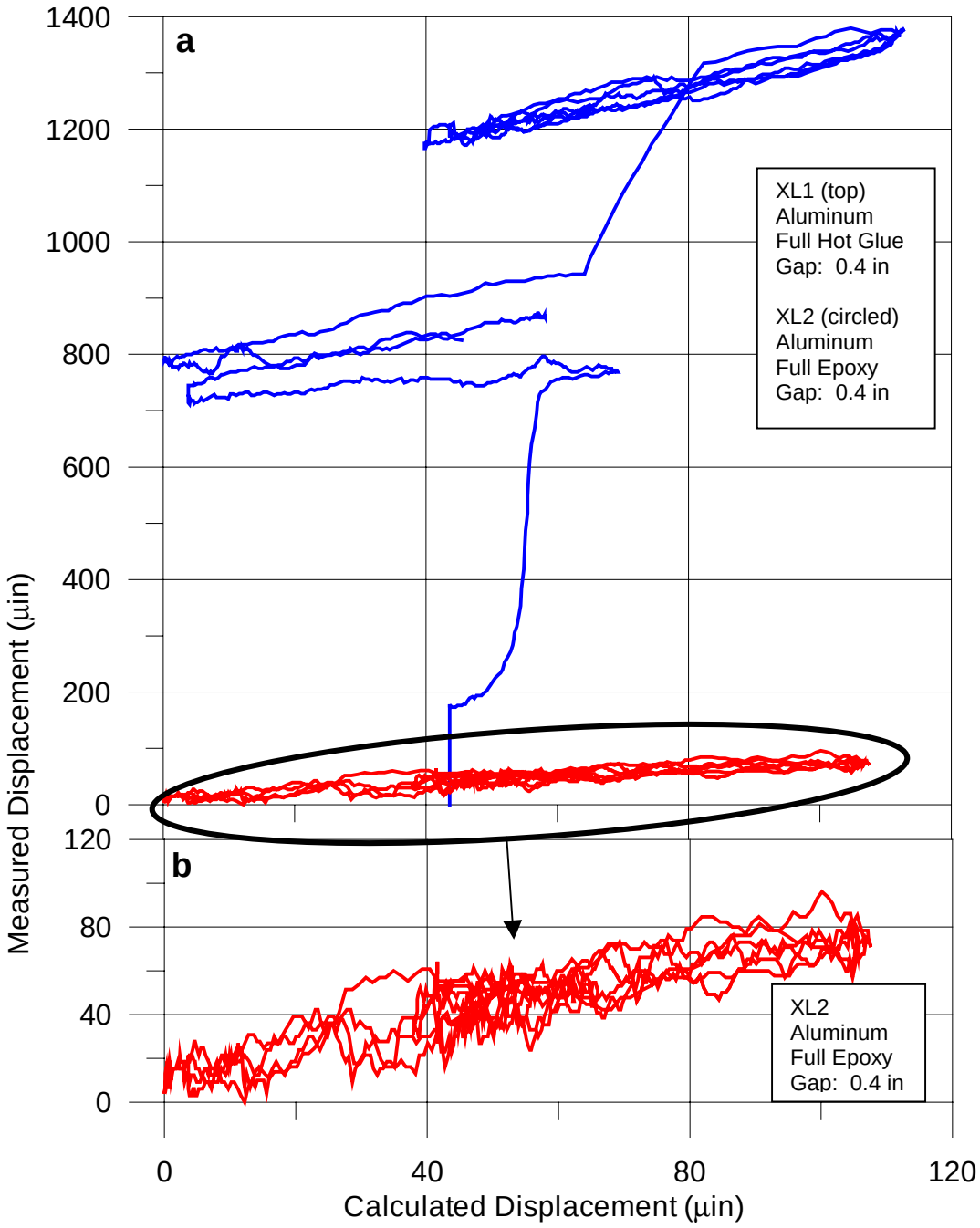

Figure A8. Comparison of adhesive attachment to aluminum plate. a. XL1 attached with ordinary "hot glue" with significant nonlinearity in wandering hysteretic loop between 700 and 950 µin, large nonlinear jumps before and after; compared to XL2 performance (circled). b. XL2 hysteretic loop magnified from A7a, showing XL2 performance relatively unchanged from System X sensors on Aluminum (see Figure A2).

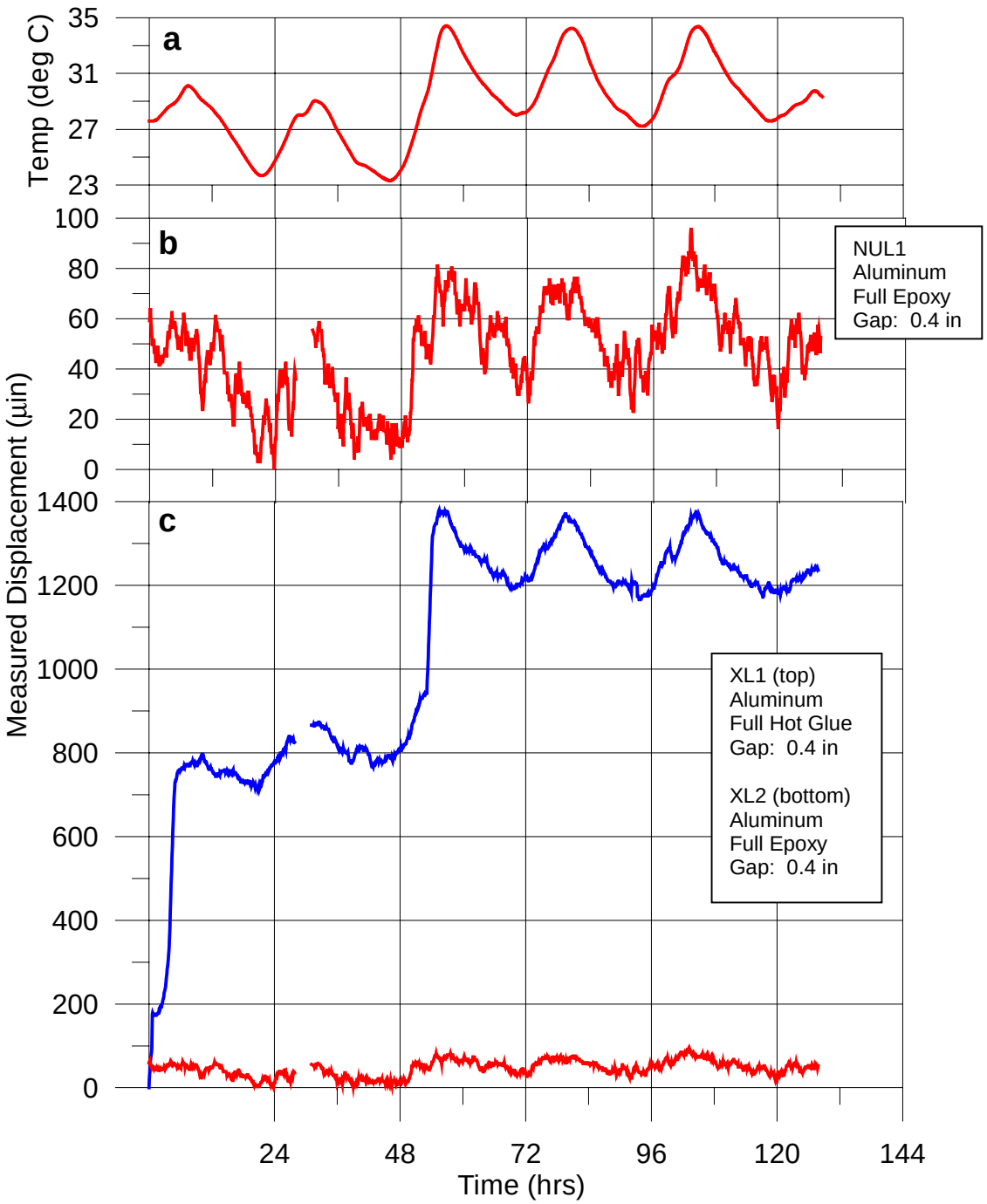

Figure A9. Time history plots of temperature and the same System X displacement data as in Figure A8. Gaps occurred when power was accidentally cut and later restored. a. Temperature, with a large sudden increase at hour 48. b. XL2 time history which tracks closely with temperature. c. Comparison of XL1 attached with ordinary "hot glue" (top plot) with nonlinearity in two places, at the beginning when the glue is hardening and during the large, rapid temperature increase near hour 48. This indicates heat instability, as does the excessive magnitude of temperature-change-tracking peaks and valleys for XL1, on the order of 200 µin, four times larger than those of XL2 despite identical gap widths for both sensors.

range of less than 2°C over several hours, likely the hardening and "settling" of the hot glue. The second radical nonlinearity occurs during a two-hour increase of almost 12°C,during which the hot glued sensor system displaces radically, by 600μin, as compared to XL2's displacement of 65 μin. Returning to Figure A8a, it is possible to see the two departures from linearity by XL1, whereas XL2 linearity is unaffected, as the large temperature swing is simply incorporated invisibly into the data, indicating the epoxy adhesive is allowing XL2 to measure accurately.

Outside interference such as magnetism can also impair ACM data, as standard ACM micro-measurement instruments rely on electromagnetic field change measurements for displacement data; Figure A10 shows how magnetism can degrade data collection.

As discussed earlier, longer rods seemed to make for less responsive LVDTs. The factory-standard Trans-Tek rods are threaded only near the top and made of brittle non-magnetic stainless steel. It was decided to thread the arm almost down to the core, to allow the thread-tapped target bracket to move farther down the rod and therefore closer to the coil, resulting in a smaller gap between target bracket and coil. While attempting to thread several such rods farther down their bodies, several were broken.

As a result, it was decided to buy cores without arNU from Trans-Tek and to replace the factory-stock rods with nonmagnetic stainless steel screws. This is standard procedure for NU Macrosensors LVDT cores, which have no rod and contain threads inside for attachment to a rod, an 18-8 stainless steel 4-40 tap screw. The core and screws are held together with thread-locking compound. Obtaining a threaded core from Trans-Tek and attaching it to a screw seemed a logical solution; unfortunately, the 18-8 stainless steel affected the Macrosensors far worse than was expected, given that 18-8

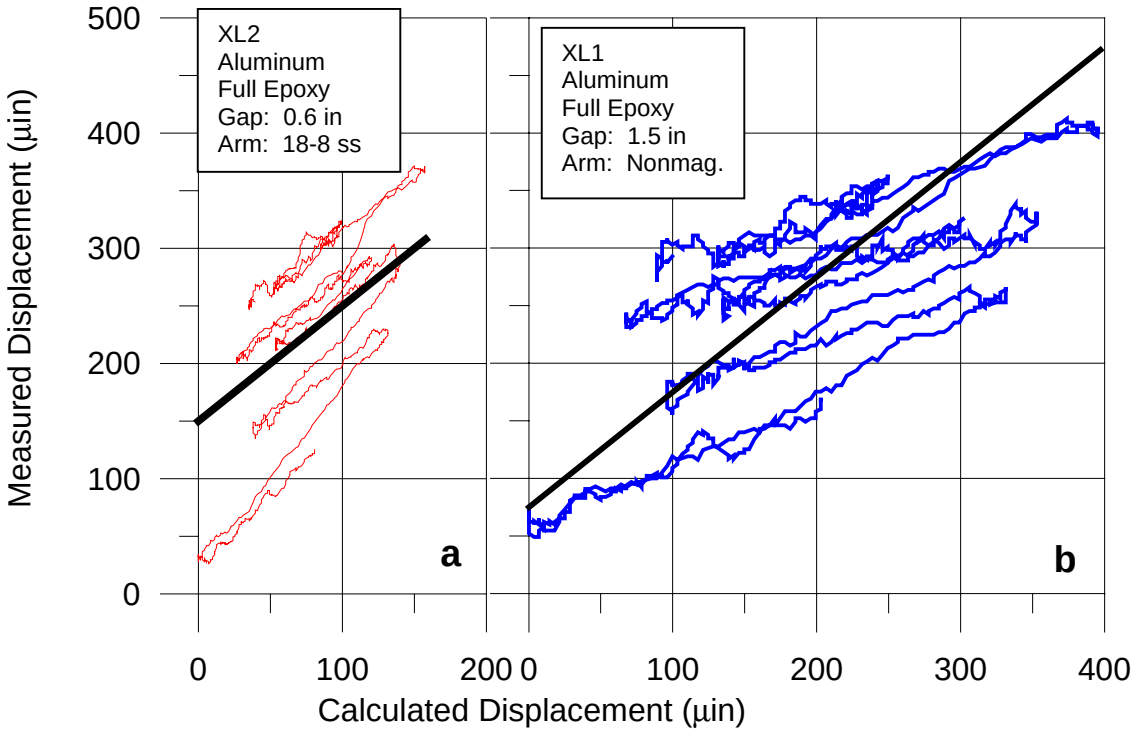

Figure A10. Effects of magnetic interference on LVDT performance. Even though only XL2 had a rod which interfered magnetically with this type of LVDT, both sensors in the test were affected. a. XL2 with 18-8 stainless steel screw as its core-holding rod. b. XL1 with its Trans-Tek factory stock nonmagnetic 312 stainless steel rod.

gives no trouble with Macrosensors LVDTs. However, the tiny 1-72 thread for the Trans-Tek core limited available material types; only the "mildly magnetic" (as described in supply house descriptions) 18-8 stainless steel, the same material as in NU Macrosensors LVDT screw rods, was readily available. As Figure A10 shows, 18-8 stainless steel apparently contains enough magnetic material to disrupt the small, delicate field of an LVDT. Both XL1 and XL2 were affected, even though only XL2 had the only 18-8 rod; XL1's rod was factory-stock 312 nonmagnetic stainless steel.

Such "wandering" behavior is unacceptable because though the material is linear, the sensor data is not, unacceptable for ACM because it becomes impossible to determine where the data is centered. The α-derived slope, the straight heavy line in Figure A10,

becomes irrelevant for comparison, and “best fit” line and standard deviation from that line become meaningless.

The test whose data is shown in Figure A10 did not differ from any other test in either mounting or data recording techniques. Therefore, it must be assumed that the replacement arm was causing magnetic nonlinearity. Custom-made short rods were ordered from Trans-Tek to solve the non-responsiveness problem.

No real-world system will be perfectly linear, and its data will not follow the ideal, or even its best-fit line, perfectly; however, data must be consistent and reproducible. Some deviation from ideal is acceptable, if understood and consistent. Performance tendencies, including attachment irregularities, must be known before an ACM system is deployed; if the system is inconsistent, it cannot be applied to ACM measuring.

One way to observe irregularities is the difference between the α-predicted slope and the best-fit line for a data set. Since sensors are typically deployed in pairs (a null sensor for an intact portion of the structure’s surface and a crack sensor to span the crack), it see NU appropriate to compare their performance to each other. Therefore, the slopes of the best-fit data lines for each center were determined and the quotient of the sensor with a consistently larger slope (numerator) and smaller slope (denominator) was taken.

Figures A11 and A12 demonstrate such consistency testing for the sensors on both test surfaces. For aluminum, only the NU system was considered, and its sensors are consistent, seen in Figure A11. During the first three tests, the ratio of NUL1 to NUL2 best fit lines seem centered around 1.2; though there are only two points, the consistent trend near a single ratio value appears to continue, in this case at 1.5.

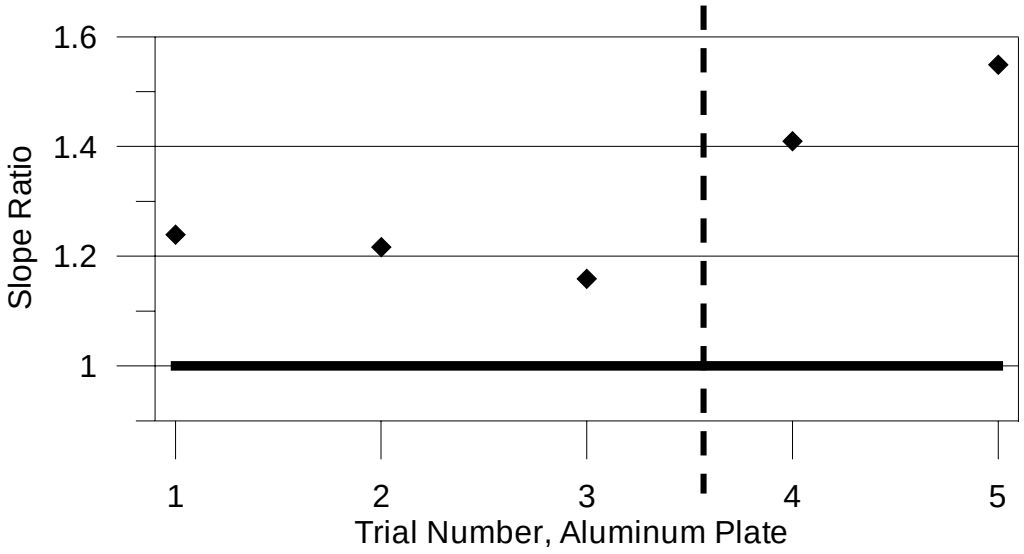

Figure A11. Slope ratios for NU LVDTs during aluminum plate tests. The slope for each sensor is determined from $\delta_{measured}/\delta_{calculated}$; then, since the sensors are always deployed in pairs, the ratio is taken of the sensor with the consistently higher slope with the second sensor.

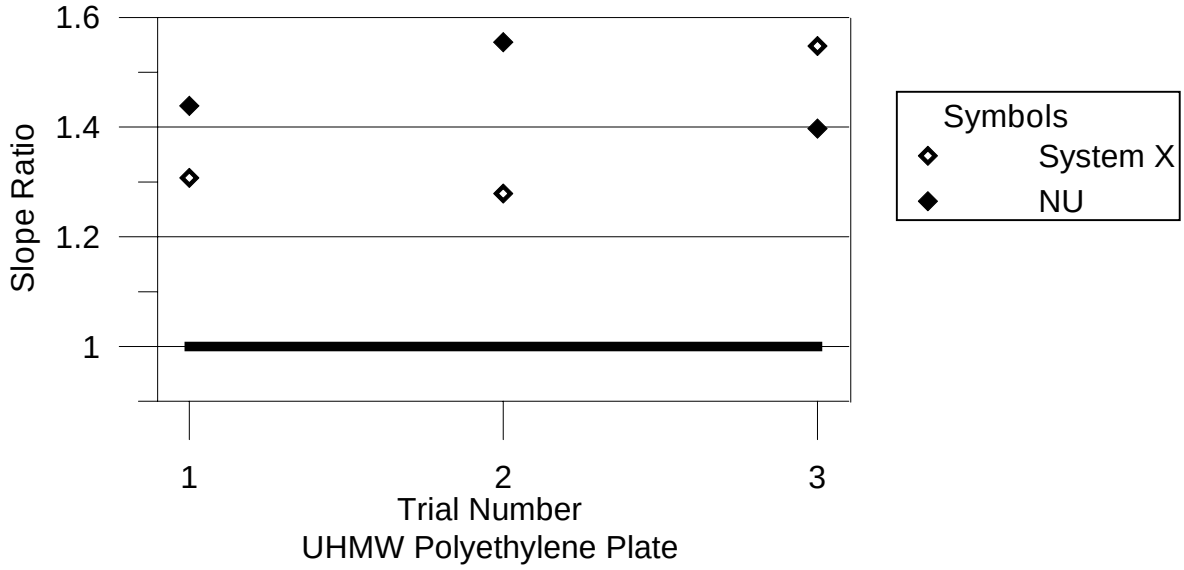

Figure A12. Slope ratios for NU and System X LVDTs during UHMW-P plate tests. The slope for each sensor is determined from $\delta_{measured}/\delta_{calculated}$; then, since the sensors are always deployed in pairs, the ratio is taken of the sensor with the consistently higher slope with the second sensor.

Similar consistency was found for the NU sensors on the UHMW-P plate tests, and System X appeared consistent, with only slight and deviation; Figure A12 summarizes the results. The NU sensors appear centered at roughly 1.5, and there appears to be no indication of a trend of departure from this pattern. The System X sensors are consistent during the first two tests, with a ratio around 1.3. The sensor- input channel swaps (XL1 into channel 2 and vice versa) during the third test appear as a changed response which though noticeable is not large.

Conclusion

Numerous laboratory and data analysis methods were tested to determine the best method for determining linearity. The results of these efforts appear above. It was found that the LVDTs performance was consistently linear on linear materials, which is of crucial importance because reliable ACM relies on sensor stability. Several factors which adversely affect system performance such as magnetism and high-α adhesive were also found. Data analysis methods and results, both analytical and empirical, justify the conclusion that a properly-built LVDT-based ACM system can be shown to be linear and consistent and therefore qualified for field installation with uncomplicated tests.

Table A1: summaries of plate test results

A1a. Aluminum plate tests, α = 13.1 μin/in/°F

Test Dates and System	T max|min °C	T max|min °F	ΔT F (top),C	Sensor	Gap in	$\delta_{calculated}$ μin	$\delta_{measured}$ μin	Best Fit Line Slope	Best Fit Slope ratio
18-29 July									
SYSTEM X	32.9	91.3	24.3	XL1	1.53	487	216	0.362	
	19.4	67.0	13.5	XL2	1.46	465	402	0.777	2.15
NU	32.9	91.3	24.3	NUL1	0.42	134	356	2.685	
	19.4	67.0	13.5	NUL2	0.40	127	263	2.166	1.24
29 Jul – 4 Aug									
SYSTEM X	32.1	89.8	20.1	XL1	1.51	397	NA	NA	
(magn. interfer.)	21.0	69.7	11.2	XL2	0.60	158	NA	NA	NA
NU	32.1	89.8	20.1	NUL1	0.42	110	305	2.672	
	21.0	69.7	11.2	NUL2	0.41	108	238	2.196	1.22
8 – 12 August									
SYSTEM X	30.2	86.4	13.2	XL1	1.50	259	97	0.351	
	22.9	73.2	7.3	XL2	0.43	74	39	0.353	0.99
NU	30.2	86.4	13.2	NUL1	0.41	71	164	2.660	
	22.9	73.2	7.3	NUL2	0.41	71	194	2.295	1.16
12 – 20 August									
SYSTEM X	33.6	92.6	16.4	XL1	1.51	324	79	0.138	
	24.5	76.2	9.1	XL2	0.43	91	120	0.910	
NU	33.6	92.6	18.9	NUL1	0.42	104	158	2.235	
	23.2	73.7	10.5	NUL2	0.41	101	214	1.585	1.41
22 – 28 August									
SYSTEM X	34.43	93.97	20.02	XL1	0.43	113	NA	NA	
(XL1 hot glue)	23.30	73.94	11.1	XL2	0.41	108	96	0.539	NA
NU	34.43	93.97	20.02	NUL1	0.42	110	161	2.200	
	23.30	73.94	11	NUL2	0.41	108	245	1.420	1.55

A1b. Ultra-High Molecular Weight Polyethylene plate tests, α = 110 µin/in/°F

Test Dates and System	T max|min °C	T max|min °F	ΔT F (top),C	Sensor	Gap in	$\delta_{calculated}$ µin	$\delta_{measured}$ µin	Best Fit Line Slope	Best Fit Slopes' ratio
28 Aug – 3 Sep									
SYSTEM X	32.1	89.8	25.6	XL1	0.42	1184	1698	1.459	
	17.9	64.2	14.2	XL2	0.40	1128	1159	1.116	1.31
NU	32.1	89.8	25.6	NUL1	0.53	1494	541	0.391	
	17.9	64.2	14.2	NUL2	0.42	1184	620	0.563	1.44
3 – 9 Sep									
SYSTEM X	30.9	87.5	27.2	XL1	0.42	1255	1747	1.348	
	15.8	60.4	15.1	XL2	0.38	1135	1246	1.054	1.28
NU	30.9	87.5	25.6	NUL1	0.56	1673	578	0.347	
	15.8	60.4	14.2	NUL2	0.42	1255	685	0.539	1.55
9 – 15 Sep									
SYSTEM X	27.8	82.1	19.9	XL1	0.42	918	1300	1.372	
	16.8	62.2	11.0	XL2	0.38	831	809	0.886	1.55
NU	30.9	87.5	27.2	NUL1	0.56	1224	403	0.310	
	15.8	60.4	15.1	NUL2	0.42	918	442	0.434	1.40

Appendix B

Field Testing

Introduction

Determining ACM system field performance is the most important part of the qualification process. System X sensors were installed alongside NU sensors in an occupied residence, a longstanding NU test site (Siebert, 2000; McKenna, 2002). ACM system performance in benign laboratory-type conditions on a linear material with no extraneous factors is only the first step. Having passed the laboratory portion of qualification, System X was ready for evaluation under actual field conditions likely to be encountered during commercial monitoring. Data herein cover winter and early spring 2004, a time of harsh weather and numerous unpredictable factors including thermal and humidity modification by a furnace, humidifier, winds, etc.

Experimental Setup

System X crack and null gauges were mounted on a ceiling crack to compare System X performance with those of the NU Kaman eddy-current sensor (chosen as the baseline) and Macrosensors DC-750 LVDT already deployed on the ceiling. The

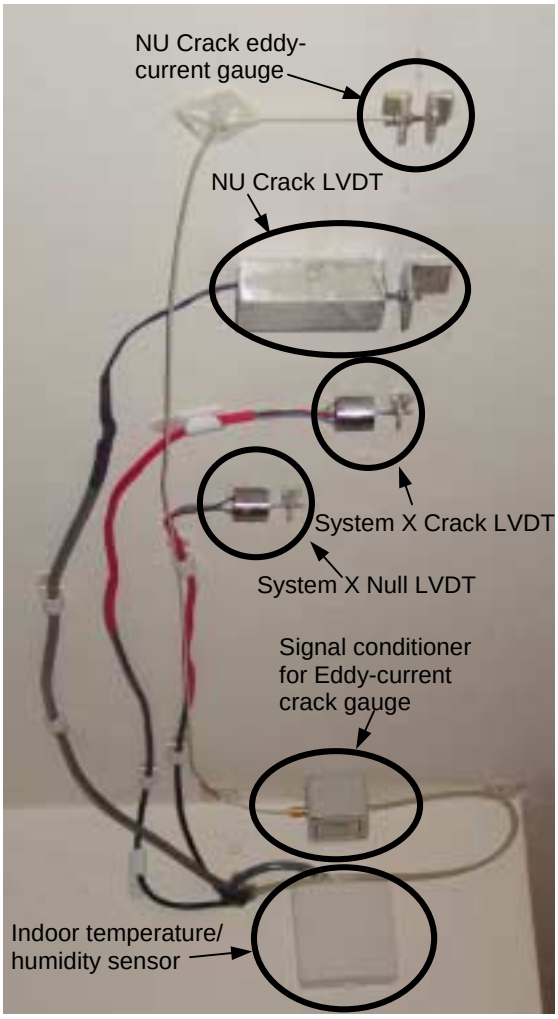

Figure B1. Sensors on ceiling crack at field test site, house near quarry, Franklin WI.

photograph of the setup appears in Figure B1. The NU eddy-current crack gauge (NUEC) was defined as the baseline because of its minimal vulnerability to thermally-induced behaviors associated with metal-rod LVDTs.

System X was attached to the ceiling with 90-second quick-drying epoxy, with System X Crack LVDT (XLC) spanning the crack, and XLN (System X Null) nearby as seen in Figure B1. The Null sensor mounted on an intact portion of the test surface has two purposes: to verify that the surface material, itself contributes little to the crack displacement, and to adjust the performance of the crack sensor for attachment effects to yield net crack movement. Placing the null sensor was relatively easy; placing the crack sensor was more difficult. Ceiling cracks tend to bow out more than wall cracks at their edges, and a certain amount of maneuvering was necessary to find a position for the XLC arm perpendicular to the crack, such that core and arm moved smoothly back and forth without binding inside the coil. Proper alignment is crucial because offset or skewing from perpendicular will result in angle-offset displacement data.

Installation and Maintenance

When System X was deployed in November 2003, a familiarization process initially ensued; the system appeared to be functioning properly in histogram mode, and in late December the data logger was returned to the manufacturer for installation of a developmental Level III trigger. Soon thereafter, in early January, actual experimental data gathering commenced, when the NU sensors were brought fully on-line. At this site, NU sensors were connected for the first time to an eDAQ, which was linked via Ethernet port to a cable modem, and data was downloaded by an NU computer over the internet. All previous data collection was with a 2100 system downloaded to NU via phone line. The eDAQ collection from NU sensors became fully operational in late December.

System X was designed for onsite downloads only; the manufacturer conceives a technician with a laptop computer and proprietary System X download software making rounds of System X installations and downloading the data individually at each site. The conscious decision to omit remote data downloads appears vindicated; NU researchers encountered numerous technical and administrative difficulties developing an internet-based method. The time and manpower required would be excessive for a commercial ACM, especially for numerous sites. NU difficulties included late arrival of the cable technician, administrative confusion surrounding upgrade of the home's existing cable television service to internet, unpredictable outages resulting in data losses, difficulties with billing, and numerous minor issues which were a nuisance to the householder and a time-consuming distraction to NU researchers. The most serious issue, cable communication outages, interrupted data collection and occasionally resulted in loss of information for several days. After more than a month of manpower-intensive

modifications, the NU automated data download became reliable, though still occasionally requiring human intervention. For an ACM system whose data may have legal implications, as little disruption as possible is crucial to the credibility of the system's data.

System Characteristics

The NU ACM system is connected both to blasting detection and crack sensors. A geophone in the yard of the house detects three channels of ground particle velocity (lateral, transverse, and vertical); a microphone detects air blast intensity. Ground motion above 0.04 inches per second (ips), the blasting industry standard detection threshold, triggers a three-second, 1000 Hz Level II recording mode for all crack and null sensors. This combined Level I / II monitoring requires complex wiring illustrated in Figure B2a-c.

Figure B2. NU data logger system installation, Franklin WI. a. Cabinet in basement showing interior and input/output wires; b. detail of interior; c. detail of cabinet top, showing communication wiring links into cabinet.

System X has a “dual” collection mode, which is designed to mimic the Level I/II collection of the NU systems. Dual mode includes both Histogram (Level I) Trigger (Level III) modes. Histogram mode is set in the normal way, with one of 14 pre-set collection periods varying from one point per second to one point per hour. Level III has a number of user-selected options to program response and recording for seismic events. There is also a capability enabling Level II triggering from a geophone, but it was decided to test this configuration at a later date.

Though System X has a nominal Level III capability, it was discovered that its crack-activated ACM-unique trigger is insufficiently developed for evaluation. Even NU systems do not have this capability, and the technology still requires development before it is sufficiently simple for installation into a compact, self-contained. The only difference between Levels II and III are the triggering method. Level III is triggered when quasi-instantaneous crack displacement exceeds an operator-selected threshold at certain preset levels of displacement. While this triggering technique is self-contained and does not require outside sensors as does Level II monitoring, it does require memory and processing capabilities. However, its self-contained nature, independent of geophones, is a crucial element of the simplicity needed for commercial monitoring.

Since Level I environmentally-induced displacement predominates crack displacement, Level I capability was assessed. All data reported are for Level I monitoring. No Dual or Trigger mode data was collected.

Crack Behavior: long-term (four-month)

Qualifying a new ACM system in the field requires accurate environmental data and already-qualified sensors for comparison. Environmental factors and system

performance are summarized in Figure B3 for the four-month trial period; gray lines represent hourly plots of one-hour rolling averages; the black lines, hourly plots of 24-hour rolling averages. The one-hour average depicts often-large daily variations in temperature and humidity, while the 24-hour average removes the jaggedness of hourly fluctuations, producing representation of weather trends or fronts. National Weather Service data for average daily high and low temperatures appears as dashed lines in Figure 3a. The colder-than-normal winter is beneficial for testing System X, as it produced greater changes in the ceiling temperature than might otherwise be the case.

Since ACM systems must be able to measure changes in displacement under varying environmental conditions without being affected themselves, it is appropriate to compare their performance to environmental factors, and sensor behavior appears in Figures B4-B7. Figures B4-B7 display the arch-like appearance for all three crack sensors, NUEC, NU crack LVDT (NULC), and XLC, while Figure B8 shows a similar plot from earlier work. The arch-like appearance effect does not appear to correspond directly either to temperature or humidity. Although the indoor temperature and humidity follow their outdoor counterparts at least to some extent when observed over the course of several weeks. However, none of the environmental factors appears to influence the shape of the crack displacement curve directly until spring, during the final six weeks of data collection.

During the winter, the indoor temperature is essentially constant with little variation as a thermostat regulates furnace operation. Besides increasing heat and temperature, the furnace also dries the air, which greatly impacts indoor humidity. Even though the householder frequently ran a humidifier, it is likely that the decreased humidity affected the moisture content of the wood. This winter heating effect is discussed in detail

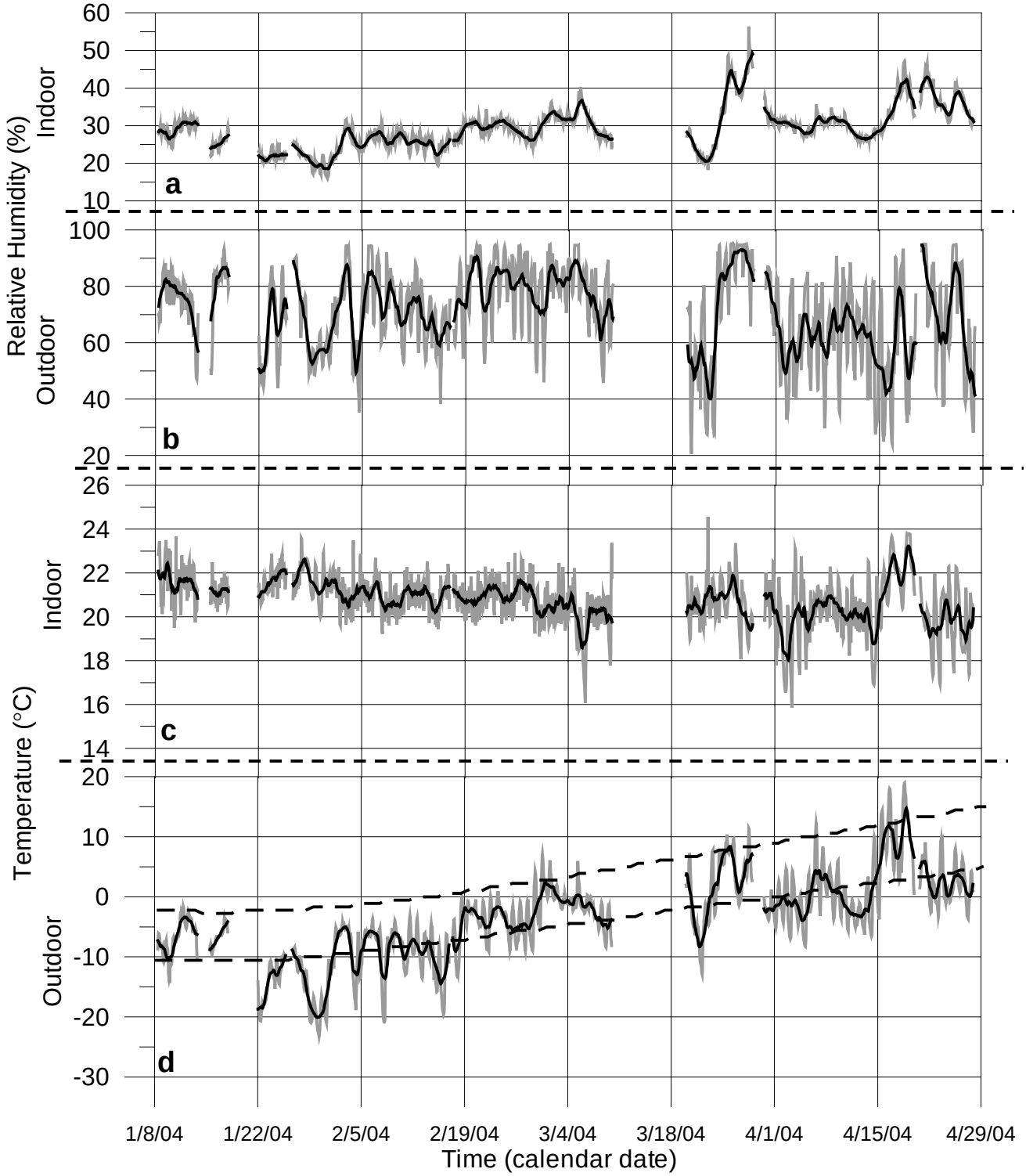

Figure B3. Environmental factors time histories for 4-month field test period. Gray lines are one-hour rolling average; black lines, 24-hour rolling average. Temperature and Humidity patterns follow each unevenly; indoor and outdoor patterns of temperature and humidity respectively parallel each other more closely. a. Indoor relative humidity; b. Outdoor relative humidity; c. Indoor temperature; d. Outdoor temperature, with National Weather Service high/low averages shown as dashed lines.

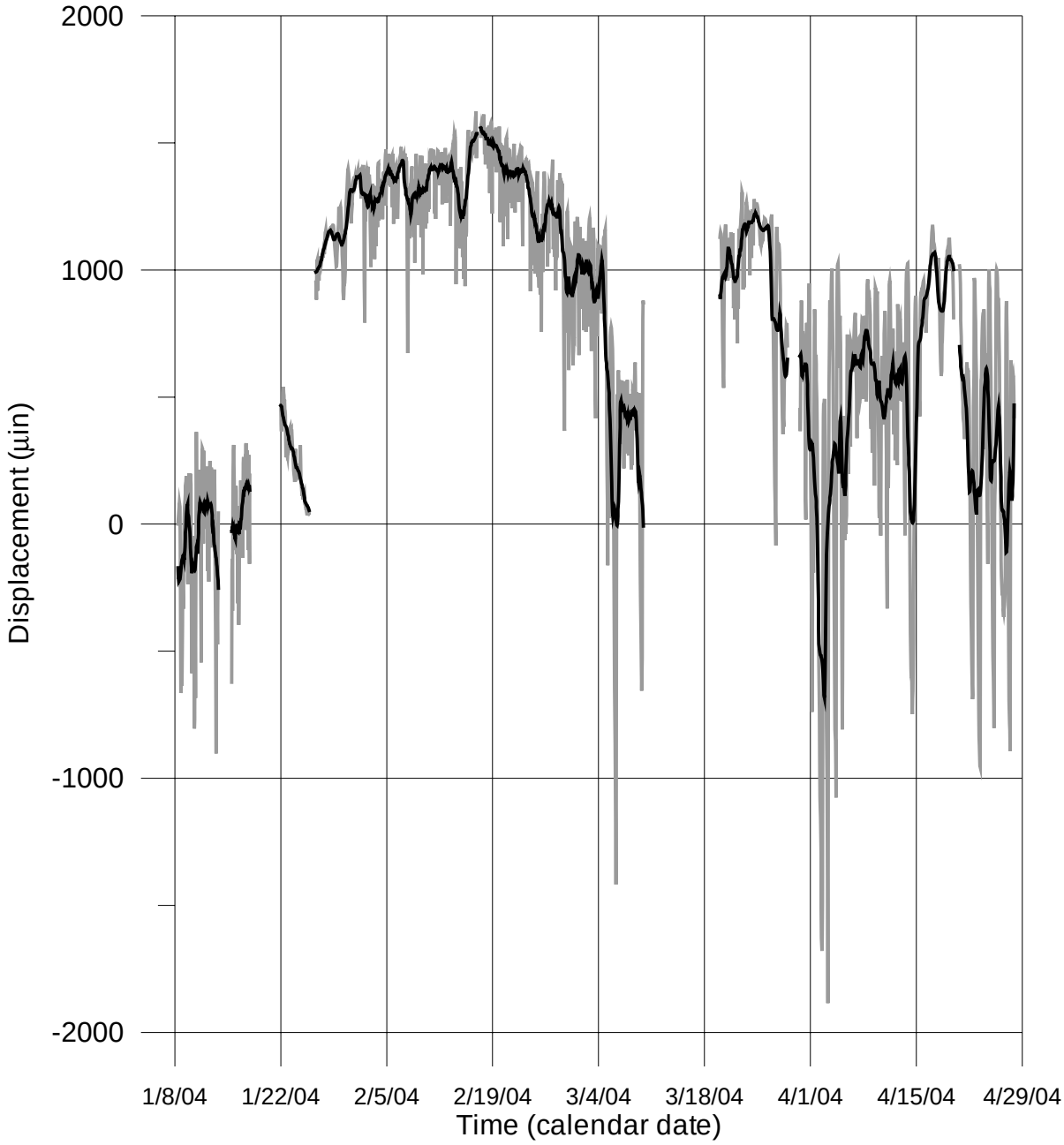

Figure B4. NU Eddy-current crack gauge (NUEC) baseline sensor data. This is the "true" baseline displacement time history for 8 January – 27 April 2004, against which all other sensors during these trials will be compared. Gray lines are one-hour rolling average; black lines, 24-hour rolling average.

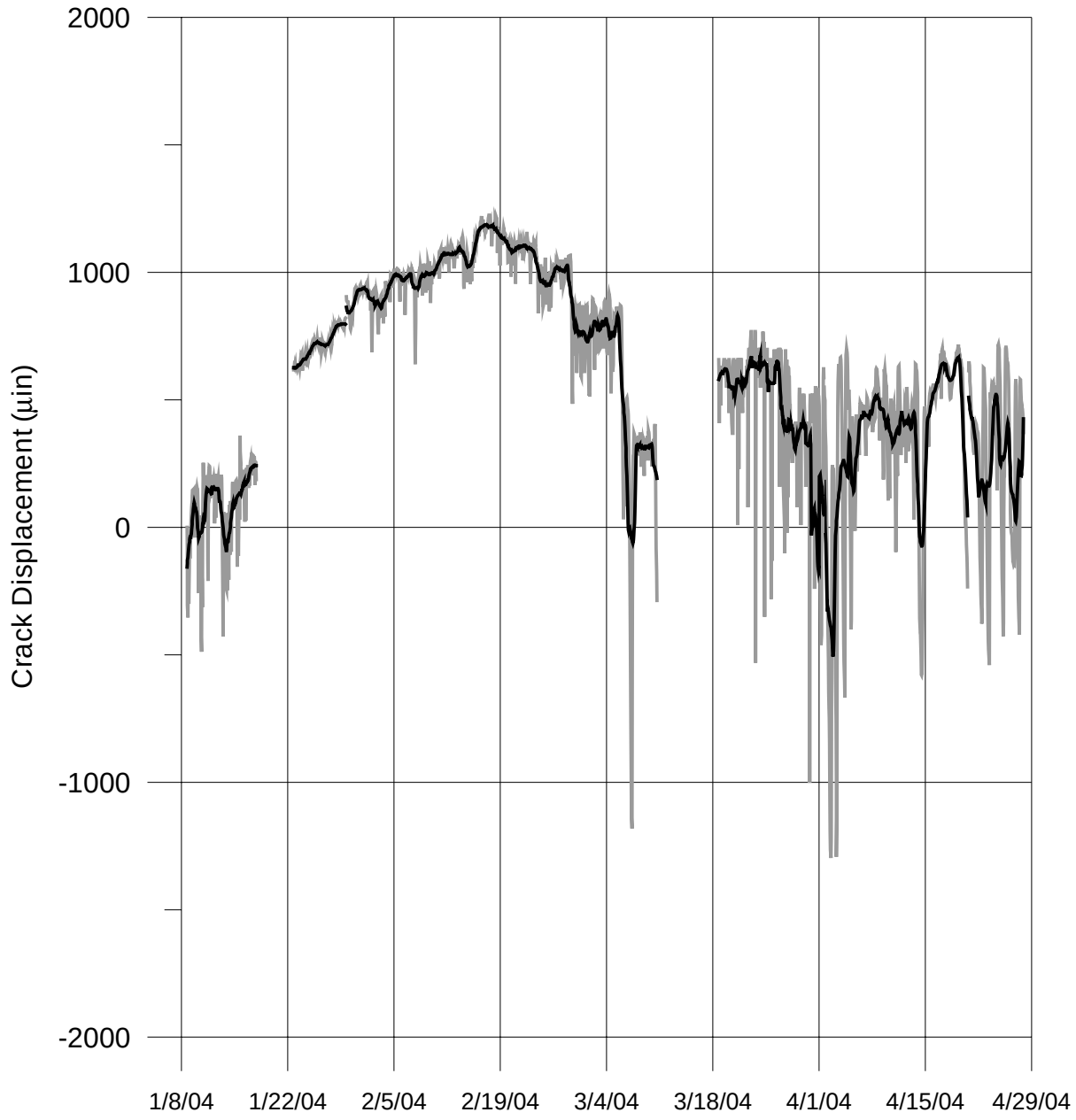

Figure B5. System X crack LVDT (XLC) displacement time history, 8 January – 27 April 2004. Gray lines are one-hour rolling average; black lines, 24-hour rolling average.

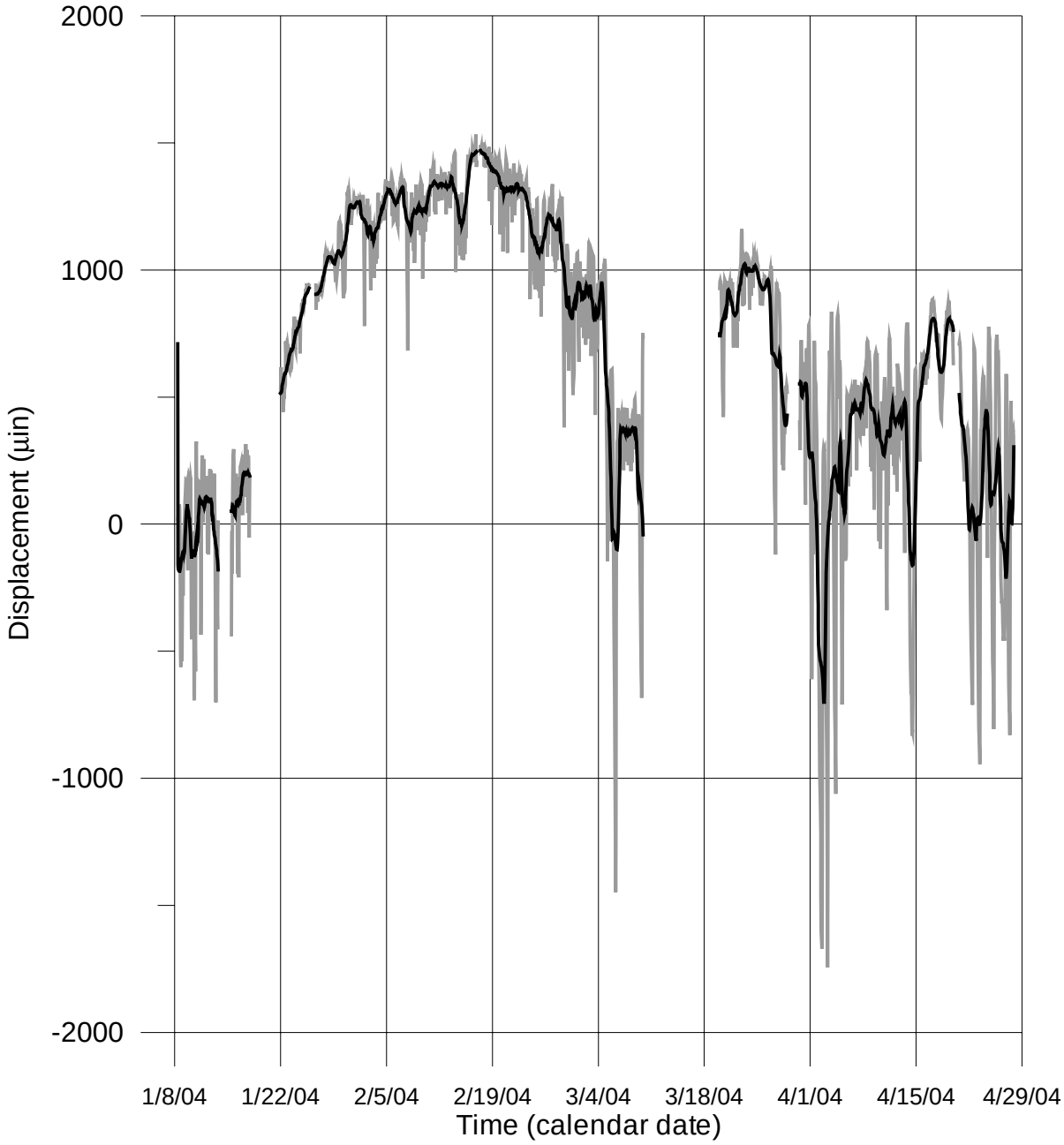

Figure B6. NU crack LVDT (NULC) displacement time history, 8 January – 27 April 2004. Gray lines are one-hour rolling average; black lines, 24-hour rolling average. This plot is very similar to the Figure B4, NUEC results.

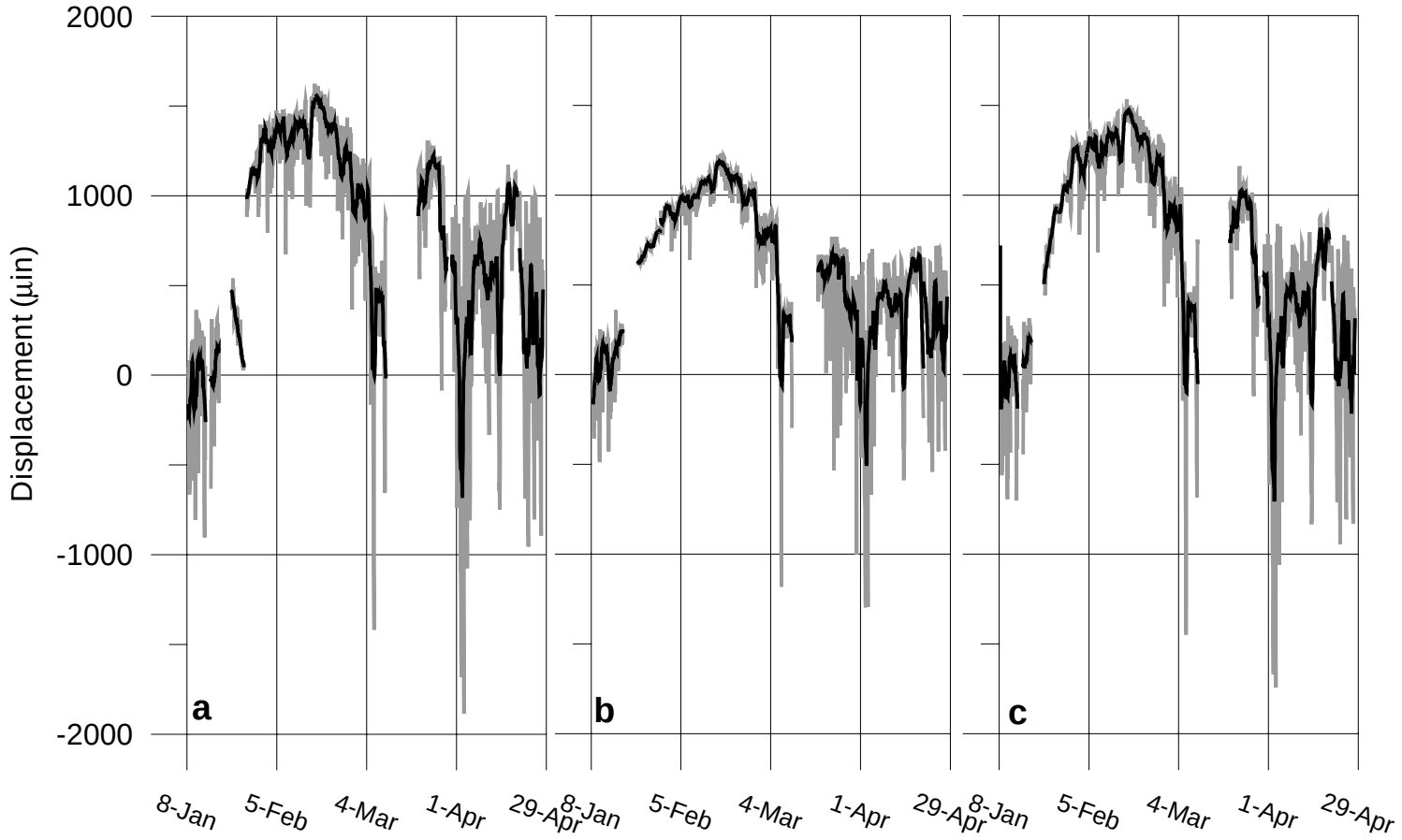

Figure B7. Figures B4-6 displayed side-by-side for comparison. a. NU eddy-current (NUEC) baseline sensor; b. System X (XLC); c. NU LVDT (NULC). Note that XLC and NULC have displacement patterns almost identical to that of NUEC. This verifies that LVDTs are appropriate for ACM, and that System X is adequate for Level I monitoring.

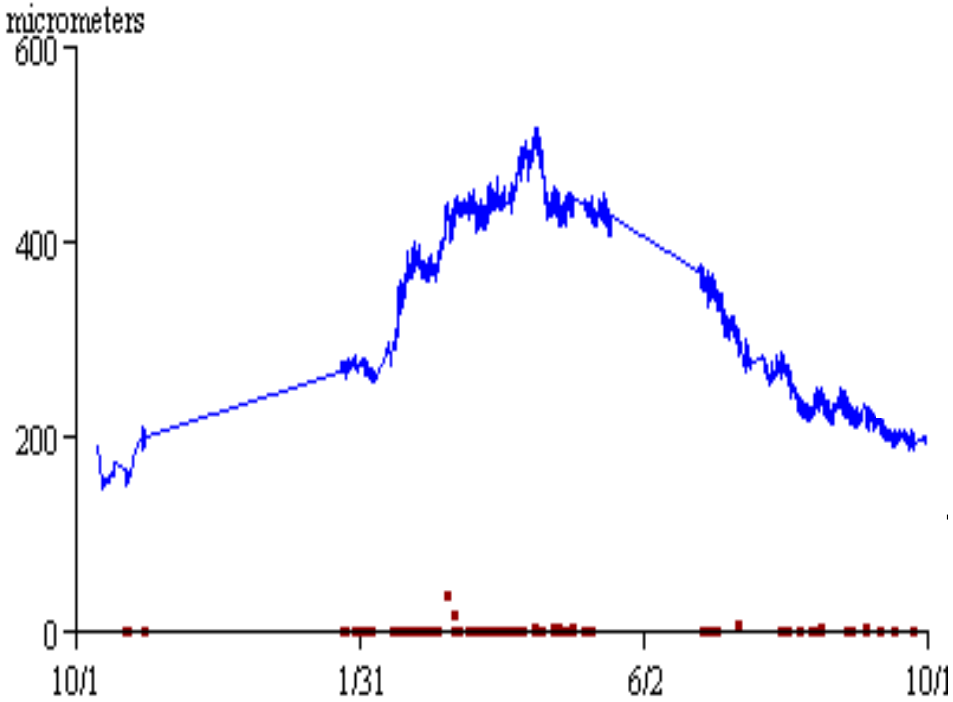

Figure B8. Up-and-down arch-like crack trend from the Franklin House site, from previous work, yearlong measurement.

in the Siebert thesis (Siebert, 2000).

As the weather becomes milder, furnace heating and humidifier operation decrease. At the same time, opening windows and doors to the outside increases the influence of outdoor temperature and humidity by allowing indoor conditions to come closer to equilibrium with outdoor conditions. Even more important, the magnitude of the proportion of indoor changes to corresponding outdoor changes will increase. Thus, the patterns will match more closely, although the magnitude of outdoor changes will still be several times larger than those indoors.

This relationship between indoor and outdoor factors is best seen with indoor temperature. Although there is always a connection between the changes of outdoor and indoor temperature, it is more tenuous during winter. During the winter months, peaks and valleys representing change in outdoor temperature are reflected indoors only at a miniscule scale. Starting 18 March 2004, indoor and outdoor temperature changes begin to correspond to one another more closely in magnitude than previously, although in the house the peaks and valleys remain smaller, as might be expected for an insulated structure.

During the "winter data" period of 8 January – 18 March 2004, the crack displacement pattern is likely a function of numerous factors acting together. The consistency of previous work and all three current sensors is likely dominated by the constant winter heating in an environment which is almost totally isolated from the outdoors.

Collection consistency

During the period 18 March – 1 April 2004, System X was set to collect data at one point per minute (ppm), but somehow reset itself without human intervention to collect data

at one point per hour (pph). Although this greatly reduced required memory, it also brought to light several heretofore unobserved collection issues.

As has been discussed elsewhere, although System X is in general adequate for ACM, its data collection channels suffer from intrusion by random noise spikes. The data recording methodology is to sample at 1000 Hz and choose the peak voltage value (which is converted to displacement) for a given period; at a collection rate of one ppm, the peak of 60,000 points is recorded, but for one pph, the peak of 3.6×10^6 points is recorded. During one pph collection, noise intrusion effects are greatly exacerbated: a spike during a given one-hour period will always be collected, but at one ppm, it will be surrounded and mitigated by 59 other points, whereas it becomes the lone data point for one pph collection. Collecting long-term, single-point/non-averaged data at one-hour intervals is not recommended.

During the 18 March – 1 April 2004 period, many anomalous points crept into the data. The XLN channel was particularly affected by noise spikes; during pph collection, the XLN raw data is subject to anomalous jumps of 500 to 5000 μin. There are stretches where every third or fourth is anomalous, and the effects, even with averaging, overwhelm the data for that period. Figure B9a shows the gross effect, while Figure B9b shows a closeup with large deviations truncated. The influence of these spikes is apparent even on the 24-hour average. Therefore, the validity of XLN data during this period is difficult to determine, and is therefore not plotted on long-term representations. Table B1 shows raw data for a particularly noisy period and Figure B10a plots crack gauge data from Table B1, while Figure B10b shows plots one ppm collection for a similar period several days later.

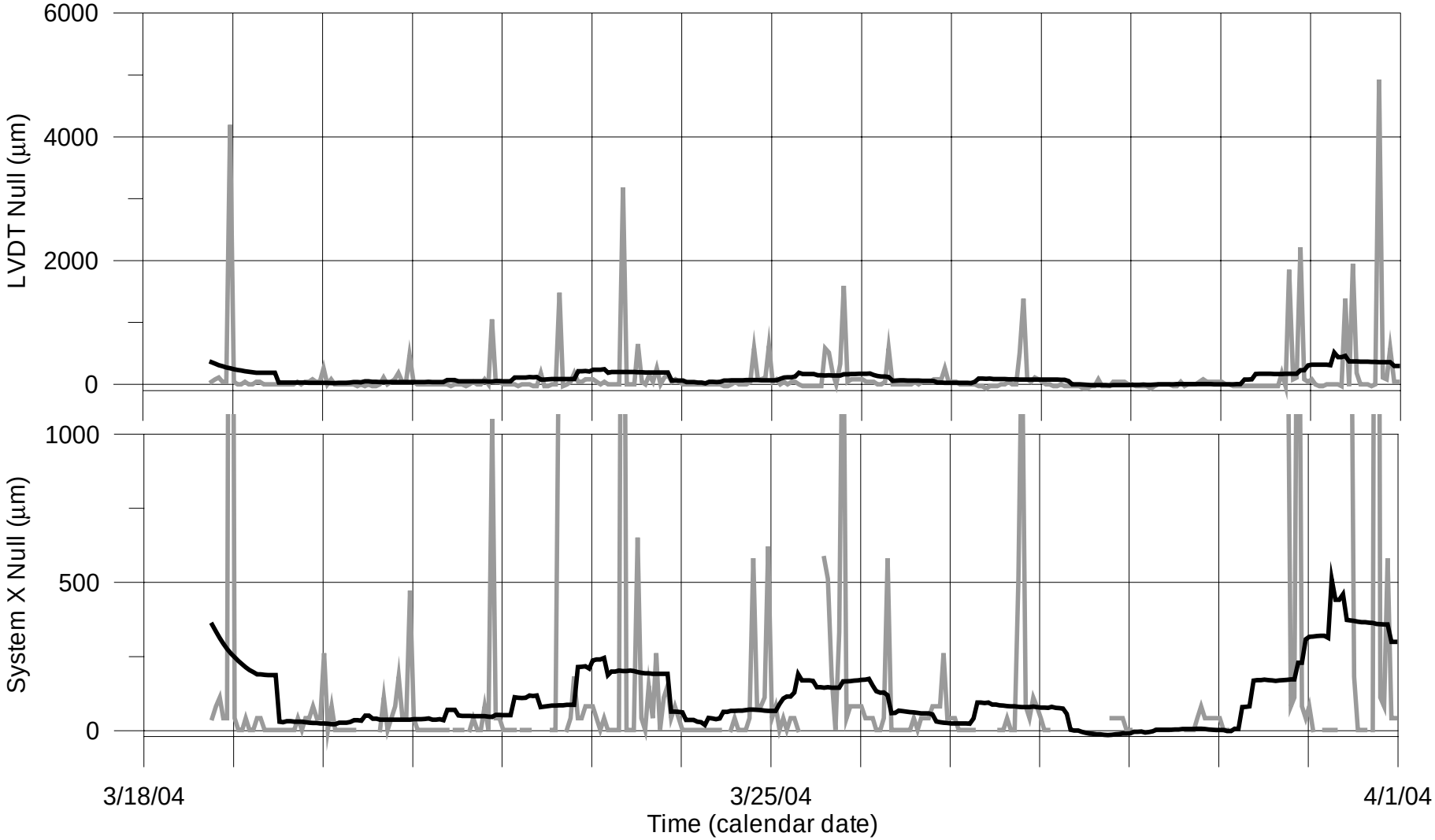

Figure B9. Effects of large noise spikes on data, XLN 18 March-1 April 2004, one point per hour data collection. Gray lines are one-hour rolling average; black lines, 24-hour rolling average. a. Entire range of y-values showing extreme effects of spikes on data. b. Truncated y-axis showing large influence of data spikes even on averaged data.

Time	System X Null mills	System X Crack mills
6:17:00	14.45	13.15
7:17:00	14.45	13.22
8:17:00	14.42	13.37
9:17:00	15.83	13.91
10:17:00	14.42	13.51
11:17:00	16.40	22.29
12:17:00	14.63	13.12
13:17:00	14.45	13.12
14:17:00	14.45	13.12
15:17:00	14.45	13.19
16:17:00	14.42	13.22
17:17:00	14.45	13.33
18:17:00	19.37	13.22
19:17:00	14.56	13.15
20:17:00	14.53	13.12
21:17:00	15.03	13.66
22:17:00	14.49	13.15

Table B1. System X data excerpt, 31 March 04; highlighted cells show exceptionally noisy data for both channels. Normally, the Null channel had far more anomalous points. The largest jump, in the Crack column between 11:17:00 and 12:17:00, is 9170 μin (233 μm).

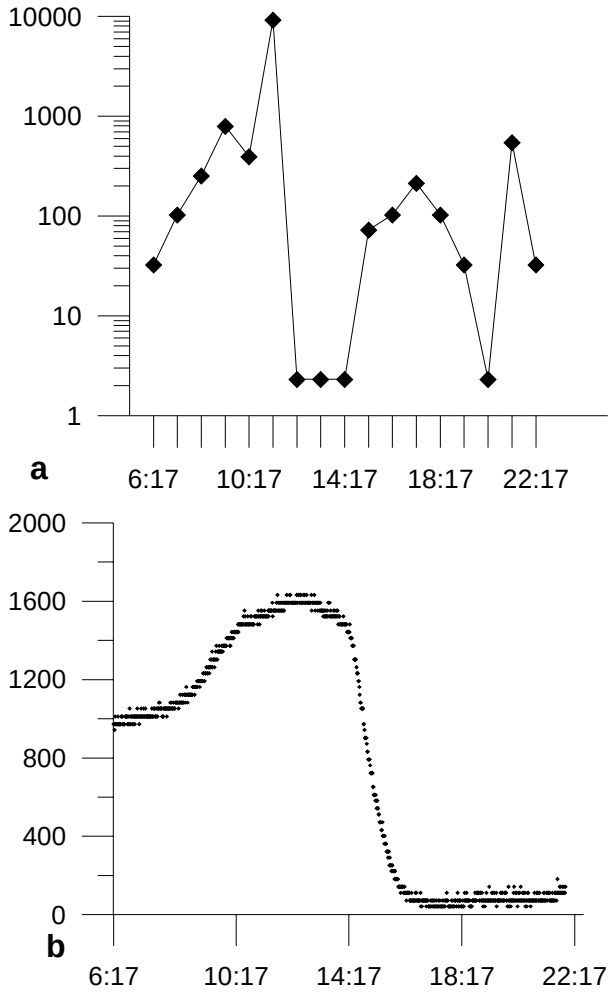

Figure B10. Collection method comparison; note different scales of plots. a. One point per hour, XLC data from Table B1. All points converted to μin and shifted to be greater than zero for plotting on logarithmic scales. b. Raw data for a similar 16-hour period, collection rate is manufacturer-recommended 1 ppm.

During the times in question, there was no blasting which could have contributed to the effects, and it is doubtful that any actions by the householder could have such large effects on the sensor: during tests on 29 January 2004, the ceiling was pounded heavily near the sensors, and neither XLC nor XLN showed any discernible reaction. Only inherent system noise could be responsible for these large departures.

Such anomalies serve to emphasize the importance of programming the ACM system to collect data within both its limits and its manufacturer specifications, whichever is more constraining. System X is designed for a collection frequency of one ppm. Collecting more frequently would be beneficial to the data, although such collection would tax the system's capability: one ppm allows three weeks of data storage, while the next, more frequent option, two ppm, cuts data capacity to ten days. Therefore, it is necessary to balance capacity, data density, and system capability. System X provided reasonably reliable data when programmed as intended.

For the XLN channel in particular, noise contamination persisted even at one ppm collection, manifested as large leaps by the gray one-hour average line from a plot which appears close to a horizontal line at this scale. Even the steadier black 24-hour average line is influenced by these significant leaps.

Focus: six-week "Spring Season Data Period," 18 March – 27 April 2004

Starting during the six-week period in Spring 2004, illustrated in Figure B11, the motion of the crack began corresponding closely to temperature patterns. As windows and doors were opened in milder weather, the influence of artificial environmental modifiers (furnace, humidifier, etc.) waned, leading to more synchronization of the crack with atmospheric influences.

The NUEC and XLC displacements closely follow temperature changes as seen in Figures B11a-c, with both sensors' peaks and valleys similar to those of interior temperature. Compared to Figure B11, Figures B4-7 are far more compressed in scale to fit all relevant data into space available. The data for the relevant time periods is identical in both plots; only the time scale is different, dramatically illustrating the importance of plotting results on a scale appropriate for the purpose. Although useful for assessing extended behavior patterns, long-term plots compress and distort data by sharpening extrema and obliterating smaller peaks and valleys. Small scale plots (more space allocated on the page per unit displacement) like Figure B11 are more faithful to minor peaks and valleys, while large scale plots like Figures B4-7 are useful for comparing long-term, "big picture" behavior of two or more sensors.

An important consideration is the magnitude of overall displacements in relation to typical anomalies. Figure B10b demonstrates the relative unimportance of noise when such anomalous points (such as one such point noticeably above the other points in the vicinity of time 22:17) are far smaller than overall displacement, and do not stand out much from the overall pattern. Figures B4-7 and B11b-c show that when noise points are much smaller in magnitude than typical gross displacement, noise has no discernible effect on averaged data.

Figures B11b and B11c also demonstrate that XLC displacement pattern is nearly identical to that of NUEC, even though XLC is less responsive and the magnitudes of its peaks and valleys are noticeably smaller. This discrepancy is somewhat mitigated by the 24-hour average, which by its nature flattens extrema. The close agreement in pattern, if not quite in magnitude, validates System X for Level I crack monitoring.

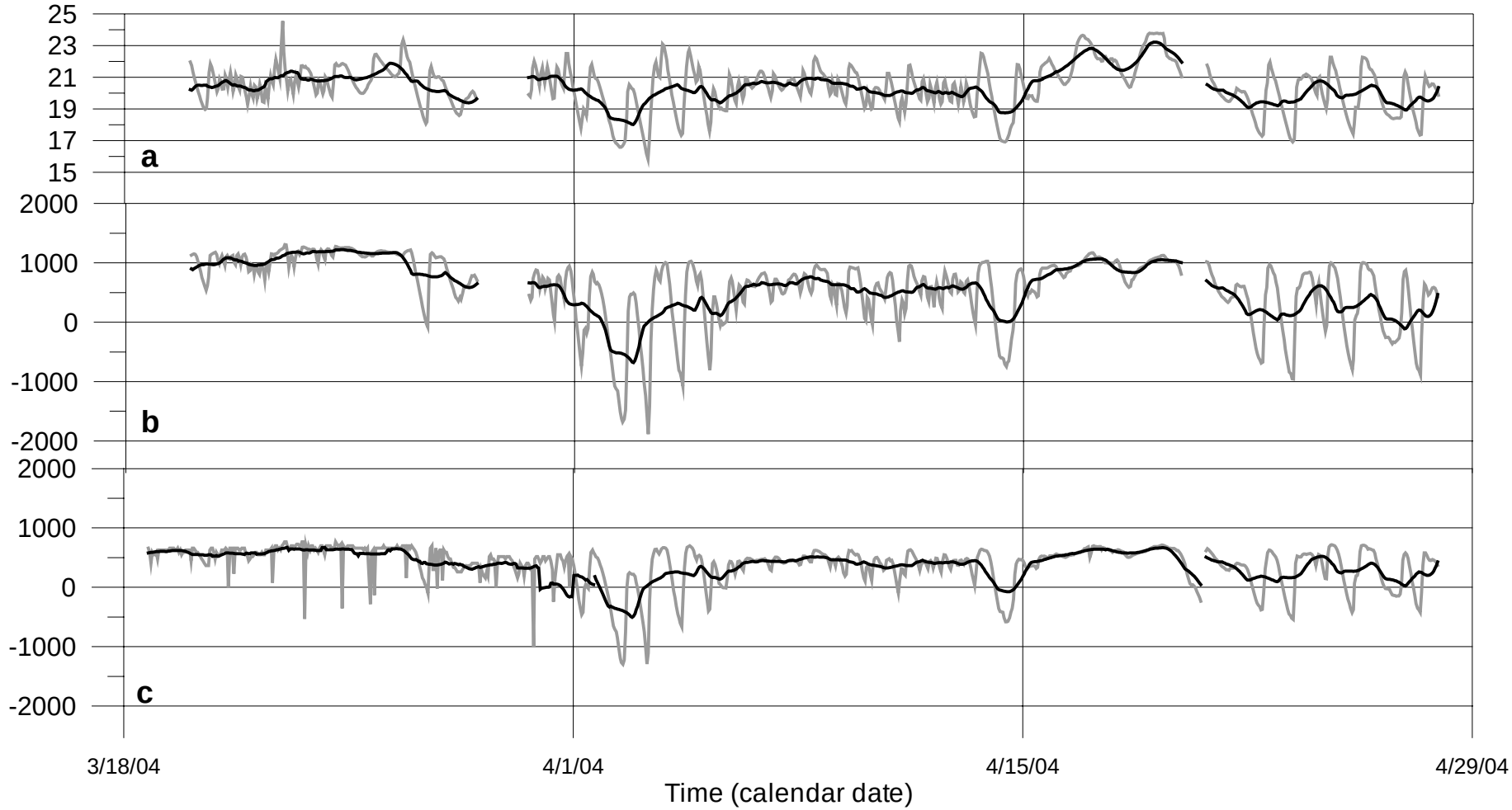

Figure B11. Comparison of indoor temperature, baseline crack sensor displacement, and System X crack sensor displacement. Gray lines are one-hour rolling average; black lines, 24-hour rolling average. Patterns are very similar for all three, demonstrating correspondence between temperature and crack movement. System X sensor displacement is smaller, but virtually identical in shape, indicating a sensor system appropriate for ACM. a. Indoor temperature; b. NU Eddy-current (NUEC) crack gauge displacement; c. System X crack LVDT (XLC) displacement; owing to monitoring period issues discussed in Figure B7 for simultaneous Null gauge recording and accompanying text, the XLC one-hour average spikes are truncated.

Measurement Significance Verified

During the entire period, XLN displacement remains relatively constant compared to the large swings in XLC, as seen in Figure B12, verifying that the crack, not the ceiling material itself, dominates XLC displacement measurements. The movements of the intact portion of the ceiling are a fraction of the displacements of crack movements, which further verifies the enormous impact of environmental factors on wall and ceiling cracks.

Measurement Calibration.

The most important aspect for an ACM system is consistency with the baseline system in following a pattern of displacements accurately and within a reasonable amount of time, neither excessively lagging nor (likely only in the case of clock mis-alignment) leading, and accuracy to within a reasonable known factor. Reasonableness is a matter of engineering judgment, depending on the purpose of the sensor; however, the difference should be no more than ±75%. A long-term test with large, gradual increases in temperature over the entire expected range can yield a conversion factor when the quotient of the difference at each point, of the absolute value of system under evaluation minus baseline and the baseline value, or |evaluated system – baseline system| / baseline system. If the variation changes depending on temperature regimes, and is not excessively large, a statistical average of some sort can be derived. At such a small scale, exactness is not possible; however, accuracy to within a reasonable factor of a given order of magnitude is sufficient to demonstrate system suitability.

System X performance is consistent with the baseline system performance. Consistent performance, not necessarily exact matching, is the hallmark of an adequate data system. A consistent-value percentage deviation can become a multiplier to define “true”

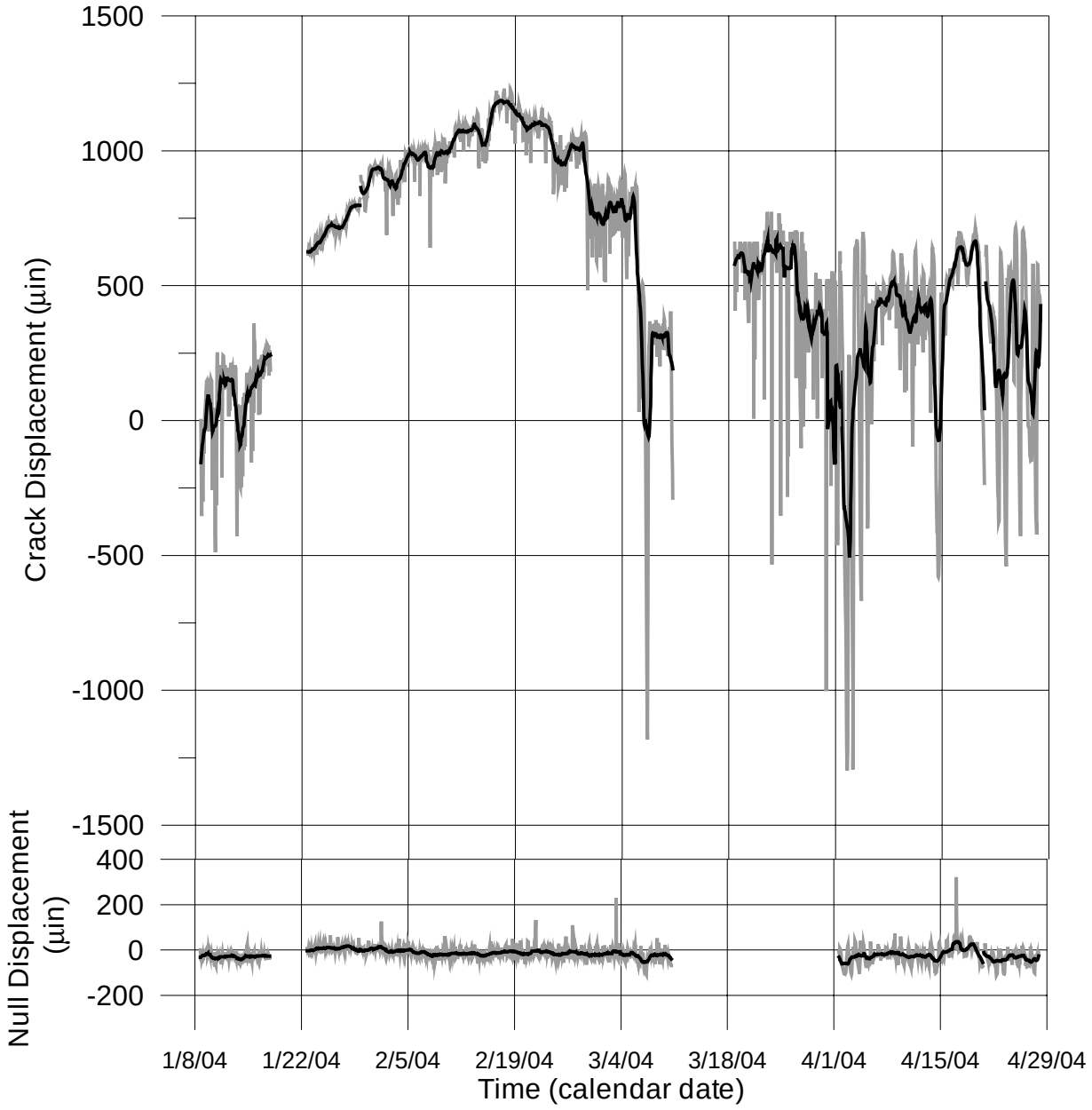

Figure B12. Comparison of System X sensors: Crack LVDT (XLC) and Null (XLN), demonstrating overwhelming dominance of crack displacement measured by XLC as opposed to wall material displacement measured by XLN. XLN data for 3/18 – 4/1 is omitted because of excessive noise; see Figure B7 and corresponding text for detailed treatment of this issue. Note that occasional noise anomalies are still present in XLN data, most notably between 2/19 – 3/4 and in the vicinity of 4/15.

movement. As Figure B11 shows, System X and NU crack displacement patterns are virtually indistinguishable. Therefore, for long-term Level I monitoring, instantaneous displacement and exact magnitude measurement are not critical as long as the large-magnitude trends are accurately recorded within a reasonable time.

Appendix C

Resolution

Analog-to-Digital resolution

Every digital electronic data logger must convert analog information to digital format, but in the process, information will always be lost. The difference in data is comparable to a tape recording and a CD: the former is the "actual" version (albeit with more noise), while the latter will always have gaps. The size of these gaps is a function of the digitization process. Chapter 2 presents calculations for determining Analog-to-Digital (A-D) conversion, or digitization, factors during ACM collection.

The two Northwestern University Analog-to-Digital (A-D) converters whose data is summarized herein are the SOMAT 2100 with its 12 bit converter with $2^{12} = 4096$ increments and the SOMAT eDAQ 16-bit converter which produces $2^{16} = 65536$ increments.

Taking the voltage range "gates" for collecting data, the minimum increment size which the data logger is capable of recording, $V_{min,\ measured}$, corresponds to several equations:

Thus, a 12 bit system with voltage gates set to ±0.06V, the standard range for 2100 detection on Aluminum can detect

$$V_{\text{min, measured}} = \frac{V_{\max} - V_{\min}}{2^{\text{processor bits}}} = \frac{0.06V - (-0.06V)}{2^{12}} = \frac{0.12V}{4096} = 2.9\text{x}10^{-5}\ \text{V}$$

By contrast, a 16-bit system increments are $1.8\text{x}10^{-6}$ V, more than a full order of magnitude smaller. These quantities are relatively meaningless until converted by a sensor scale factor, the manufacturer-specified quantity in volts per inch, simply a conversion factor and as such equal to unity, allowing the numerator and denominator to be exchanged for each other.

$$\delta_{\text{min, measured}} = V_{\text{min, measured}} * \text{Scale Factor} = \frac{V_{gate(\max)} - V_{gate(\min)}}{2^{\text{processor bits}}} * \text{Scale Factor}$$

For a system with 12-bit resolution, set to ±0.06V for LVDTs with scale factor = 200 V/in = 1in/200V:

$$\delta_{\text{min, measured}} = 2.9\text{x}10^{-5}\text{V/increment} * \frac{1\,in}{200\,V} = 0.1\text{x}10^{-6}\text{in} = 0.1\ \mu\text{in}$$

where for a 16-bit system the resolution is much finer, $9\text{x}10^{-9}$ in/increment, or 2.5 and 0.16 μin respectively.

Resolution is a function of both range and A-D converter. If the data collection range is too large, the ability of even 16-bit processors to discriminate between points can be compromised. Detected points smaller than the resolution are rounded up or down to the next interval, where the rounding method is a proprietary software technique of each individual manufacturer. To see this, it is necessary to examine a narrow range of data, in which exact repetition of certain decimal values occurs. Therefore, it is necessary to set the correct range in a processor with adequate resolution.

Characterization

System X, the off-the-shelf commercial ACM system which was tested, had a large, preset range which the end-user could not modify. The large range ensured that measurements of even the largest conceivable motion were possible, but this range also results in a resolution on the order of 35μin (≈1μm). For ACM, a typical displacement during a five-minute interval as measured by the NU SOMAT systems is less than 1μin, and likely even smaller during System X's one-minute increments. Therefore, averaging becomes a major factor in interpreting data from a logger with the resolution of System X.

System X was qualified for field installation during laboratory testing on two materials, aluminum and Ultra-High Molecular Weight Polyethylene (UHMW-P). Both materials have linear thermal expansion properties, the coefficient of thermal expansion (α) for aluminum is 13.1 μin/in/°F; for UHMW-P, 110 μin/in/°F.

The α units signify a length by which each inch of material will expand for a 1°F temperature increase; a one-inch length of aluminum heated by 1°F will expand 13.1 μin; UHMW-P, 110 μin. For ACM, the length corresponds to the gap between the target and the motion detector, in the case of the LVDT, between the bracket edge facing the coil, and edge of the coil facing the bracket, shown in Figure 1. ACM gaps are on the order of 0.5 inches. Given a daily temperature swing of 40°F or less and a gap of 0.5 inches, the largest motion predicted for testing on a UHMW-P plate will be on the order of 100 μin per hour, or less than 2 μin per minute. On less-responsive aluminum, displacements are 10 μin per hour, or far less than 1μin per minute.

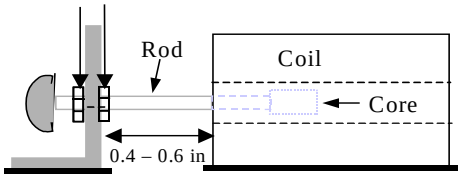

Figure C1. ACM LVDT setup showing rod (in this case a screw), coil, core, and gap, typically 0.4-0.6 inches wide.

This enormous difference, combined with the fact that aluminum does not realistically represent wall movement, prompted the move to the plastic plate for qualification.

Resolution in actual testing

Data is much less discernible when the A-D step is larger than the plate's "test-specific α" quantity, i.e., α*L*1°F; as the gaps were typically one-half inch or smaller, this corresponded to less than 7μin of movement per degree Fahrenheit of temperature increase. System X, with 35μin resolution and a gap of 0.4 inches, required much larger temperature changes than the 0.1 μin resolution NU SOMAT 2100 system. As seen in Figure C2a, the temperature change for this hot two-day summer period were relatively small, with a maximum change of slightly more 10°F. It is not surprising that a low-resolution system would have trouble detecting movement under these conditions. However, such small movements do not accurately simulate wall behavior; as seen elsewhere in this work, walls expand at a rate many times that of aluminum. Therefore, aluminum is not a realistic test surface, and UHMW-P was selected because of its high α which more closely mimics the linear aspect of wall thermal expansion.

UHMW-P plastic has a high α for a conventional linear material, and it requires less than 1°F to induce a response from a system with 35μin resolution, as seen in Figure C3. In Figure C3a, the first seven hours alone produce a temperature increase equal to the entire temperature range of Figure C2a. In this temperature range, System X has more than 20 A-D steps for plastic, as seen in Figure C3b, forming a distinctive, recognizable, and accurate pattern even without averaging, whereas the five legitimate A-D step levels in Figure C2b make it difficult to interpret both raw and averaged data.

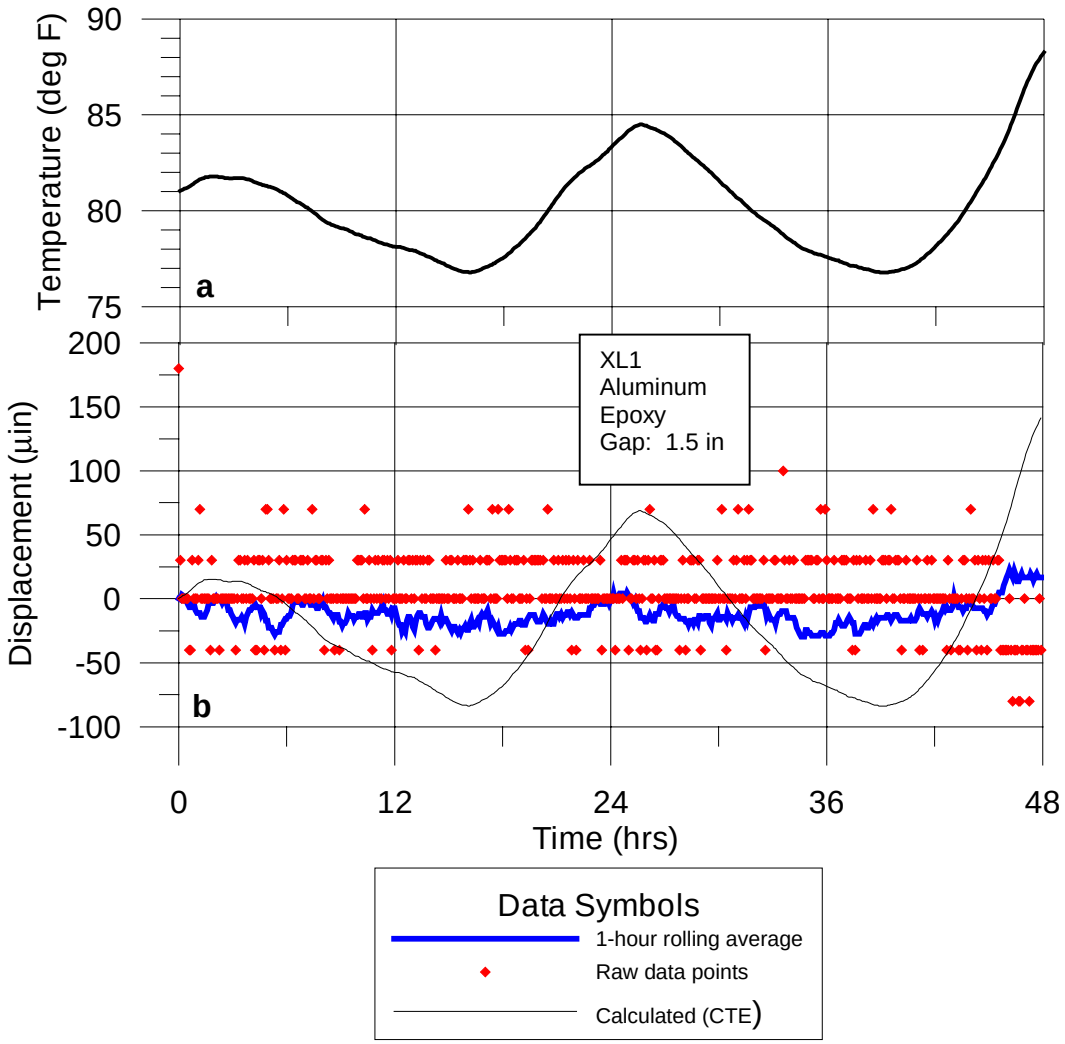

Figure C2. a.Temperature for a 48 hour period corresponding to C2b. Displacement detected by System X over a 48-hour period on an Aluminum sheet. Note the quantum levels corresponding to 35µin steps of the A-D converter, the indistinguishable pattern, and the average-data plot that does not clarify the meaning of the raw data.

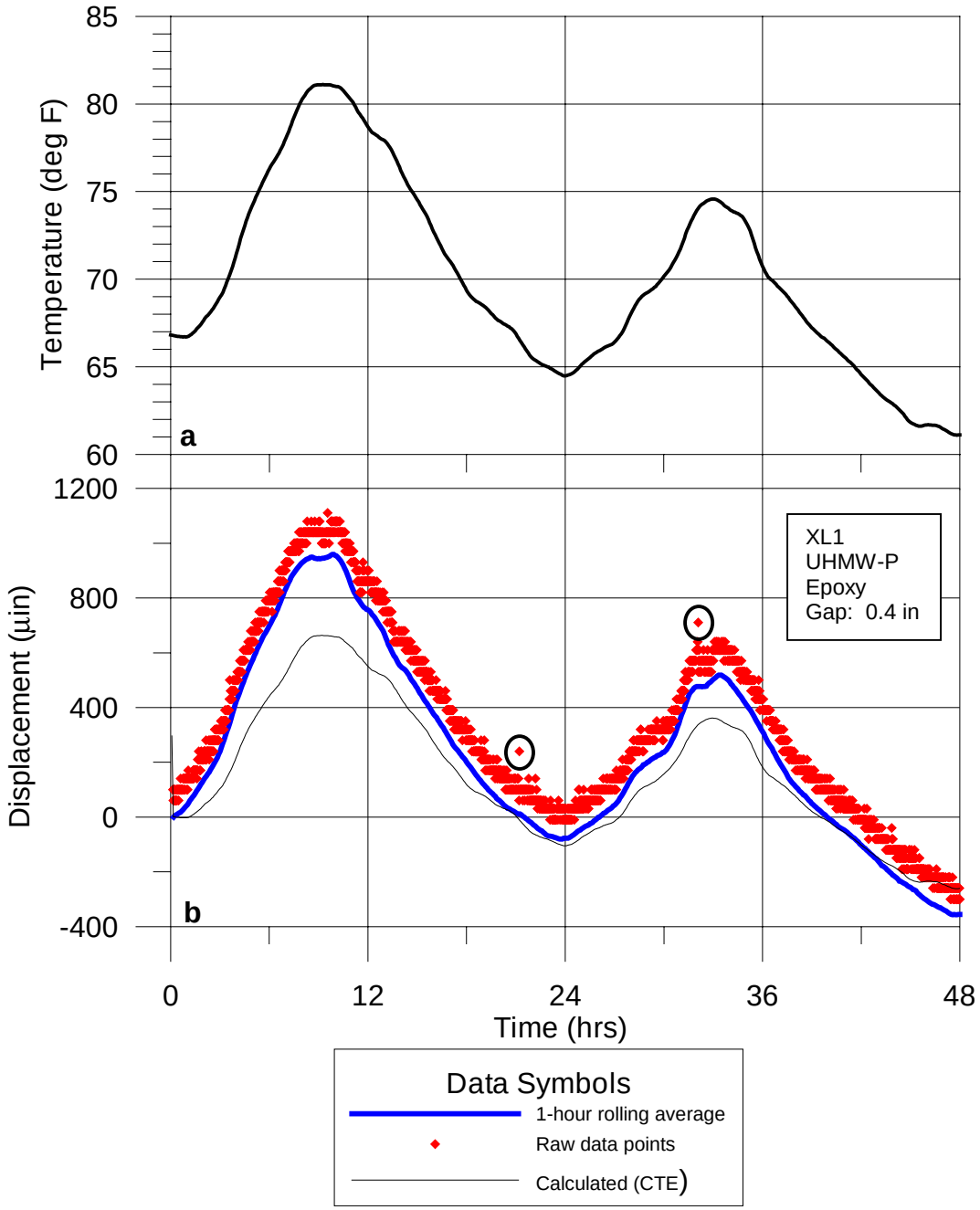

Figure C3 a. Temperature for a 48 hour period corresponding to C3b. Displacement detected by System X over a 48-hour period on a plastic sheet. Note the quantum levels corresponding to 35µin steps of the A-D converter, and the easily-distinguished pattern. Note also the noise spikes at hours 21 and 31 (circled) that are of little consequence as shown by the average-line plot.

Fortunately, aluminum thermal expansion does not realistically represent structural crack displacement, and an ACM system does not need the fine resolution necessary to measure aluminum displacement. Testing on the plastic sheet, which more accurately simulates crack movement magnitude, verified the fitness of System X for field deployment, where System X proved to be an adequate ACM system. Therefore, it is imperative to evaluate equipment with realistic testing methods; large A-D steps do not necessarily bar a system from ACM. At the same time, system design should aim to minimize A-D steps as much as possible in an expected operational range to improve data precision.

Appendix D

Data Processing

Storage and retrieval

Automated Crack Monitoring produces large volumes of data which must be properly handled and stored for analysis. A coherent, logical, easily-understandable computer filing scheme is crucial for proper organization. Without it, retrieving the desired information from the large volume of data spanning long periods of time becomes confusing and time-consuming. File manipulation procedures during analysis, for averaging, plotting, and reporting, must be orderly, logical, and systematic.

System X collected data once per minute, producing 1440 points per day, which were stored in a single file. Minutes 1 to 1440 were stored in the file during minute 1441 minute; data was not recorded for minute 1441 to eliminate partial minutes. Thus, minute1442 in relation to the first data set became the first data point of the new file.

The files were consolidated in a spreadsheet, and for the blank minute 1441, the value for minute 1440 was inserted. The difference between minutes 1440, 1441, and 1442 was always small, given that this was Level I collection with short-term displacement changes which do not vary much between points.

During data download periods for both NU systems and System X, no recording took place, as the processor was occupied with data transfer. This led to gaps whose magnitude is a function of the data file size and transfer speed. Ethernet downloads (eDAQ) took less than 60 seconds, while serial downloads (System X, 2100) could take as long as 30 minutes.

In one case, the time gap between a download and collection re-start was less than an hour. There were no seismic events during this time, and to leave it as it was would have caused an interruption. For each quantity (displacement, temperature) the difference between the first point of the new data set and the last point of the old data set was divided by the number of missing minutes; starting with the last recorded value before the gap, this differential was added to each preceding point, eliminating the short break. This procedure allowed uninterrupted averaging of one long file instead of two shorter files. The former resulted in a smooth line; the latter resulted in lines with different endpoints because of the termination of data on either side.

NU systems were set to collect three points every five minutes. The system was sufficiently stable and electronically quiet for this collection method to be acceptable, since the long-term averaging would mitigate any short term effects. These points were downloaded automatically into a data collection computer, converted from voltage to engineering units and placed in a file via an algorithm written by a research engineer, who passed the data to the author.

Seismic data recording

Level II recording mode is triggered by an external geophone. The Level II ACM system maintains a buffer of one thousand or more continuously-updated crack sensor data

points sampled at the same frequency as that of Level II recording. When Level II recording is triggered, the buffer is "frozen," saved, and becomes the beginning of several more seconds of high-frequency data from the crack sensors. Such a "pre-trigger" buffer is necessary because the trigger lags the actual seismic reaction of the wall crack by a fraction of a second. In the absence of seismic activity, the buffer points are continuously updated, with new points added to the most recent data while older points at the end of the data set are discarded, until a seismic event triggers high-frequency crack recording.

Level III, triggered by the crack itself, has more complex computing requirements. As for Level II, the data logger must continuously maintain a memory buffer of points collected at high frequency for a pre-set time period; for example, 3000 points from three seconds of data at 1000 Hz. This buffer is like the Level II buffer; new points are continuously added while points whose age exceeds the buffer period are discarded. These points are continuously averaged, with newest points at the front end forcing out the "oldest" points at the back end. In Level III, the trigger is activated by quasi-instantaneous large displacements, defined as the absolute value of the rolling average exceeding a certain threshold for a certain time period. When such a displacement occurs, the Level III trigger initiates the same type of short-term, high-frequency collection as Level II.

Calculations

Selective averaging reduced these large volumes of data to more manageable size. For System X, which collected one point per minute, a starting point was selected as a baseline, then points was taken every five minutes thereafter, and a one-hour rolling average (the point itself and 30 minutes of data preceding and following it) was taken.

Spreadsheet calculation and sorting for such data created unwieldy files. Matlab averaging became the standard practice.

An example of such a spreadsheet with points every five minutes appears in Figure D1. To reduce visual clutter, decimal places were minimized: one decimal place for displacement and environmental quantities, and as few decimal places as needed to see change between one point and the next. Although a point every five minutes was consistent with the laboratory testing method, the files became too large for several months of data from the field, leading to consideration of data once per hour.

The Matlab program in Figure D2 reads a data file consisting of points every 100 seconds, as collected at the field test location, and calculates a one-hour rolling average with output points every five minutes. Figure D3 averages 100-point bursts as for laboratory tests; a program similar to D2 performs the rolling average. Quality control is easier if averaging is performed in several smaller steps, as opposed to in one large, omnibus program performing all averaging calculations.

When inputting data sets into input files, it was necessary to ensure that the first data point corresponded to the proper minute, i.e., if the time of the first point is 12:00, then it is necessary for all subsequent files to start with a point ending in :00. This sometimes necessitated discarding nearly an hour of data, which in the end amounted to only one point in a set of well over 2000 points.

If a programming language is not available, Figure D4 shows the clumsy, memory-intensive spreadsheet calculations for taking a one-hour rolling average of one point per hour, where collection is one ppm. The spreadsheet method requires that every point be averaged and then sorted.

The program in Figure D5 averages each one-hour rolling average points every five minutes, with twelve points (twelve hours) on either side for a 24-hour rolling average. Output consists of four points per hour: the sorted one-hour average points and calculated 24-hour average points in both English and SI units. The results are written into a text file.

The computer program text file output was opened in an Excel Spreadsheet, and the data pasted into a master spreadsheet containing information for the entire test period. There was no discernible difference between the appearance of plots whose points were at five and 60 minute intervals, respectively.

When there is more than one data point per for the time of averaging, i.e., more than one point per minute for System X and more than one point per five minutes for NU systems, data handling is described in Chapter 4. However, calculation programs must take this into account, particularly at the beginning and end of data series, one of the more confusing aspects of rolling-time averages.

For a one-hour rolling average, the first or last 30 minutes of points do not have 30 minutes of points preceding or following them respectively. Therefore, it is necessary to truncate the calculations for available points. The averaging routines, both computer program and spreadsheet, are slightly different at the beginning and end to account for the absence of data.

As previously discussed, estimated data was “filled in” during short data gaps during periods when no seismic activity took place. When a data series is truncated at either end, it does not have the benefit of the following data series for averaging, and even though there may be just a few minutes’ gap between he two data sets. Truncation may cause

Date	Time	Time	Days	Temp (ave)	MS1CTE>0	MS1 ave	MS1 zero	MS1 pos	MS1 CTE	MS1CTE0	MS1 Raw	MS1Raw0
	actual	hrs		Deg C	μin	μin	77.8	34.5	μin	μin	μin	50.0
Tue 12 Aug	3:20 PM	0.00	0.000	27.2	40.3	77.8	0.0	42.8	445.8	0.0	76.427	26.4
Tue 12 Aug	3:25 PM	0.08	0.003	27.3	40.5	78.1	0.3	43.1	446.0	0.2	77.117	27.1
Tue 12 Aug	3:30 PM	0.17	0.007	27.3	40.7	78.6	0.8	43.6	446.2	0.4	76.924	26.9
Tue 12 Aug	3:35 PM	0.25	0.010	27.3	41.0	79.0	1.2	44.0	446.5	0.7	76.217	26.2
Tue 12 Aug	3:40 PM	0.33	0.014	27.3	41.1	79.4	1.6	44.4	446.6	0.8	78.547	28.5
Tue 12 Aug	3:45 PM	0.42	0.017	27.3	41.3	79.9	2.1	44.9	446.8	1.0	79.043	29.0
Tue 12 Aug	3:50 PM	0.50	0.021	27.4	41.5	80.3	2.5	45.3	447.0	1.2	80.146	30.1

Figure D1. Data sheet, point every five minutes from hysteresis testing. Excerpt of data for only one sensor, an NU Macrosensors DC-750-050, here called MS1, is shown. For the four-month experiment period, such a plot contained close to 30,000 points. While suitable for brief runs of several weeks for laboratory testing, such frequent data points are overwhelming for long collection periods.

Explanation of symbols:

MS1	Macrosensors LVDT DC-750-050 connected to data logger channel 1.
MS1CTE>0	Quantity α*L*Temp(ave), where α = 13.1 μin/in/°F and L=0.41 in are constant, and Temp(ave) is from the column immediately to the left; all data points in this column are ≥ 0, so that this quantity on the x-axis and MS1ave on the y-axis is always in the +x, +y quadrant.
MS1ave	1-hour rolling average of MS1 data
MS1zero	Adjusted so that time history of MS1 data begins at the origin; the quantity subtracted appears immediately below the label MS1 zero.
MS1pos	MS1ave – min(all MS1ave points) = MS1ave –34.5, so that hysteresis plot is in the +x, +y quadrant when plotted with MS1CTE>0 on the x-axis.
MS1CTE	α*L*Temp(ave), gross quantity. MS1CTE>0 and MS1CTE0 are this quantity minus a constant.
MS1CTE0	MS1CTE-445.8, so that time history plot of MS1CTE begins at the origin
MS1Raw	Raw data logger points for MS1
MS1Raw0	Raw data logger points for MS1 plotted so that time history of MS1 raw points begin above MS1ave points; this quantity is to compare averaged and raw MS1 data.

```
%Read data
file_type = 1;
if file_type == 1
      [filename pathname] = uigetfile('*.txt', 'Select file to read');
            fullname = [pathname filename];
      Input = dlmread(fullname,'\t');
else
      [filename pathname] = uigetfile('*.xls', 'Select file to read');
            fullname = [pathname filename];
      Input = xlsread(fullname);
end

%Determine number of points
num_col = length(Input(1,:));
numpoints1 = length(Input(:,1));
array_length = round(numpoints1/3-0.5);
      numpoints = array_length * 3;

%Compute first six averages
for i = 1:7
    index1 = 3*(i-1)+1;
    Average(i,:) = mean(Input(1:index1+18,:));
end

for m = 8:array_length-6
      index2 = 3*(m-1)+1;
      Average(m,:) = mean(Input(index2-20:index2+18,:));
end

%Compute last six averages

for n = array_length-5:array_length
      index3 = 3*(n-1)+1;
      Average(n,:) = mean(Input(index3-20:numpoints1,:));
end

for p = 1:array_length
    index4=3*(p-1)+1;
    Output_av(p,1) = Input(index4,1);
    Output_av(p,4) = Input(index4,2);
end

Output_av(:,2) = 39.37*(Average(:,1));
Output_av(:,3) = Average(:,1);
Output_av(:,5) = 39.37*(Average(:,2));
Output_av(:,6) = Average(:,2);

%Write data
[filename pathname] = uiputfile('*.txt', 'Enter name of output file');
      fullname = [pathname filename];
dlmwrite(fullname, Output_av, '\t');
fclose('all')
```

Figure D2. Matlab program calculates one-hour rolling average of displacements every five minutes, where input data is one point per hundred second (0.01 Hz collection frequency) in μm and output is in both μin and μm. Easily modified to include other data taken at the same collection intervals.

```
%Read data
file_type = 1;
if file_type == 1
      [filename pathname] = uigetfile('*.txt', 'Select file to read');
            fullname = [pathname filename];
      Input = dlmread(fullname,'\t');
else
      [filename pathname] = uigetfile('*.xls', 'Select file to read');
            fullname = [pathname filename];
      Input = xlsread(fullname);
end

%Determine number of points
numpoints = length(Input(1,:));
array_length = numpoints/100;

%Compute average of every 100-point group

for j = 1:array_length
    Output(1,j) = mean(Input((j-1)*100+1:j*100))/5*1000000;
end

%Write data
[filename pathname] = uiputfile('*.txt', 'Enter name of output file');
      fullname = [pathname filename];
dlmwrite(fullname, Output, '\t');
fclose('all')
```

Figure D3. Matlab program calculates average of 100 bursts every five minutes, where input data is mV and output is in μin. This is a simplified algorithm; it is easier to run the resulting output through another program for one- and 24-hour rolling averages. It is easier to perform intermediate quality assurance on data with several smaller steps, rather than writing an omnibus program to perform all calculations.

A	B	C	D	E	F	G	H	I	J	K
		Elapsed	Crack	Null	Crack ave	Null ave		Elapsed	Hrly Crack	Hrly Null
		Time	Gauge	Gauge	μin	μin		Time	Gauge ave	Gauge ave
		(min)	mills	mills	**14.44516**	**13.19968**		(min)	μin	μin
16:26:00	16:27:00	0	14.45	13.22	0.0	0.0		0	0.0	0.0
16:27:00	16:28:00	1	14.45	13.22	0.2	-0.3		60	4.0	0.7
16:28:00	16:29:00	2	14.45	13.19	0.3	0.3		120	5.5	-9.3
16:29:00	16:30:00	3	14.45	13.22	0.4	0.9		180	23.9	-25.9
16:30:00	16:31:00	4	14.42	13.19	0.6	1.5		240	25.8	-30.7
16:31:00	16:32:00	5	14.45	13.22	0.7	2.0		300	16.0	-31.3
16:32:00	16:33:00	6	14.45	13.19	0.8	1.7		360	27.8	-29.0
16:33:00	16:34:00	7	14.45	13.22	0.9	1.4		420	17.3	-36.1
16:34:00	16:35:00	8	14.42	13.19	1.0	1.1		480	5.7	-36.4
16:35:00	16:36:00	9	14.45	13.22	0.3	0.8		540	-7.9	-21.6
16:36:00	16:37:00	10	14.45	13.19	0.4	0.6		600	-11.9	15.6
16:37:00	16:38:00	11	14.45	13.19	0.6	0.3		660	-18.3	75.1
16:38:00	16:39:00	12	14.45	13.22	0.7	0.1		720	-23.2	160.7
16:39:00	16:40:00	13	14.45	13.19	0.7	-0.1		780	-23.2	270.8
16:40:00	16:41:00	14	14.45	13.19	0.2	0.3		840	-23.7	406.4
16:41:00	16:42:00	15	14.42	13.19	0.3	0.1		900	-39.6	488.4
16:42:00	16:43:00	16	14.45	13.22	0.4	-0.1		960	-54.0	521.6
16:43:00	16:44:00	17	14.45	13.19	0.5	-0.3		1020	-56.0	548.5
16:44:00	16:45:00	18	14.45	13.19	0.6	0.1		1080	-54.0	590.5
16:45:00	16:46:00	19	14.45	13.19	0.6	-0.1		1140	-46.1	620.0
16:46:00	16:47:00	20	14.45	13.22	0.7	-0.3		1200	-45.0	646.9
16:47:00	16:48:00	21	14.42	13.19	0.8	-0.4		1260	-36.3	593.8
16:48:00	16:49:00	22	14.45	13.19	0.9	-0.1		1320	-27.1	535.2
16:49:00	16:50:00	23	14.42	13.19	0.9	-0.2		1380	-25.2	454.7
16:50:00	16:51:00	24	14.45	13.19	1.0	-0.4		1440	-21.7	399.7
16:51:00	16:52:00	25	14.45	13.19	1.1	-0.6		1500	-6.5	251.6
16:52:00	16:53:00	26	14.45	13.19	1.2	-0.2		1560	18.8	46.6
16:53:00	16:54:00	27	14.45	13.19	1.9	-0.4		1620	23.7	-17.9
16:54:00	16:55:00	28	14.45	13.22	2.0	0.0		1680	17.3	-21.5
16:55:00	16:56:00	29	14.45	13.19	2.0	-0.2		1740	8.8	-11.2
16:56:00	16:57:00	30	14.45	13.19	2.1	-0.3		1800	16.6	16.1
16:57:00	16:58:00	31	14.45	13.19	2.1	-0.8		1860	5.2	17.5

Figure D4a. Averaging calculations in a spreadsheet. The elapsed time appears in Column C, raw data for the data channels in Columns D and E. The boldface quantities in Columns F and G are equal to the rolling average for the first point; this quantity is subtracted from all subsequent averages and the result multiplied by 1000 to convert mills to μin and start the time-history plot at the origin. If this were a continuation of previous data, the boldface quantities would be equal to the rolling average of the very first point, which might be several months before. Column I represents the minutes of every hour, while Columns J and K sort through all the data in Columns F and G to extract data corresponding to the minutes in Column C.

	C	D	E	F	G	H	I	J
1	Elapsed	Crack	Null	Crack ave	Null ave			Crack
2	Time	Gauge	Gauge	μin	μin		Time	Gauge ave
3	(min)	mills	mills	=AVERAGE(D4:D34)	=AVERAGE(E4:E34)		(min)	μin
4	0	14.45	13.22	=(AVERAGE(D4:D34)-Crack0)*1000	=(AVERAGE(E4:E34)-Null0)*1000		0	=VLOOKUP($I4,$C$1:$G$12981,4,FALSE)
5	=C4+1	14.45	13.22	=(AVERAGE(D4:D35)-Crack0)*1000	=(AVERAGE(E4:E35)-Null0)*1000		=I4+60	=VLOOKUP($I5,$C$1:$G$12981,4,FALSE)
6	=C5+1	14.45	13.19	=(AVERAGE(D4:D36)-Crack0)*1000	=(AVERAGE(E4:E36)-Null0)*1000		=I5+60	=VLOOKUP($I6,$C$1:$G$12981,4,FALSE)
7	=C6+1	14.45	13.22	=(AVERAGE(D4:D37)-Crack0)*1000	=(AVERAGE(E4:E37)-Null0)*1000		=I6+60	=VLOOKUP($I7,$C$1:$G$12981,4,FALSE)
8	=C7+1	14.42	13.19	=(AVERAGE(D4:D38)-Crack0)*1000	=(AVERAGE(E4:E38)-Null0)*1000		=I7+60	=VLOOKUP($I8,$C$1:$G$12981,4,FALSE)
9	=C8+1	14.45	13.22	=(AVERAGE(D4:D39)-Crack0)*1000	=(AVERAGE(E4:E39)-Null0)*1000		=I8+60	=VLOOKUP($I9,$C$1:$G$12981,4,FALSE)
10	=C9+1	14.45	13.19	=(AVERAGE(D4:D40)-Crack0)*1000	=(AVERAGE(E4:E40)-Null0)*1000		=I9+60	=VLOOKUP($I10,$C$1:$G$12981,4,FALSE)
11	=C10+1	14.45	13.22	=(AVERAGE(D4:D41)-Crack0)*1000	=(AVERAGE(E4:E41)-Null0)*1000		=I10+60	=VLOOKUP($I11,$C$1:$G$12981,4,FALSE)
12	=C11+1	14.42	13.19	=(AVERAGE(D4:D42)-Crack0)*1000	=(AVERAGE(E4:E42)-Null0)*1000		=I11+60	=VLOOKUP($I12,$C$1:$G$12981,4,FALSE)

Figure D4b. Calculations for Figure D3a. Elapsed time appears in Column C. The quantities in Columns F3 and G3 are constants, defined as Crack0 and Null0, respectively equal to the rolling average for the first point; this quantity is subtracted from all subsequent averages and the result multiplied by 1000 to convert mills to μin and start the time-history plot at the origin. Column I represents the minutes of every hour, while Columns J and K sort through all the data in Columns F and G to extract data corresponding to the minutes in Column C.

	C	D	E	F	G
	Elapsed Time (min)	Crack Gauge mills	Null Gauge mills	Crack ave μin	Null ave μin
34	=C33+1	14.45	13.19	=(AVERAGE(D4:D64)-Crack0)*1000	=(AVERAGE(E4:E64)-Null0)*1000
35	=C34+1	14.45	13.19	=(AVERAGE(D5:D65)-Crack0)*1000	=(AVERAGE(E5:E65)-Null0)*1000
36	=C35+1	14.45	13.22	=(AVERAGE(D6:D66)-Crack0)*1000	=(AVERAGE(E6:E66)-Null0)*1000
37	=C36+1	14.45	13.22	=(AVERAGE(D7:D67)-Crack0)*1000	=(AVERAGE(E7:E67)-Null0)*1000
38	=C37+1	14.45	13.22	=(AVERAGE(D8:D68)-Crack0)*1000	=(AVERAGE(E8:E68)-Null0)*1000

Figure D4c. Calculations for the middle portions of the data, when there are 30 minutes of data on either side of the data point around which the one-hour rolling average is being taken.

	C	D	E	F	G
	Elapsed Time (min)	Crack Gauge mills	Null Gauge mills	Crack ave μin	Null ave μin
12970	=C12969+1	14.45	13.3	=(AVERAGE(D12940:D12981)-Crack0)*1000	=(AVERAGE(E12940:E13000)-Null0)*1000
12971	=C12970+1	14.45	13.26	=(AVERAGE(D12941:D12981)-Crack0)*1000	=(AVERAGE(E12941:E13001)-Null0)*1000
12972	=C12971+1	14.45	13.26	=(AVERAGE(D12942:D12981)-Crack0)*1000	=(AVERAGE(E12942:E13002)-Null0)*1000
12973	=C12972+1	14.45	13.26	=(AVERAGE(D12943:D12981)-Crack0)*1000	=(AVERAGE(E12943:E13003)-Null0)*1000
12974	=C12973+1	14.45	13.3	=(AVERAGE(D12944:D12981)-Crack0)*1000	=(AVERAGE(E12944:E13004)-Null0)*1000
12975	=C12974+1	14.45	13.26	=(AVERAGE(D12945:D12981)-Crack0)*1000	=(AVERAGE(E12945:E13005)-Null0)*1000
12976	=C12975+1	14.45	13.26	=(AVERAGE(D12946:D12981)-Crack0)*1000	=(AVERAGE(E12946:E13006)-Null0)*1000
12977	=C12976+1	14.45	13.26	=(AVERAGE(D12947:D12981)-Crack0)*1000	=(AVERAGE(E12947:E13007)-Null0)*1000
12978	=C12977+1	14.45	13.26	=(AVERAGE(D12948:D12981)-Crack0)*1000	=(AVERAGE(E12948:E13008)-Null0)*1000
12979	=C12978+1	14.45	13.3	=(AVERAGE(D12949:D12981)-Crack0)*1000	=(AVERAGE(E12949:E13009)-Null0)*1000
12980	=C12979+1	14.49	13.3	=(AVERAGE(D12950:D12981)-Crack0)*1000	=(AVERAGE(E12950:E13010)-Null0)*1000
12981	=C12980+1	14.42	13.3	=(AVERAGE(D12951:D12981)-Crack0)*1000	=(AVERAGE(E12951:E13011)-Null0)*1000

Figure D4d. Calculations for the end of the data, when there are less than 30 minutes of data between the point around which the one-hour rolling average is being taken and the end of the data.

```
%Read data
file_type = 1;
if file_type == 1
       [filename pathname] = uigetfile('*.txt', 'Select file to read');
              fullname = [pathname filename];
       Input = dlmread(fullname,'\t');
else
       [filename pathname] = uigetfile('*.xls', 'Select file to read');
              fullname = [pathname filename];
       Input = xlsread(fullname);
end

%Determine number of points
num_col = length(Input(1,:));
numpoints1 = length(Input(:,1));
array_length = round((numpoints1-1)/12-0.5);
       numpoints = array_length * 12;

%Extract points every hour from a series of every 5th minute
for m = 1:array_length
    Hrly(m,1) = Input(12*(m-1)+1,1);
    Hrly(m,2) = Input(12*(m-1)+1,4);
end

%Compute first six averages
for i = 1:12
    Average(i,:) = mean(Hrly(1:i+12,:));
end

for j = 13:array_length-12
    Average(j,:) = mean(Hrly(j-12:j+12,:));
end

%Compute last six averages

for k = array_length-11:array_length
    Average(k,1) = mean(Hrly(k-12:array_length,:));
end

for p = 1:array_length
    Output_av(p,1) = Hrly(p,1);
    Output_av(p,3) = Hrly(p,2);
end

Output_av(:,2) = Average(:,1);
Output_av(:,4) = Average(:,2);

%Write data
[filename pathname] = uiputfile('*.txt', 'Enter name of output file');
       fullname = [pathname filename];
dlmwrite(fullname, Output_av, '\t');
fclose('all')
```

Figure D5. Program to calculate 24-hour rolling average from input data of one-hour rolling average with points at five-minute intervals. Sorts one point per hour, performs 24-hour rolling average, and outputs once-per-hour one-hour rolling average data and calculated 24-hour rolling average data.

visible deviation and mismatch in end-points and slopes of the last and first averaged points of two sets, respectively. "Filling in" leads to smooth, continuous curves. Caution must be exercised, however, to ensure that times of seismic activity are not thus being "erased."

The best fit line and standard variance from the best-fit-line for hysteresis data sets were calculated with standard linear regression (Haldar and Mahadevan, 2000) calculated by the computer program in Figure D6. A spreadsheet is too unwieldy and confusing for such an analysis. To check output, the slope of the best-fit line calculated by the program was compared to an automatic spreadsheet "best fit line" function. The slopes typically agreed to at least two decimal places.

Presentation and plotting

Graph presentation was via Excel spreadsheet data plotted in Golden Software Grapher 3. For this application, it is important not to add columns between existing columns once a plot has been saved, as the software is linked to a specific column, not a data set. For example, a Grapher file is set to plots Column A (time) on the x-axis and Column B (displacement) on the y-axis. If another column is added between the two, for example, temperature, the new Column B will be temperature, and all other columns will be shifted right. Thus, when Grapher opens the file again, it will plot Column A (time) on the x-axis and the new Column B (temperature) on the y-axis.

Spreadsheet presentation is crucial for data management, and the whole should be well-organized and consistent. Every spreadsheet must have easily-understood headings, with units (e.g., μin, hours, etc.). A template makes for much easier data management, and inclusion of data description, including date and time, is necessary not only for plotting, but also for keeping track of data. The template for this project appears in Figure D7.

```
%Read data
file_type = 1;
if file_type == 1
	[filename pathname] = uigetfile('*.txt', 'Select file to read');
		fullname = [pathname filename];
	Input = dlmread(fullname,'\t');
else
	[filename pathname] = uigetfile('*.xls', 'Select file to read');
		fullname = [pathname filename];
	Input = xlsread(fullname);
end
%Determine number of points
num_col = length(Input(1,:));
numpoints = length(Input(:,1));
array_length = numpoints;
sumx = 0;
sumy = 0;
sumxy = 0;
sumxisq = 0;
Sxy = 0;
Sxx = 0;
MSE = 0;

for z = 1:numpoints
    x(z) = Input(z,1);
    y(z) = Input(z,2);
end

for i = 1:numpoints
    sumx = sumx + x(i);
    sumy = sumy + y(i);
    sumxy = sumxy + x(i)*y(i);
    sumxisq = sumxisq + x(i)^2;
end
xbar = sumx/numpoints;
ybar = sumy/numpoints;

for j =1:numpoints
    Sxy = Sxy + y(j) * (x(j) - xbar);
    Sxx = Sxx + (x(j) - xbar)^2;
end

b1 = Sxy/Sxx;
b0 = ybar - b1*xbar;

for k = 1:numpoints
    MSE = MSE + (y(k) - (b0 + b1*x(k)))^2;
end

MSE = MSE/(numpoints-2);
Dev = MSE^0.5;

Output(1) = b0;
Output(2) = b1;
Output(3) = Dev;

%Write data
[filename pathname] = uiputfile('*.txt', 'Enter name of output file');
	fullname = [pathname filename];
dlmwrite(fullname, Output, '\t');
fclose('all')
```

Figure D6. Linear regression Matlab program.

Date/Time	Julian Date	1hrAv OutdrT	24hrAv OutdrT	1hrAv OutdrRH	24hrAv OutdrRH	1hrAv IndrT	24hrAv IndrT	1hrAv IndrRH	24hrAv IndrRH	1hr avg LVDTm	24hrAvg LVDTm	1hrAvg LVDTm0	24hrAvg LVDTm0	1hrAvg LVDTin0	24hrAvg LVDTin0
		deg C	deg C	%	%	deg C	deg C	%	%	μm	μm	μm	μm	μin	μin
1/8/2004 10:04	37994.4194	-8.7	-7.3	70.0	72.9	22.9	22.1	27.8	28.4	91.2	87.9	0.0	-3.3		
1/8/2004 11:04	37994.4611	-7.8	-7.4	70.2	73.5	23.0	21.9	27.9	28.5	91.7	87.1	0.5	-4.1	19.7	-161.0
1/8/2004 12:04	37994.5028	-6.5	-7.5	66.9	74.3	23.2	21.9	28.1	28.6	92.0	86.7	0.8	-4.5	31.2	-177.1
1/8/2004 13:04	37994.5444	-6.1	-7.6	67.2	75.0	23.3	21.8	28.0	28.6	92.5	86.7	1.3	-4.6	50.9	-179.1
1/8/2004 14:04	37994.5861	-6.1	-7.6	67.9	75.7	23.5	21.8	28.2	28.7	92.7	86.7	1.5	-4.6	57.5	-179.6
1/8/2004 15:04	37994.6278	-6.4	-7.7	70.0	76.2	23.1	21.7	29.8	28.8	93.2	86.5	2.0	-4.7	77.2	-185.2

Figure D7. Spreadsheet data organization for managing and plotting field test data from Franklin, WI; note headings and units.

1hr Av	One-hour rolling average, i.e., the data point and all data 30 minutes preceding and following it.
24hrAv	24-hour rolling average, i.e., the data point and all data 12 hours preceding and following it.
Outdr	Outdoor
Indr	Indoor
T	Temperature
RH	Relative Humidity
LVDTm	NU LVDT displacement in SI units (μm)
1hr Avg LVDTm0	NU LVDT displacement in SI units (μm)set so that time history begins at origin, here by subtracting 91.2 μm, the starting point, from both 1hrAv
24hr Avg LVDTm0	NU LVDT displacement in SI units (μm)set so that 24 hrAvg0 = 24hrAvg –91.2 μm, so that this column's data differential is the same as that of 1hrAvg plots allowing the 24hrAvg line to show up in near the middle of the 1hrAvg plot line.
1hr Avg LVDTin0	NU LVDT displacement in English units (μin) set so that 1hrAvgLVDTm0*39.37; the first point is not used because the 0 SI value does not necessarily correspond to a 0 English unit value.
24hr Avg LVDTin0	NU LVDT displacement in English units (μin) set so that 24hrAvgLVDTm0*39.37; the first point is not used because the 0 SI value does not necessarily correspond to a 0 English unit value.

Other calculation techniques are described in Chapters 2 and 4 of this work. The techniques described herein were arrived at after much trial and error. Although the computations are not themselves complicated, their application is non-standard and the volume of data is massive. The necessity crucial importance for adequate organization cannot be understated.

Appendix E

LVDT Mounting Procedures

- Plate Test Mounting Procedures
  - Prepare LVDT coil and bracket for gluing
    - Remove all old epoxy
      - Large chunks can be pried off
      - Smaller chunks carefully sliced off with straight razor blade
      - Small residue sanded down with medium-fine sandpaper
    - Take care not to nick or gouge metal surface
    - Sandpaper surface of LVDT coil (or tube containing coil) and bracket where they contact the test surface
      - Curved LVDT coil/coil tube (coil tubes are usually square nonmagnetic tubes into which LVDTs are epoxied to make mounting the LVDT easier)
        - Choose portion of coil surface to contact plate
        - Ensure this surface is clean from front to back of coil
      - Flat coil/coil tube (see Figure 1): choose bottom surface, ensure entire bottom is clean

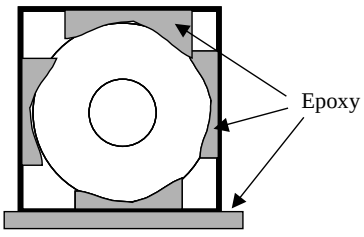

Front view:
LVDT mounted in square tube
on Test Plate

Figure 1. Appearance of round LVDT coil mounted inside square tube to simplify attachment.

      - Sandpaper down to reach first stage of uniform, hard, bright metal

        - Ensure sandpaper abrades evenly across the entire surface
        - Avoid gouging or causing uneven surface with sandpaper
    - Apply denatured (grain) alcohol to cloth or paper towel
        - Rub sanded metal with alcohol-moistened cloth
        - Continue cleaning until cloth in contact with sanded area stops picking up debris (“comes clean”)
- Prepare bracket for test
    - Option 1: LVDT core attached to prefabricated threaded arm, Figure 2.
        - Attach nut corresponding to thread size to arm
        - Position nut about 1/3 of distance from free end of arm
        - Pass threaded arm through bracket hole
            - Nut should be between coil and bracket when setup is complete
            - If bracket hole is tapped, turn carefully to prevent stripping the bracket hole threads.
        - Attach a second nut to the portion of rod extending outside the bracket.
        - Position both nuts to touch the bracket; finger tighten only!

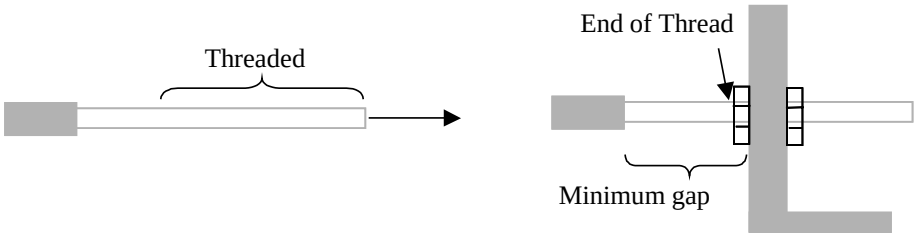

Figure 2. Pre-manufactured rod mounting in bracket.

- Option 2a: LVDT core separate from arm; construct arm with nonmagnetic stainless steel sheet metal screw, Figure 3.
  - Ensure end of screw is intact, all threads are intact and undamaged
  - Attach one nut, move close to the screw head
  - Pass free end of screw through the bracket hole
  - Attach a second nut, move it up and well clear of the screw end
  - Apply thread-locking compound to the end of the screw
    - Apply over a distance slightly longer than the length of the core
    - Screw core onto the end of the screw
  - Hold screw-core assembly near the screw head
    - Hold for manufacturer specified set time
    - Keep screw off surfaces while waiting for this initial set
    - Skewing results if assembly rests on surface before thread lock sets
  - When thread lock hardens, place assembly on a flat, clean surface; wait 10-15 minutes for "hard set"

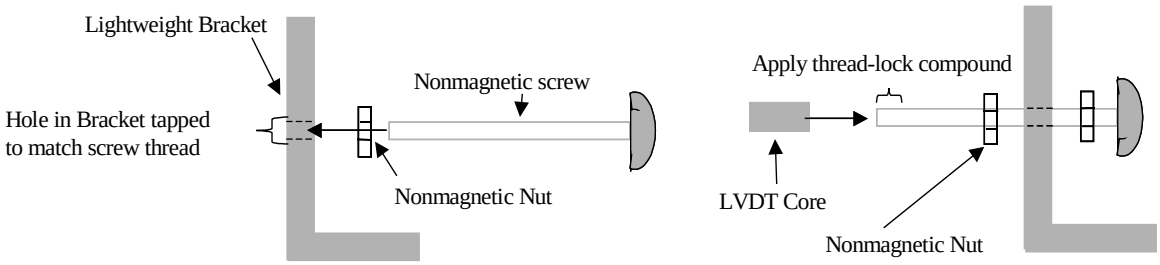

Figure 3. Custom-built LVDT rod with manufacturer-supplied LVDT core.

- Option 2b: LVDT core separate from arm, construct arm with prefabricated rod
  - Attach core to threaded rod as to the screw in Option 2a above
  - Attach nuts and bracket as in Option 1 above

o Prepare test plate
- Ensure proposed attachment points are free of dirt, debris
- Place LVDT coil and bracket on plate in desired position of attachment
  - Leave ≈0.5 in (1.3 cm) between bracket's inside edge and coil's outside face
  - Ensure this set-up allows the core to enter the coil completely
    - If not, loosen nuts and adjust arm to allow core to enter coil completely
    - Re-align nuts to touch both sides of bracket
    - Tighten nuts just enough to hold this position
    - This step is critical for proper bracket-plate attachment!
  - Mark arrangement on plate; place marks just outside areas epoxy will be applied
- Remove LVDT coil and bracket, very lightly abrade attachment areas with fine sandpaper
- Apply denatured (grain) alcohol to cloth or paper towel
  - Rub abraded portions of the plate with alcohol-moistened cloth
  - Continue cleaning until cloth in contact with sanded areas stops picking up debris

o Mix epoxy for LVDT coil
- Important: if epoxy resin-curing compound portions are not equal, poor bonding and a bad experiment will result!
- Mix equal amounts of epoxy resin and curing compound; total volume ≈ 2/3 teaspoon
  - Mix with thin tongue depressor or (e.g.) non-cotton end of wooden-shafted laboratory grade disposable cotton swab
  - Ensure thorough mixing
    - Every 8-10 seconds, scrape sides of mixing stick onto mixing surface, work scrapings into mixture
    - Compound is well-mixed when it takes on a "cloudy" or "milky" appearance with bubbles inside
  - Carefully monitor time: 30 seconds of mixing for 90 second curing epoxy!

- Flat bottom, Figure 4:
  - Apply thin (≈1/3 mm) layer of epoxy to entire bottom
  - Ensure layer is uniform and smooth
  - Mixing stick is a convenient epoxy trowel/smoothing instrument
  - Should take no more than 10-15 seconds

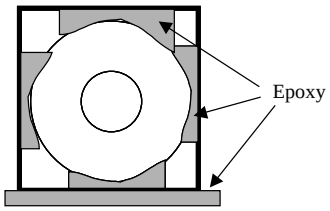

Front view:
LVDT mounted in square tube
on Test Plate

Figure 4. Tube-contained LVDT coil mounted on plate.

- Rounded bottom, Figure 5
  - Apply sufficient epoxy to leave ≈1/3 mm layer at desired attachment surface
  - Apply enough for a cushion of epoxy to support sloping sides
- Before set time elapses, press LVDT coil onto plate in desired (pre-surveyed) area
- Hold down for 8-10 minutes
  - Very important step: this ensures proper bonding!
  - If not held down long enough, epoxy will "drift" and coil will move
- With sufficient practice and skill, two LVDTs can be mounted simultaneously.

o

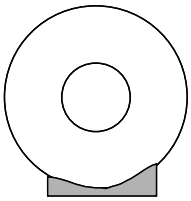

Front view:
LVDT mounted on epoxy "bed"
on Test Plate

Figure 5. LVDT coil mounted directly on test plate.

Attach LVDT bracket to plate, Figure 6

- For LVDT coils open at both ends, place a small, thin tube or spacer into the coil
  - Spacer should fit between core and coil channel without binding; may be electrical shrink-wrap tubing, custom-machined aluminum insert, etc.
  - Allows even alignment horizontally and longitudinally; prevents skewed core
  - Do not insert a spacer if coil is open only at one end! (Exception: eg, spacer short enough to fit between glued-down coil and bracket with longitudinal split)
- Mix a fresh batch of epoxy as described above
- Spread epoxy along entire bottom of bracket, taking care not to apply epoxy to core, arm, or nuts
- Place bracket in the designated place, carefully moving core into coil hole
  - Previous layout and adjustments should make this easy
  - Ensure core is not bumping sides of the coil
  - While epoxy is still wet, move coil in-and-out very slightly to ensure core does not bind with sides
  - Take care to complete alignment before epoxy set time!
- When properly placed and aligned, hold down bracket for 10 minutes
- NOTE: failure to hold down bracket until epoxy sets firmly will result in epoxy drift, skewed bracket and mis-alignment of core inside coil!

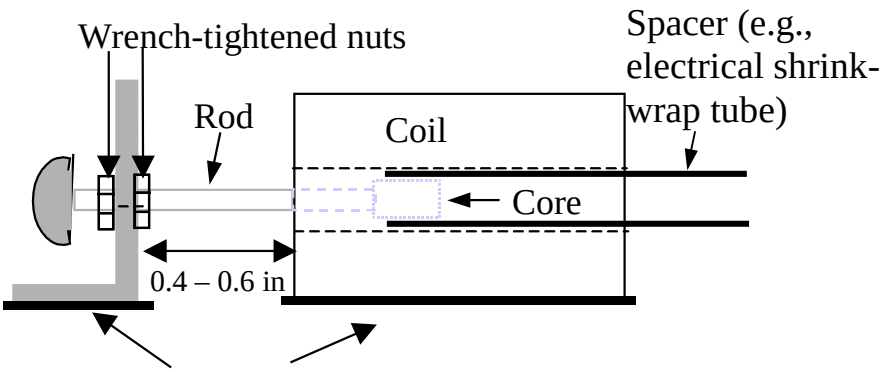

Figure 6. Completed LVDT assembly, including bracket, mounted on plate.

Appendix F

Proposed ASTM Standard: "Qualification of Systems to Measure Micro-inch Crack Opening and Closing"

1. Scope

1.1. This practice outlines procedures to determine suitability of linear variable displacement transducers (LVDT) and similar displacement sensors to measure micro-inch opening and closing of cracks in structures subject to construction vibration characterized by high frequency and small displacement. This practice covers any purpose-built or component-assembled system for Automated Crack Monitoring (ACM), the electronic sensor measurement of structural crack displacement.

1.2. This procedure determines behavior of crack-measurement systems under gradually changing temperature. The material to which the sensor is attached will expand and contract one-dimensionally as a function of the material's coefficient of thermal expansion (CTE).

1.3. This calibration procedure determines fidelity of the system being tested compared to a highly-accurate, previously-characterized reference system of known behavior.

1.4. *This standard does not purport to address all the safety concerns, if any, associated with its use. It is the responsibility of the user of this standard to establish appropriate safety and health practices and determine the application of regulatory limitations prior to use.*

2. Referenced Documents

2.1. *ASTM Standards*

D6027-96 Standard Practice for Calibrating Linear Displacement Transducers for Geotechnical Purposes

3. Terminology

3.1. *Definitions*—Definitions of terms used in this practice are in accordance with Terminology D 653.

3.2. *Definitions of Terms Specific to this Standard:*

3.2.1. *ACM, n*—Automated Crack Monitoring, measurement of structural crack oepning with electrical detecting and data systems.

3.2.2. *LVDT, n*—Linear Variable Differential Transducer, detects small linear displacements through electromagnetic changes linearly proportional to displacement.

3.2.3. *reference system, n*—displacement and temperature measurement/recording system of known characteristics, previously qualified for ACM,

3.2.4. *bracket, n*—nonmagnetic metal piece to which LVDT rod is attached and from which it extends across a crack.

3.2.5. *coefficient of thermal expansion (CTE), n*—defines material microstrain per degree of temperature change.

3.2.6. *test plate, n*—a smooth, stiff slab of known CTE whose thermally-induced displacements are measured by electronic sensors along a single axis.

3.2.7. *coil, n*—an LVDT component which produces an electromagnetic field, changes in which are induced by linear displacement of an independently-moving core.

3.2.8. *coil channel, n*—a channel through the center of the LVDT coil parallel to its long axis into which the core fits.

3.2.9. *core, n*—small cylinder of ferromagnetic material which fits into the LVDT coil channel. Back-and-forth core motion inside the coil changes the coil's electromagnetic field proportional to displacement.

3.2.10. *data logger, n*—electronic equipment to detect and record voltage or current signals representing displacement and temperature.

3.2.11. *signal conditioner, n*—specialized electrical component, such as but not limited to multiplexers, to convert sensor data to data logger-compatible electronic signals.

3.2.12. *displacement sensor, n*—an electrical or electro-mechanical device to measure relative displacement by detecting changes in an electromagnetic field.

3.2.13. *eddy-current sensor, n*—sensor that measures displacement by detecting changes in an electromagnetic field continuously transmitted against a reflecting target.

3.2.14. *rod, n*—LVDT non-magnetic threaded shaft cantilevered from a bracket, across a crack, and into an LVDT coil channel, where it holds the LVDT core.

3.2.15. *readout equipment, n*—devices to detect data logger information real-time; can be anything from a voltmeter to a computer.

3.2.16. *multiplexer, n*—device to convert sensor electrical signals into signals compatible with a data logger.

3.2.17. *hysteresis, n*—a quasi-linear loop representing displacement versus temperature or a function thereof; ideally, on a material with linear thermal expansion properties, a specific temperature will always correspond to a specific displacement, and the hysteretic loop is a line.

3.2.18. *test surface, n*—wall, ceiling, or other surface of a structure on which LVDT assemblies are mounted; both intact and cracked surfaces provide data.

3.2.19. *crack gauge, n*—LVDT coil-core-rod-bracket assembly whose rod spans a structural crack to measure linear crack displacement.

3.2.20. *null gauge, n*—LVDT coil-core-rod-bracket assembly whose rod spans an intact portion of the same material as a nearby crack gauge to measure intact material expansion.

3.2.21. *null surface, n*—undamaged surface of the same material as and close to a crack being measured.

3.2.22. *null correction, n*—crack gauge data minus simultaneous null gauge data yields net "crack-only" displacement.

3.2.23. *zero, n*—user-defined initial point from which LVDT voltage changes represent differential displacements. Displacement gauges' beginning, or "zero" point is user-defined.

3.2.24. *transmitter, n*—source of measuring device electromagnetic field that is changed during crack opening and closing.

3.2.25. *target, n*—displacement sensor component, whose movement is measured relative to the electromagnetic field-producing sensor component. Reflector for eddy-current sensor, bracket holding rod for LVDT.

4. Summary of Test Method

4.1. Part I: Temperature Stability Qualification.

4.1.1. Two sensors and brackets are mounted with epoxy-resin compound on a test plate with a gap of approximately 0.5 inches between LVDT coil and bracket.

4.1.2. Plate is placed in an environment with temperature variations normal for the test area, e.g., an uninsulated shed.

4.1.3. Ensure recording equipment is functional and record for 15 to 30 days as continuously as possible, minimizing data collection interruptions.

4.1.4. All sensor displacements and plate temperature are recorded at intervals adequate to secure data or in accordance with manufacturer's recommendations for purpose-built ACM systems, whichever is more strict, during the experimental period.

4.1.5. Plot measured displacement versus calculated displacement; the former is collected data, while the latter is $\delta = CTE*L*T$, where L is the gap between LVDT coil and bracket, T is temperature which corresponds to a simultaneous displacement.

4.1.6. Data linearity is assessed by linear regression: best fit line and variation from best-fit line (standard deviation from best fit divided by total displacement during the test).

4.2. Stage II: Temperature Stability Field Test.

4.2.1. Attach reference system and test system sensor to walls/ceilings across cracks.

4.2.2. Leave in place 30-60 days.

4.2.3. Subtract null gauge from crack gauge displacements for net crack movement; assess test system performance by comparing to reference system data.

5. Significance and Use

5.1. LVDT and similar electromagnetic sensors can accurately measure changes in the width of structural cracks on the order of micro-inches.

5.2. Temperature changes typically cause larger changes in crack width than seismic events, meaning LVDT and measuring apparatus must be stable under a wide variety of conditions.

5.3. An accurate, thermally-stable reference system installed side-by-side with system(s) under evaluation provides a reference to evaluate stability and accuracy.

6. Apparatus

6.1. *LVDT or similar electronic displacement sensors*, two per system, one to measure crack strain, one to measure strain of non-cracked portion of same structural member nearby.

6.2. *Power supply with output*, equal to that required by the sensor.

6.2.1. *Discussion: ensure that proper power supply (AC or DC) is provided for the LVDT to prevent shocks and damage to personnel and equipment.*

6.3. *Signal conditioning, data logging and readout equipment, and related cables and fittings.*

6.4. *Sensor target*, sensor component producing no electromagnetic field, perpendicular to a structural crack; corresponds to LVDT rod spanning the crack and bracket to which rod is attached, or eddy-current sensor reflector bracket.

6.5. *Sensor electromagnetic signal generator*, corresponds to LVDT coil or eddy-current signal transmitter/receiver.

7. Hazards

7.1. Safety Hazards:

7.1.1. This practice involves electrical equipment. Verify that all electrical wiring is connected properly and that the power supply, signal conditioner, and data logger are grounded properly to prevent electrical shock to the operator. Take necessary precautions to avoid exposure to power signals.

7.1.2. This practice involves potentially toxic adhesives. Ensure manufacturer safety recommendations are followed to prevent toxic reactions.

7.2. Safety Precautions:

7.2.1. Smooth sharp edges or burrs on sensors.

7.2.2. Ensure sensors are properly connected to power supplies, signal conditioning units, and data loggers to prevent short circuits and arcing.

7.2.3. Ensure AC-DC conversions are properly insulated to prevent shock hazards.

7.2.4. Ventilate areas where epoxy will be applied, and prevent contact with skin and eyes.

7.2.5. Follow manufacturer safety recommendations.

7.3. Technical Precautions

7.3.1. Interchange LVDT cores and coils, or components between other types of sensors, only if manufacturer verifies that parts are interchangeable.

7.3.2. Replace LVDT core if gouged, significantly dented, or otherwise damaged in a manner that may create electromagnetic inconsistencies; consult manufacturer, if necessary.

7.3.3. Replace LVDT rods if sufficiently bent to be visible from the side; slight bends visible only looking parallel to the long axis of a rod are generally acceptable. The rod should be replaced if a bend causes the core to come into contact with the coil channel walls.

7.3.4. Properly store sensors and signal conditioner to prevent damage when not in use.

7.3.5. Do not exceed manufacturer-specified maximum voltage and current.

7.3.6. Ensure sensors are sufficiently separated to prevent magnetic co-interference.

7.3.7. Take care not to clog or damage equipment with epoxy-resin adhesive.

8. Calibration and Standardization

8.1. Reference system: eddy-current sensor

8.2. Highly accurate, with no moving parts. Note: to be effective for ACM, apparatus must be able to tolerate gaps widths on the order of 0.5 inches.

8.2.1. Eddy-current sensor may be nonlinear, with displacement as a polynomial function of voltage. Determine voltage corresponding to center of displacement range, either analytically or by manipulating the polynomial equation in a spreadsheet.

8.2.1.1. Insert minimum and maximum voltages into a spreadsheet formula for the polynomial to determine minimum and maximum displacement

8.2.1.2. Input voltage values into the spreadsheet; determine voltage corresponding to displacement center point by trial and error.

8.2.2. Attach to metal plate.

8.2.2.1. Ensure bottom surfaces of transmitter and target bracket are smooth and clean.

8.2.2.2. Lightly scratch a line onto the surface, and another parallel to the first at 0.5 ± 0.1 inches. These marks denote the position of the target edge facing the transmitter and the edge of the electromagnetic field transmitter.

8.2.2.3. Mix 90-second set epoxy per procedure outlined below. Attach target first and then transmitter separately. Apply a thin coat to the bottom of the bracket, ensuring no epoxy is applied to the reflective surface; press into place. Apply firm, steady pressure. Excessive pressure will cause the target to "wander" on its epoxy layer.

8.2.2.4. Transmitter and target must be properly aligned to yield proper results; check manufacturer specifications. Carefully apply a thin coat of epoxy to the bottom of the transmitter, and align as required with a gap, previously marked.

8.2.2.5. See Figure 1 for layout.

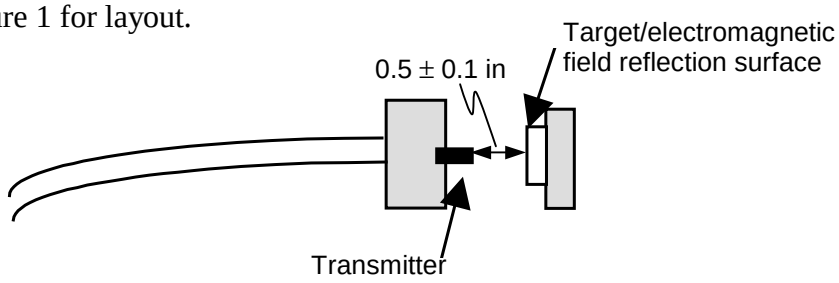

Figure 1. Test plate arrangement of an eddy-current sensor.

8.2.3. Ensure proper operation with data logger and readout equipment. Set voltage as close as possible to the point corresponding to the center of the displacement range.

8.3. Ensure reference system is functioning properly by running two four-day tests before qualifying a new system. Time thus spent ensures accurate reference.

8.3.1. Temperature time history and sensor displacement time history should have virtually identical patterns.

8.3.2. Adjust if necessary, then repeat test.

8.4. Disregard data during five days following epoxy-resin attachment for all systems; as the adhesive cures and the bond stabilizes, unreliable data may result.

8.5. Ensure sufficient temperature swings (minimum 10°C over the course of the test) for proper hysteresis observations.

8.6. System is considered calibrated and validated as reference for testing a system of unknown characteristics if displacement sensor and temperature time histories have identical patterns.

9. Procedure

9.1. Pre-test fabrication

9.1.1. If necessary, build brackets of non-magnetic material to hold end of LVDT rod or to reflect eddy-current electromagnetic signal.

9.1.2. A small block of aluminum may be milled to form an "upright," then tapped with a hole corresponding to the rod's size and thread, as seen in Figure 2. The center of the bracket hole must be precisely at the height corresponding to the center of the coil resting on the same surface, allowing the core to enter the coil channel parallel to the channel walls without touching them. This arrangement also holds the rod parallel to the test surface.

9.1.3. If LVDT manufacturer does not provide a rod, fabricate with non-magnetic screw.

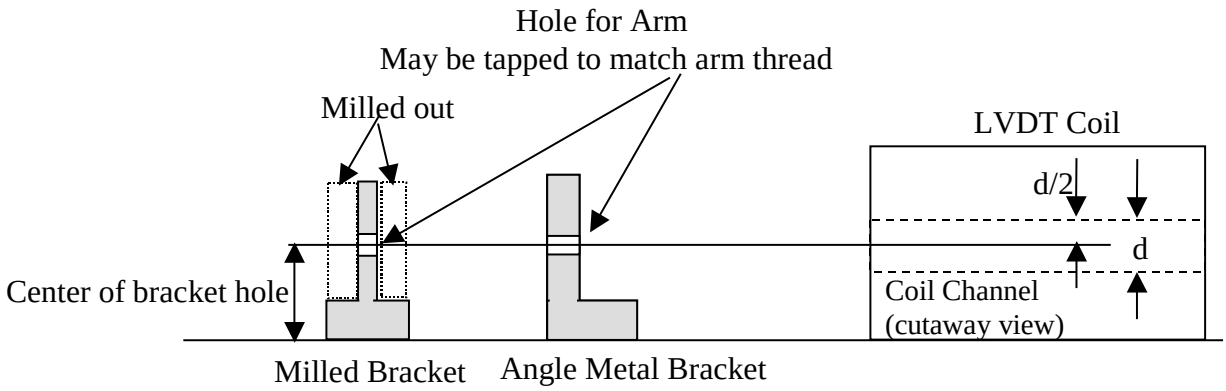

Figure 2. LVDT brackets, proportioning and construction.

9.1.4. LVDT rod assembly:

9.1.4.1. User-assembled, Figure 3. Pass screw or threaded rod through: 1) outside nut, 2) bracket, 3) inside nut; 4) apply dab of thread lock to screw tip; 5) insert into core deeply enough for stable, stiff support; 6) wait for thread lock to dry.

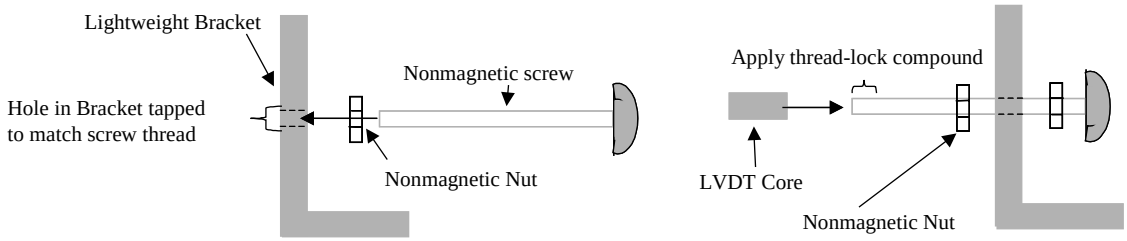

Figure 3. Setting up custom-built LVDT rod with manufacturer-supplied LVDT core.

9.1.4.2. Manufactured rod (core attached to threaded rod by manufacturer), Figure 4. Pass rod through 1) inside nut, 2) bracket, 3) outside nut.

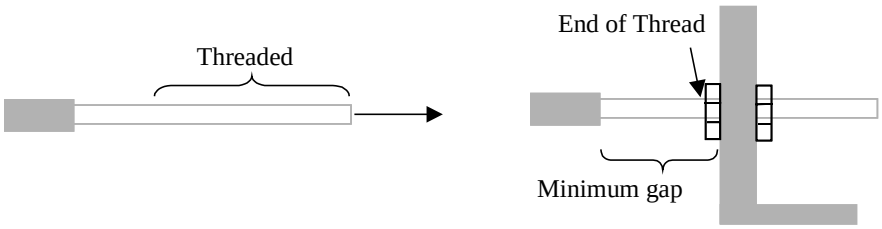

Figure 4. Setting up manufactured core-rod assembly in bracket.

9.1.5. Attach LVDT to test plate of known CTE. Ultra High Molecular Weight (UHMW) Polyethylene (CTE=110 µin/in/°F) has been found to simulate crack movement adequately. Three-quarter inch (¾") test plates balance stiffness, price, and workability.

9.2. Part I: Linearity Determination Data Collection

9.2.1. Mix 90-second set-time epoxy-resin compound and apply to entire underside of LVDT coil; hold coil on plate with gentle, steady pressure for ten minutes to ensure firm bond. If pressure is released before adhesive sets, coil will "wander" out of position.

9.2.2. Space subsequent coils sufficiently far from each other to prevent magnetic co-interference. If possible, determine such spacing by powering sensors and observing voltage outputs for both real-time on readout equipment display. Otherwise, raw data must be examined after several minutes of high-frequency collection. Such co-interference is rarely observed.

9.2.3. Measure surface 0.5±0.1 in (1.5 cm) perpendicular to coil face; mark with pencil or small, shallow scratch, keeping marks outside area where epoxy will be laid down.

9.2.4. Mix and apply a thin but comprehensive layer of epoxy to entire underside of bracket. Line up core/rod to be parallel to coil channel. Place bracket edge to be nearest to coil at 1.5 cm mark made in 9.2.3. Ensure core/rod assembly is parallel to coil interior channel by very slightly moving bracket backward and forward to verify absence of binding. If binding occurs, maneuver bracket slightly to stop the binding.

9.2.4.1. *Caution: excessively long duration or movement during bracket adjustment may lead to epoxy being rubbed off or beginning to set, requiring removal of epoxy from bracket and test surface, then repeating step 9.2.4.*

9.2.5. When bracket is in position, hold bracket down with light pressure. Adjust slightly to if bracket drifts on adhesive. If adhesive is properly mixed, drifting should stop within 10 minutes. Apply light, constant pressure; excessive force pressure causes the bracket to drift on its adhesive bed.

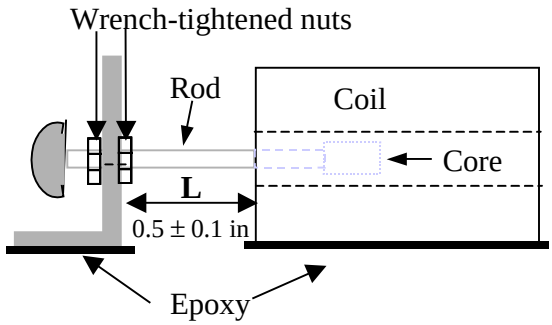

Figure 5. Complete LVDT assembly, including bracket, mounted on a plate.

9.2.6. Figure 5 shows completed LVDT assembly.

9.2.7. Wait 3-5 days before taking data for the record. Epoxy will set completely during this interval.

9.2.8. Place test plate on a flat surface in the testing area.

9.2.9. Measure and record gap between coil and bracket for all LVDT; this measurement yields the important value L (per Figure 5) from which δ is calculated for the x-axis of the hysteretic plot.

9.2.10. With all power off, connect sensors to power supply, any necessary signal conditioning unit, and data logger; Figure 6 shows custom-built system wire junction assembly for power and signal routing.

9.2.10.1. For exterior power supply, ensure power supply is unplugged, place power supply output wires into slot opposite LVDT power cable per manufacturer instructions.

Jumper wires from power supply inputs may be necessary to accommodate additional LVDT units.

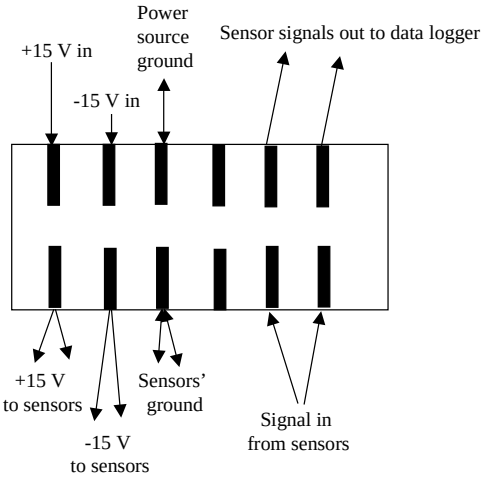

Electrical wire junction. Lines represent wires for 2-sensor system.

Figure 6. Power/signal electrical wire junction for 2-sensor system.

9.2.10.2. Connect sensor signal output into slots opposite appropriate data logger input wires. It is necessary to note which LVDT unit is connected to which data logger channel. Sensor and (if possible) signal wires should be marked with channel designation.

9.2.10.3. Connect temperature signal wire to data logger, via multiplexer if necessary. Attach temperature sensor directly on plate near gap of between sensor transmitters and targets. Strong non-magnetic duct tape works well for thermocouples.

9.2.11. When all signal and power wires are connected, turn on power.

9.2.11.1. Discussion. Regulated laboratory-quality power supply sources connected to an uninterrupted power system (UPS) unit are recommended to minimize ambient electrical noise. Electrical filters are not used to prevent loss of small movement data.

9.2.12. Data Logger Calibration.

9.2.12.1. Calculate "worst case" expected displacement δ_{tot} as a function of predicted low and high temperature conditions, δ_{tot} = CTE * L * ΔT, where L is from 9.2.9 above, and ΔT is expected temperature range (expected maximum temperature minus expected minimum temperature) for the time period. Convert δ_{tot} to voltage: e.g., for LVDT with 200 Volts/inch scale factor, voltage range = 200 V/in * δ_{tot} (in).

9.2.12.2. Connect readout equipment to data logger communication port.

9.2.12.3. Slightly loosen nuts on both sides of the bracket.

9.2.12.4. Zero the data logger. Observing readout equipment, twist rod to move core backward and forward inside coil. Adjust until readout is zero volts or at manufacturer-recommended starting point.

9.2.12.4.1. Start with large voltage range on the readout, and adjust LVDT rod close to zero.

9.2.12.4.2. Zoom in to smaller voltage range, and re-adjust until sensor is as close to zero as practicable; repeat until sensor is adjusted to zero (volts or amps) in the readout's finest data discrimination mode.

9.2.12.5. Taking care to prevent the core from moving excessively, tighten the nuts on both sides to lock in the rod stiffly to the bracket. Monitor the readout; iterative adjustments involving nut loosening, rod adjustment, and nut tightening will probably be necessary. Tighten carefully with pliers or wrench, but ensure force is not sufficient to compromise bracket-plate adhesive bond.

9.2.12.6. Adjust voltage or current detection limit ("gates") in the data logger by multiplying voltage range obtained in 9.2.12.1 above by 1.5 to 2, and set the voltage detection gates by this amount above and below the zero point.

9.2.12.7. *Discussion: Purpose-built systems may be factory-calibrated and no end-user adjustment necessary or possible. Custom-assembled systems require voltage range adjustment.*

9.2.12.8. If possible, observe sensor and temperature measurement performance during real-time on readout equipment. Ensure temperature is reasonable and within acceptable range for the equipment, and sensor LVDT is near zero. Re-set and troubleshoot if displacements appear excessive or signals other than ordinary electronic noise appear.

9.2.12.9. *Discussion: Sinusoidal noise spikes are unavoidable with AC power. Only DC battery power eliminates such spikes. Electronic noise is "filtered" during data averaging.*

9.2.12.10. Displacement and temperature data collection:

9.2.12.10.1. Burst-collection capable signal processor: 0.1 seconds @ 1000 Hz every five (5) minutes = 100 points every five minutes. This averaging procedure eliminates sinusoidal interference (see Figure 7). To reduce data file size, if on-board processing is available and reliable, average these 100 points and store the averaged data every five minutes. Record time (relative to start of test or absolute) for each data point.

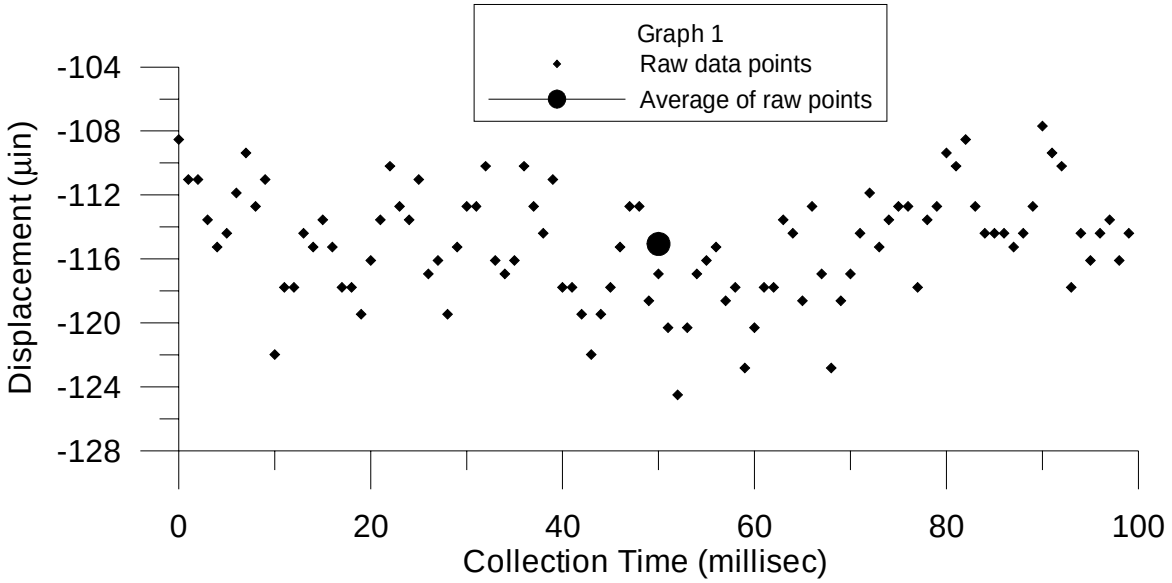

Figure 7. 100-point raw data burst in a 0.1 second time interval. The dot in the center represents the average of the 100 points. Note sinusoidal pattern of systemic noise even during this brief period.

9.2.12.10.2. No burst collection capability: one to four points per minute, depending on memory available. Record time for each data point.

9.2.12.11. Download data every 7-10 days for analysis. System should have sufficient memory for this length of time.

9.3. Field test.

9.3.1. Locate a crack in a structure.

9.3.2. Attach crack sensors of system under evaluation with transmitter on one side of a crack, target on the other, with both perpendicular to crack. See Figure 8.

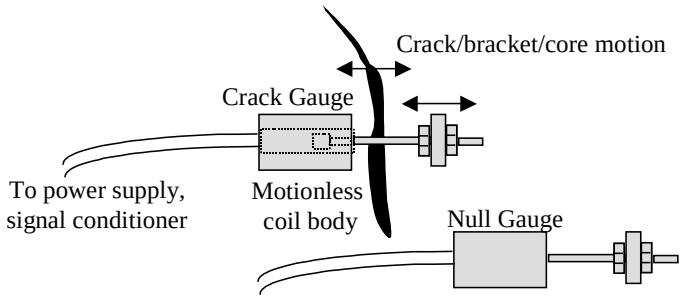

Figure 8a. LVDT field setup: crack gauge across a structural crack, null gauge nearby on same, but intact, material.

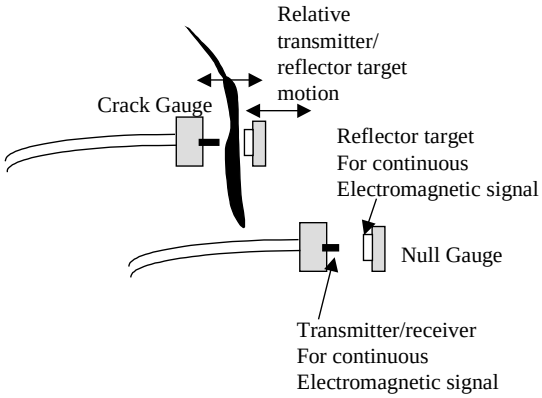

Figure 8b. Field setup, eddy-current sensors: similar to LVDT setup in Figure 7a.

9.3.3. Attach reference system crack sensor across the same crack as in 9.3.2 near the LVDT of system being evaluated, ensuring no magnetic co-interference occurs.

9.3.4. Attach null sensors on the same surface (same wall, ceiling, post, etc.) as the crack sensors.

9.3.5. Set data collection for one burst (as previously described) per five minutes.

9.3.6. Data logger memory should be sufficient to store several weeks' data. Online or telephone downloads are possible with data loggers configured for such operations; however, the troublesome nature of arranging such capability in the field may dictate on-site manual downloads.

10. Calculation.

10.1. If necessary, convert raw data from data logger proprietary format to standard text files for processing.

10.2. The following data quantities are relevant:

t_i = individual time increment, i

$T_{i,raw}$ = measured temperature collected by data logger at time increment i.

$T_{i,avg}$ = one-hour rolling average of raw temperature data at time i.

$T_{i,s,avg}$ = one-point-per-hour one-hour rolling average, sorted from $T_{i,avg}$ data set

$\delta_{i,raw,nl}$ = averaged-burst or single-point null sensor data directly from data logger, at time increment i.

$\delta_{i,raw,c}$ = averaged-burst or single-point null sensor data directly from data logger, at time increment i.

$\delta_{i,avg,nl}$ = one-hour rolling average of $\delta_{i,raw,nl}$ data

$\delta_{i,avg,c}$ = one-hour rolling average of $\delta_{i,raw,c}$ data

$\delta_{i,s,avg,nl}$ = one-point-per-hour one-hour rolling average from $\delta_{i,avg,nl}$ data set

$\delta_{i,s,avg,c}$ = one-point-per-hour one-hour rolling average from $\delta_{i,avg,c}$ data set

$\delta_{i,s,avg,net}$ = $\delta_{i,s,avg,c}$ - $\delta_{i,s,avg,nl}$ at time increment i.

$T_{i,24}$ = 24-hour rolling average of temperature at time increment i.

$\delta_{i,24nl}$ = 24-hour rolling average of null sensor measured displacement at time increment i.

$\delta_{i,24c}$ = 24-hour rolling average of crack sensor measured displacement at time increment i.

$\delta_{i,24net}$ = $\delta_{i,24c}$ - $\delta_{i,24nl}$ at time increment i.

L = gap between LVDT coil and bracket measured in step 9.2.8 above.

CTE = coefficient of thermal expansion, μin/in/°F or μm/m/°C

$\delta_{i,calc,nl}$ = calculated displacement as a function of CTE and $T_{i,avg}$ for null sensor

$\delta_{i,calc,c}$ = calculated displacement as a function of CTE and $T_{i,avg}$ for crack sensor

σ = standard deviation from best-fit line of $\delta_{i,avg}$ vs $\delta_{i,calc}$ plot

V = variance, a function of σ and $\delta_{i,avg}$

10.3. Plate testing:

10.3.1. Perform one-hour rolling average for all data. For data points at five-minute intervals, average the data point with the six data points preceding and following it, with either a spreadsheet or computer program. This procedure eliminates anomalies and smooths data. At the beginning and end of data sets, average as many points as are available within one-half hour on either side. Thus, for five minute intervals:

$$T_{i,avg} = \frac{\sum_{n=i-6}^{n=i+6} T_{n,raw}}{13} \qquad (1a)$$

$$\delta_{i,avg} = \frac{\sum_{n=i-6}^{n=i+6} \delta_{n,raw}}{13} \quad (1b)$$

10.3.2. Determine theoretical, or calculated, displacement for an ideal system, corresponding to each time point

$$\delta_{i,calc} = CTE * L * T_{i,avg} \quad (2)$$

10.3.3. Enter data into a spreadsheet in the following columns (Figure 8): elapsed time (five minute increments) t_i, averaged temperature $T_{i,avg}$, calculated displacement $\delta_{i,calc,nl}$ and $\delta_{i,calc,c}$, raw measured displacements $\delta_{i,raw,nl}$ and $\delta_{i,raw,c}$, and averaged measured displacement $\delta_{i,avg,nl}$ and $\delta_{i,avg,c}$. For all columns headed H (corresponding to hysteresis), determine minimum $\delta_{i,calc}$ and $\delta_{i,avg}$ values and subtract these from all data points in that column; this adjusts plots into Quadrant I (+x, +y). For all columns headed TH (corresponding to time history) determine subtract the first values in each column (i.e., $\delta_{1,calc}$ and $\delta_{1,avg}$, etc.) from all data points in that column; this adjusts plots to start time history at the origin.

t_i	$T_{i,avg}$	H	TH	TH	H	TH
		$\delta_{i,calc,nl}$	$\delta_{i,calc,nl}$	$\delta_{i,raw,nl}$	$\delta_{i,avg,nl}$	$\delta_{i,avg,nl}$
minutes	°C	μin	μin	μin	μin	μin
0		$\delta_{1,calc,nl} - \min(\delta_{i,calc,nl})$	$\delta_{1,calc,nl} - \delta_{1,calc,nl}$	$\delta_{1,raw,nl} - \delta_{1,raw,nl}$	$\delta_{1,avg,nl} - \min(\delta_{i,avg,nl})$	$\delta_{1,avg,nl} - \min(\delta_{1,avg,nl})$
5		$\delta_{2,calc,nl} - \min(\delta_{i,calc,nl})$	$\delta_{2,calc,nl} - \delta_{1,calc,nl}$	$\delta_{2,raw,nl} - \delta_{1,raw,nl}$	$\delta_{2,avg,nl} - \min(\delta_{i,avg,nl})$	$\delta_{2,avg,nl} - \min(\delta_{2,avg,nl})$

Figure 8. Data table example. Space limitations do not allow other recommended columns, e.g., time in hours and days, calendar days for reference, Julian dates for plotting program manipulations, etc.

10.3.3.1. Repeat for reference system that should have been operating simultaneously with system being tested. Enter data in spreadsheet columns for reference system $\delta_{i,calc,nl}$, $\delta_{i,calc,c}$, $\delta_{i,raw,nl}$, $\delta_{i,raw,c}$, $\delta_{i,avg,nl}$, and $\delta_{i,avg,c}$.

10.3.3.2. Plot $\delta_{i,avg}$ (y-axis) versus $\delta_{i,calc}$ (x-axis) for each sensor, and with linear regression methods, determine the best-fit line and standard deviation σ from the best-fit line for each sensor's data set for each test run. For such calculations, $\delta_{i,calc}$ is the independent variable and $\delta_{i,avg}$ is the dependent variable.

10.3.3.3. Divide standard deviation by measured displacement range to yield variance,

$$V = \frac{\sigma}{\delta_{i,avg}(\max) - \delta_{i,avg}(\min)} \quad (3)$$

A value of 0.1 or less is desirable. This procedure assesses linearity.

10.3.3.4. Plot measured displacement versus time for all sensors, and compare to temperature versus time. To start all data sets' time histories at the origin shift all points:

$$\delta_{i,avg} = \delta_{i,avg} - \delta_{1,avg} \quad (4)$$

10.3.3.5. Reference sensor displacement time history pattern should agree closely with temperature time history pattern. Significant deviations or irregularities by reference system indicate invalid test, by system under evaluation, sensor instability. Definition of "significant" is a matter of engineering judgment, and depends on accuracy required and legal and professional implications of data.

10.3.3.6. Repeat with at least two more data sets to verify data.

10.3.4. If desired, for systems proven linear and stable, a scale factor to convert that system's displacement sensor data to "true" data may be determined.

10.3.4.1. Plot averaged displacement time histories $\delta_{i,avg}$ for each sensor being tested with the reference system sensor deemed most reliable. Ensure all data begins at the origin.

10.3.4.2. Plots of test system sensors should be above or below the reference sensor plot at roughly constant magnitude. If not, the transition between above and below should be in distinct regimes, and the differences should be constant in those regimes.

10.3.4.3. Sensor correction factor: determine average fractional difference in each regime yielding a multiplier to obtain "true" displacement as defined by the reference system:

$$\text{Scale Factor} = \overline{\left(\frac{\delta_{i,avg}(\textit{sensor being evaluated})}{\delta_{i,avg}(\textit{baseline sensor})} \right)} \qquad (5)$$

10.4. Field testing.

10.4.1. Perform one-hour rolling average of all data.

10.4.2. Sort all data so that one, one-hour rolling average data point is taken for every hour at one-hour intervals. A computer program is recommended; spreadsheets become large and unwieldy for this operation.

10.4.3. For data at five-minute intervals, 12 points per hour corresponds to:

$$[\delta_{1,s,avg} = \delta_{1,avg}, \delta_{2,s,avg} = \delta_{13,avg}, \delta_{3,s,avg} = \delta_{26,avg}, \ldots] \qquad (6)$$

10.4.4. Perform 24-hour rolling average of all data, taking the data point at time i and data points 12 hours before and after it, e.g. as for measured displacement below:

$$\delta_{i,24} = \frac{\sum_{n=i-12}^{n=i+12} \delta_{n,s,avg}}{25} \qquad (7)$$

10.4.5. Subtract null sensor $\delta_{i,24nl}$ and $\delta_{i,s,avg,nl}$ from crack sensor $\delta_{i,24c}$ and $\delta_{i,s,avg,c}$ for all i:

$$\delta_{i,24net} = \delta_{i,24c} - \delta_{i,24nl} \qquad (8a)$$

$$\delta_{i,s,avg,net} = \delta_{i,s,avg,c} - \delta_{i,s,avg,nl} \qquad (8b)$$

10.4.6. Plot one-hour and 24 hour time histories of Temperature, $\delta_{i,s,avg,net}$, $\delta_{i,s,avg,nl}$, $\delta_{i,24net}$, $\delta_{i,24nl}$ and all sensors' measured displacement, and net displacement from equations 7a and 7b above. Shift all data to start at the origin per Equation 4 above. For a test with several intermediate downloads, apply the $\delta_{1,24} = \delta_{1,s,avg}$ point determined in the very first data set to all data.

10.4.7. Reference system one-hour and 24-hour sensor measured displacement time histories should match temperature time history. Test is invalid if significant deviations occur.

10.4.8. Assess fidelity of system under evaluation $\delta_{i,s,avg,net}$ and $\delta_{i,24net}$ to reference system $\delta_{i,s,avg,net}$ and $\delta_{i,24net}$ graphs. View in various scales. Exactness of both magnitude and contemporaneous time is not as important as pattern fidelity.

10.4.9. If desired, "correction to true" may be applied as a function of sensor correction factor from 10.3.3.4 above.

11. Interpretation of Results.

11.1. Repeated values of $V > 0.1$ as determined in Equation 3 are not desirable because of significant dispersion of system response.

11.2. Significant deviations from the temperature time history pattern that persist over the course of several tests disqualify the sensor as unstable.

12. Report

12.1. Plate testing. The report for each sensor for each test run consists of:

12.2. A hysteretic curve of measured displacement $\delta_{i,avg}$ versus calculated displacement $\delta_{i,calc}$ showing best-fit line, with annotated standard deviation σ and variance V (Figure 9);

12.3. A time history curve of measured displacement versus time $\delta_{i,avg}$ versus time t_i for both system being tested and reference system (Figure 10);

12.4. A time history curve of average temperature, $T_{i,avg}$ versus time, t_i (Figure 11).

12.5. Field testing. The report for each sensor for each test run consists of:

12.6. A time history curve of measured displacement versus time $\delta_{i,avg}$ versus time t_i for both system being tested (Figure 12a) and reference system (Figure 12b), one-hour and 24-hour rolling averages;

12.7. A time history curve of one-hour and 24-hour rolling average temperature, $T_{i,avg}$ versus time, t_i (Figure 12c).

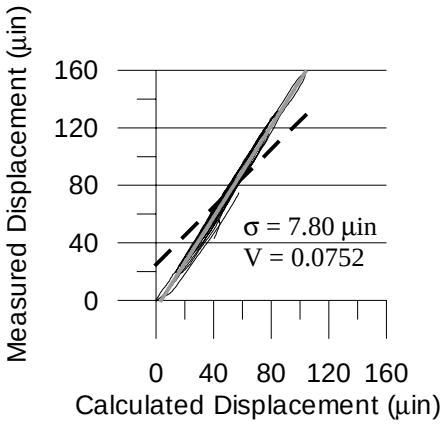

Figure 9. Hysteretic curve, with predicted displacement (dashed line, slope = 1.0) offset for visibility. Gray line through center of hysteretic curve is best-fit line. Many graphics programs can automatically calculate and plot such a line.

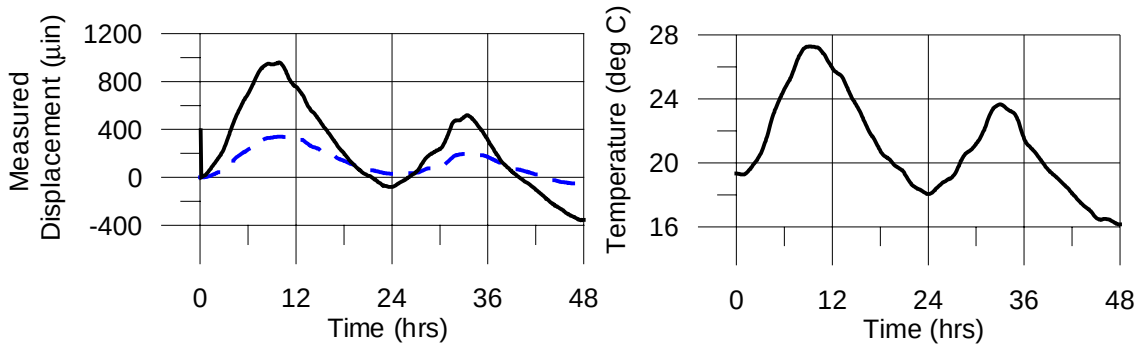

Figure 10. Time history curves, measured displacement ($\delta_{i,avg}$) versus time (t_i)for both system being tested (dashed line) and reference system (solid line).
Figure 11. Time history curves, averaged temperature (Ti,avg) versus time (ti) .

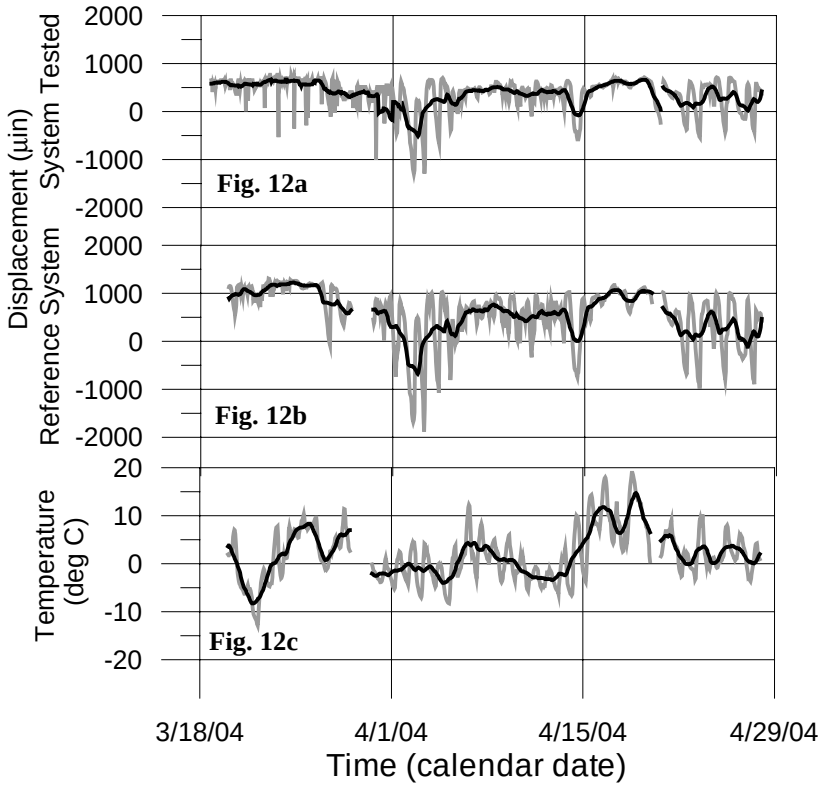

Figures 12. Gray lines are one-hour rolling averages; black lines are 24-hour rolling averages.
Figures 12a-b. Displacement time histories of: a. System being tested; b. Reference system across a crack in a nonlinear material, the sheetrock ceiling of a wood frame house.
Figure 12c. Temperature time history. Note pattern does not always match displacement patterns on a nonlinear material under actual conditions, unlike close agreement on a linear, predictable material.

13. Keywords: Calibration; displacement; instrumentation; strain; hysteresis; linearity; time history; displacement pattern; correction factor.